Range Alignment for ISAR Imaging of Sea Vessels

Inverse Synthetic Aperture Radar

Prepared by:

Azhar Ebrahim

EBRAZH001

Department of Electrical Engineering
University of Cape Town

Prepared for:

Dr M. Y. Abdul Gaffar

DEPARTMENT OF ELECTRICAL ENGINEERING
University of Cape Town

May 2022

Submitted to the Department of Electrical Engineering at the University of Cape Town in partial fulfilment of the academic requirements for a Bachelor of Science degree in Mechatronics Engineering**.**

Abstract

This project covers range alignment for ISAR imaging of sea vessels. Radar concepts as well radar signal processing concepts were investigated. Subsequently, inverse synthetic aperture radar (ISAR) concepts were looked at before a focus on range alignment algorithms was placed.

The rationale behind the study was to review the range alignment techniques found in the literature and to assess the strengths and weaknesses of the techniques. Furthermore, the study was done to determine the performance of range alignment algorithms across different datasets.

The analysis was done by implementing the techniques on MATLAB, across different measured datasets. These datasets came from maritime vessels, namely a Spanish vessel and a CSIR vessel.

The measures used to quantify the performance of the algorithms were both qualitative and quantitative. The qualitative measure included looking at high range resolution (HRR) profile plots and comparing them. The quantitative measures used were contrast and entropy.

It was found the sub-integer envelope correlation techniques performed better than the integer-shift envelope correlation techniques. The best performing technique qualitatively, and in terms of the contrast, was the single reference profile envelope correlation (sub-integer shift) technique. The cumulative averaging reference profile envelope correlation technique achieved the best entropy across the measured datasets. Furthermore, in this study, it was found that the techniques have consistent performance across different datasets, with minor differences.

Acknowledgements

Firstly, I would like to thank the Almighty for giving me the strength and knowledge to complete my project.

I extend my sincere appreciation to all the following individuals who assisted me in my research project.

I would like to express my heartfelt gratitude to my supervisor, Dr Abdul Gaffar. He stood by me throughout my project and was always there for me when I needed guidance and direction. Words cannot express my appreciation for him. It was an honour working with someone with so much knowledge and insight in the field.

My mom and sister for their prayers, sacrifices, and unwavering support. Their faith in me has encouraged me to reach my full potential. They have instilled important values in me from a young age for which I will always be grateful.

My peers, Salmaan, Crystal, Raees, Muneeb, Kavir, Taqi, Reesen, and Trivaan have all been a pillar of strength throughout my studies. I am thankful for their moral and emotional support.

Also, to my other friends who steered me in the right direction and had confidence in me. I will always have fond memories of the experiences we shared as a group and our UCT days.
I am also thankful to all my lecturers who provided me with the necessary skills and knowledge to achieve my goals.

I express my sincere gratitude to the Council of Scientific and Industrial Research (CSIR) for providing the measured datasets that were used in this work.

Lastly, to the University of Cape Town, where I have acquired so much knowledge and received a good education.

Plagiarism declaration

1. I know that plagiarism is wrong. Plagiarism is to use another's work and pretend that it is one's own.
2. I have used the IEEE convention for citation and referencing. Each contribution to, and quotation in, this final year project report from the work(s) of other people, has been attributed and has been cited and referenced.
3. This final year project report is my work.
4. I have not allowed, and will not allow, anyone, to copy my work with the intention of passing it off as their work or part thereof.

Page count: 69

Name: **Azhar Ebrahim**

Signature: **A.Ebrahim** **Date:** 29 May 2022

Table of Contents

Abstract i
Acknowledgements ii
Plagiarism declaration iii
Table of Contents iv
List of Figures vii
List of Tables ix
Nomenclature x
1. Introduction 1
1.1 Introduction 1
1.2 Background 1
1.3 Problem statement 1
1.4 Objectives 2
1.5 Thesis contributions 2
1.6 Scope and limitations 2
1.7 Plan of development 3
2. Literature Review 4
2.1 Introduction 4
2.2 Radar Concepts 4
2.2.1 Introduction to Radar 4
2.2.2 The Radar Concept 5
2.2.3 The Physics of electromagnetic waves 6
2.2.4 The bandwidth of electromagnetic waveforms 7
2.2.5 Basic radar configurations and waveforms 7
2.2.6 Range resolution 7
2.2.7 Pulse compression or matched filtering [for Pulse-Doppler Radars] 8
2.2.8 Range concepts – pulse compression and waveforms [for Pulse-Doppler Radars] 8
2.2.9 Doppler concepts 8
2.3 Radar Signal Processing Concepts 8
2.3.1 Sampling the radar's received signal 8
2.3.2 Range bins 9
2.3.3 Radar data matrix: fast time vs slow time 9
2.3.4 Measuring Doppler with multiple pulses 9
2.3.5 High Resolution Radar (HRR) 9
2.3.6 Radar Imaging 9
2.3.7 Synthetic Aperture Radar (SAR) 10
2.3.8 Inverse Synthetic Aperture Radar (ISAR) 10
2.3.9 Motion Compensation and Autofocus 11
2.3.10 Target Feature Extraction 12
2.4 Inverse Synthetic Aperture Radar Concepts 12
2.4.1 Detailed introduction to ISAR 12
2.4.2 Waveforms used to obtain high range resolution 13
2.4.3 Range alignment vs phase adjustment 13
2.4.4 ISAR motion compensation 13
2.4.5 Effect of Coherent Processing Interval Window Length (CPIWL) on ISAR images 14
2.5 Overview of range alignment techniques 14
2.5.1 Peak alignment 14
2.5.2 Envelope correlation 14

2.5.3 The spectral domain phase difference 15
2.5.4 Minimum entropy of the average range profile 16
2.5.5 Sub-integer range bin alignment 16
2.5.6 Hough transform 17
2.5.7 Global Method 17
2.5.8 Other range alignment techniques 18
2.6 Quality measures of alignment techniques 18
2.6.1 Sum Envelope Contrast 18
2.6.2 Sum Envelope Entropy 18
2.6.3 Global Envelope Correlation 20
2.6.4 The variance of the peak location 20
2.6.5 Mean squared envelope difference 20
2.6.6 Burst Derivative 21
2.7 Critical Literature Survey 21
2.7.1 Strengths and weaknesses of the literature 21
2.7.2 Gaps in the literature and topics out of the scope 21
2.7.3 Link to Objectives 22
2.8 Conclusion 22
3. Methodology 23
3.1 Overview 23
3.2 The Measured datasets and loading them into MATLAB 23
3.2.1 Spanish Dataset 23
3.2.2 CSIR Dataset 24
3.3 Method for integer shift range alignment algorithms 25
3.4 Method for sub-integer shift range alignment algorithms 26
3.5 Method for the quality measures 26
3.5.1 Contrast 26
3.5.2 Entropy 27
3.5.3 Qualitative measure 27
3.6 Testing across the different datasets 27
3.7 Plotting the HRR profiles and bin shifts 27
3.7.1 HRR profile plots 27
3.7.2 Bin shift plots 27
3.7.3 Quality measure comparison plots 27
4. Algorithm Implementations and Results 28
4.1 Introduction and structure of the chapter 28
4.2 Contrast and Entropy techniques 30
4.3 Single Reference Profile envelope correlation Alignment (Integer shift) 32
4.3.1 Spanish Dataset 33
4.3.2 CSIR Dataset 34
4.3.3 Discussion and comparison of both datasets 35
4.4 Adjacent Reference Profile Alignment (Integer shift) 37
4.4.1 Spanish Dataset 38
4.4.2 CSIR Dataset 39
4.4.3 Discussion and comparison of both datasets 41
4.5 Non-coherent Cumulative Average Reference Profile Alignment (Integer shift) 42
4.5.1 Spanish Dataset 43
4.5.2 CSIR Dataset 44
4.5.3 Discussion and comparison of both datasets 45
4.6 Sliding-Window Average Reference Profile Alignment (Integer shift) 47

4.6.1 Spanish Dataset 48
4.6.2 CSIR Dataset 49
4.6.3 Discussion and comparison of both datasets 51
4.7 Overview of Sub-integer shift algorithms 52
4.8 Single Reference Profile envelope correlation Alignment (Sub-integer shift) 53
4.8.1 Spanish Dataset 53
4.8.2 CSIR Dataset 54
4.8.3 Discussion and comparison of both datasets 56
4.9 Adjacent Reference Profile Alignment (Sub-integer shift) 57
4.10 Non-coherent Cumulative Average Reference Profile Alignment (Sub-integer shift) 57
4.10.1 Spanish Dataset 57
4.10.2 CSIR Dataset 58
4.10.3 Discussion and comparison of both datasets 60
4.11 Sliding-Window Average Reference Profile Alignment (Sub-integer shift) 60
4.11.1 Spanish Dataset 60
4.11.2 CSIR Dataset 61
4.11.3 Discussion and comparison of both datasets 63
5. Discussion of the algorithms on different blocks within a dataset 64
5.1 Spanish Dataset intra-block performance 64
5.2 CSIR Dataset intra-block performance 65
6. Conclusion 68
6.1 Review of Range alignment techniques 68
6.2 Implementation and assessment of Range alignment techniques 68
6.3 Performance of the different algorithms on different datasets 68
6.4 Intra-dataset performance 68
6.5 Future work 68
6.5.1 Exploring more techniques 68
6.5.2 Exploring more quantitative measures 69
6.5.3 Using more datasets 69
6.5.4 Phase correction and autofocus 69
Appendices 72
Appendix A: Sub-Integer algorithm steps and derivation 72
Appendix B: Global Method flow diagram 73
Appendix C: Sum Envelope Entropy derivation 74
Appendix D: Code to obtain the results 75

List of Figures

Figure 2.1 Literature Review Structure 4
Figure 2.2 Radar process [12] 5
Figure 2.3 Radar transmission and reception [13] 6
Figure 2.4 Effect of bandwidth on range resolution [12] 7
Figure 2.5 Trajectory of the research [4] 10
Figure 2.6 A ship with its ISAR image [18] 11
Figure 2.7 How pitch, yaw and roll affect the orientation [19] 11
Figure 2.8 a) Spotlight SAR configuration to b) an ISAR configuration [21] 12
Figure 2.9 Motion compensation procedure for ISAR imaging [21] 13
Figure 2.10 Effect of standard deviation on the entropy value [4] 19
Figure 2.11 Using a shifted Sinc function to highlight the influence of misalignment [4] 19
Figure 3.1 Image of the Altera vessel [28] 23
Figure 3.2 Transmitted waveform 24
Figure 3.3 Image of the Zayaan Vessel 24
Figure 3.4 Wrapping of profiles [900 964] 25
Figure 4.1 Structure of algorithm presentation 28
Figure 4.2 HRR unaligned profiles 1:256 29
Figure 4.3 HRR unaligned profiles 1536:1599 30
Figure 4.4 Code snippet to calculate the sum envelope S(n) 30
Figure 4.5 Code Snippet to calculate the contrast 30
Figure 4.6 Code snippet to calculate the entropy 31
Figure 4.7 Code snippet to show the conversion to dB scale 31
Figure 4.8 Single reference profile (integer) process 32
Figure 4.9 HRR profiles plot of the envelope correlation single reference profile algorithm 33
Figure 4.10 Plot of the bin shifts per profile for alignment 34
Figure 4.11 HRR profiles plot of the envelope correlation single reference profile algorithm 34
Figure 4.12 Plot of the integer bin shifts per profile for alignment 35
Figure 4.13 Single reference profile (integer) process 37
Figure 4.14 HRR profiles plot of the envelope correlation adjacent reference profile algorithm 38
Figure 4.15 Plot of the integer bin shifts per profile for alignment 39
Figure 4.16 Plot of profile 1 and profile 2 to show similarities 39
Figure 4.17 HRR profiles plot of the envelope correlation adjacent reference profile algorithm 40
Figure 4.18 Plot of the integer bin shifts per profile for alignment 40
Figure 4.19 Plot of profile 1 and profile 2 to show similarities 41
Figure 4.20 Cumulative average reference profile (integer) process 42
Figure 4.21 HRR profiles plot of the envelope correlation cumulative average reference profile algorithm 43
Figure 4.22 Plot of the integer bin shifts per profile for alignment 44
Figure 4.23 HRR profiles plot of the envelope correlation cumulative average reference profile algorithm 45
Figure 4.24 *Plot of the integer bin shifts per profile for alignment* 45
Figure 4.25 Sliding window average reference profile (integer) process 47
Figure 4.26 HRR profiles plot of the envelope correlation sliding window average reference profile algorithm 48
Figure 4.27 Plot of the integer bin shifts per profile for alignment 49
Figure 4.28 HRR profiles plot of the envelope correlation sliding window average reference profile algorithm 50
Figure 4.29 Plot of integer the bin shifts per profile for alignment 51
Figure 4.30 Sub-integer shift process 52

Figure 4.31 HRR profiles plot of the envelope correlation single reference profile algorithm (sub-integer shift) 54
Figure 4.32 Plot of the bin shifts per profile for alignment with a first order polynomial 54
Figure 4.33 HRR profiles plot of the envelope correlation single reference profile algorithm (sub-integer shift) 55
Figure 4.34 Plot of the bin shifts per profile for alignment with a first order polynomial 56
Figure 4.35 HRR profiles plot of the envelope correlation cumulative average reference profile algorithm (sub-integer shift) 57
Figure 4.36 Plot of the bin shifts per profile for alignment with a first order polynomial 58
Figure 4.37 HRR profiles plot of the envelope correlation cumulative average reference profile algorithm (sub-integer shift) 59
Figure 4.38 Plot of the bin shifts per profile for alignment with a first order polynomial 59
Figure 4.39 HRR profiles plot of the envelope correlation sliding window average reference profile algorithm (sub-integer shift) 61
Figure 4.40 Plot of the bin shifts per profile for alignment with a first order polynomial 61
Figure 4.41 HRR profiles plot of the envelope correlation sliding window average reference profile algorithm (sub-integer shift) 62
Figure 4.42 Plot of the bin shifts per profile for alignment with a first order polynomial 63
Figure 5.1 Plot of the block number vs normalised contrast (dB) 65
Figure 5.2 Plot of the block number vs normalised entropy (dB) 66
Figure 5.3 Plot of the block number vs normalised contrast (dB) 66
Figure 5.4 Plot of the block number vs normalised entropy (dB) 67

List of Tables

Table 3.1 Radar parameters 23
Table 3.2 Parameters of the X-band radar 25
Table 4.1 Table showing the contrast and entropy values in dB 29
Table 4.2 Table showing the contrast and entropy values in dB 30
Table 4.3 Table showing the contrast and entropy values in dB 33
Table 4.4 Table showing the contrast and entropy values in dB 35
Table 4.5 Table showing the contrast and entropy values in dB 38
Table 4.6 Table showing the contrast and entropy values in dB 40
Table 4.7 Table showing the contrast and entropy values in dB 43
Table 4.8 Table showing the contrast and entropy values in dB 44
Table 4.9 Table showing the contrast and entropy values in dB 49
Table 4.10 Table showing the contrast and entropy values in dB 50
Table 4.11 Table showing the contrast and entropy values in dB 53
Table 4.12 Table showing the contrast and entropy values in dB 55
Table 4.13 Table showing the contrast and entropy values in dB 57
Table 4.14 Table showing the contrast and entropy values in dB 58
Table 4.15 Table showing the contrast and entropy values in dB 60
Table 4.16 Table showing the contrast and entropy values in dB 62
Table 5.1 Performance of the algorithms on different blocks 64

Nomenclature

Acronym	Term
ISAR	Inverse Synthetic Aperture Radar
RCS	Radar Cross-Section
CPI	Coherent Processing Interval
PGA	Phase Gradient Autofocus
RF	Radiofrequency
T/R	Transmit/Receive
IF	Intermediate Frequency
ADC	Analgoue-to-Digital
PRI	Pulse Repetion Interval
PRF	Pulse Repetition Frequency
SNR	Signal-to-Noise Ratio
CPIWL	Coherent Processing Interval Window Length
FMCW	Frequency-Modulated Continuous Waveform
FFT	Fast-Fourier Transform
HRR	High Resolution Radar
SAR	Synthetic Aperture Radar
LFM	Linear Frequency Modulated
IFFT	Inverse Fast Fourier Transform
IFT	Inverse Fourier Transform
HRR profiles	High Range Resolution profiles

1. Introduction

1.1 Introduction

Inverse synthetic aperture radar (ISAR) is a signal processing and imaging technique used to provide an electromagnetic image of a target [1]. An ISAR image of a target is achieved by using wide bandwidth pulses which echo off a moving target [1]–[3].

The technique has gained a lot of popularity due to its wide variety of usability. ISAR images contain an abundance of information which is valuable for target classification. Targets can range from aircraft to sea vessels and many other moving objects [4], [5]. This is particularly useful for environmental monitoring and surveillance systems [2]. Another application of ISAR is its use in measuring the Radar Cross-Section(RCS) of platforms to subsequently reduce large hotspot areas. The following report focuses on using ISAR for the classification of sea vessels.

Radar technology is well suited for this application of target classification due to its many advantages. Firstly, radar can provide a high spatial resolution which is unconstrained by the distance to the image target area. The same cannot be said for optical sensors which have a much lower operating range. This is due to the resolution only being dependent on wavelength, bandwidth and the relative movement between the object and the radar. Secondly, since radar is an active sensor it operates independently from the sun and time of the day. Furthermore, the electromagnetic waves are not affected by visual hindrances such as fog, smoke and clouds, making the quality of images independent of the weather. Once more, radar proves better than optical sensors, which are dependent on sunlight and weather conditions. This also gives it an advantage over LiDAR, which generally has a better accuracy [2]. Some disadvantages of radar include its inability to distinguish between multiple similar targets, and also to distinguish between colours.

1.2 Background

The formation of an ISAR image, a technique that focuses on translational motion compensation, is a result of two main processes, namely range alignment and phase correction. The first step which is range alignment is the focal point of the project. Therefore it is crucial that a good range alignment is achieved, as poor range alignment would lead to errors which cannot be corrected with algorithms down the processing chain. That is, the remaining processing such as autofocus(phase correction) and polar-reformatting are unable to correct the errors of a weak range alignment algorithm. This would result in unfocused ISAR images.[6]

1.3 Problem statement

In providing effective solutions, the following challenges relating to compensation for translational motion and rotational motion need to be overcome. As aforementioned range alignment and autofocus are used to compensate for translational motion, and polar-reformatting for rotational motion compensation. Adapting and improving already implemented algorithms for compensation is one such challenge. Additional challenges include finding suitable intervals within the datasets which provide adequate data for the formation of effective 2-D ISAR images, for classification. Suitable intervals for both non-cooperative vessels as well as cooperative vessels are discussed by Martorella [7] and Abdul Gaffar [8] respectively. The paper by Abdul Gaffar [8] also describes the challenge of finding the Coherent Processing Interval (CPI) which is investigated.

Solutions to the above-mentioned range alignment challenges have been extensively addressed in the literature by Van Rensburg [4] and Zyweck [5]. The range alignment techniques discussed in Van Rensburg's work [4] are, peak alignment, envelope correlation, spectral domain phase difference, minimum entropy of average range profile, sub-integer bin alignment, Hough transforms and the global method. The performance of these

algorithms is quantified using contrast, entropy, variance, mean squared envelope difference and burst derivative. In Zyweck's [5] work the Haywood algorithm for sub-integer shift alignment is explored as well as in a paper by Munoz-Ferreras [9].

An autofocus algorithm based on a time domain phase gradient is presented in work done by Nel [10], along with its relation to phase gradient autofocus (PGA). Algorithms published in the field relating to polar formatting include the tiered subaperture algorithm, space-variant post-filtering and the widefield polar formatting algorithm [11].

There has been insufficient work in addressing the problem of differentiating between datasets and quantifying the performance improvement between basic range alignment methods. Moreover, designing more robust algorithms is an area for research, as well as identifying an appropriate quantitative measure for the performance of range alignment.

The problem that was addressed in this work was exploring the above gaps in research. That is, adapting existing algorithms and exploring new ones which are more robust, while simultaneously testing the solutions on different datasets. Lastly, the effectiveness of these solutions was quantified with existing and new measures.

By solving the stated problems, the advantages that are gained are more robust systems, as well as quantitative and qualitative feedback on the performance of range alignment algorithms among different datasets.

1.4 Objectives

The objectives of this report are listed as follows:

- Review range alignment algorithms in the literature.
- Implement range alignment algorithms on the measured data to understand their strengths and weaknesses.
- Compare the range alignment performance for different algorithms on different datasets.

1.5 Thesis contributions

The main contribution of this thesis was to identify range alignment algorithms and a combination thereof that lead to robust alignment. This was attempted using theories and algorithms that have been implemented, specifically on a variety of different datasets, quantifying the difference in performance.

1.6 Scope and limitations

The work in this project was limited to range alignment techniques. There are 8 algorithms analysed as stated below:

1. Single Reference Profile envelope correlation Alignment (Integer shift)
2. Adjacent Reference Profile envelope correlation Alignment (Integer shift)
3. Non-coherent Cumulative Average Reference Profile envelope correlation Alignment (Integer shift)
4. Sliding-Window Average Reference Profile envelope correlation Alignment (Integer shift)
5. Single Reference Profile envelope correlation Alignment (Sub-integer shift)
6. Adjacent Reference Profile envelope correlation Alignment (Sub-integer shift)
7. Cumulative Average Reference Profile envelope correlation Alignment (Sub-integer shift)
8. Sliding-Window Average Reference Profile envelope correlation Alignment (Sub-integer shift)

These algorithms were implemented and analysed on different datasets.

The work excluded autofocus and ISAR imaging (Doppler images). Furthermore, range alignment algorithms not implemented include the spectral domain phase difference, Hough transform and the global method.

Time was a constraint for the project. The project spanned the first semester of the 2022 academic year. A 13-week duration meant that efficiency was important and there was not much room for error.

Moreover, the software used (MATLAB), is computationally taxing. It uses up a lot of ram and memory and needs to be run on a good processor. All simulations and designs shown in the report are run on a 16Gb ram laptop with an I5 processor.

1.7 Plan of development

The project has the following sequential order:

Chapter 2 presents the **Literature review**. This covers radar and radar signal processing concepts. It also covers ISAR concepts, as well as an overview of range alignment algorithms and their quality measures. Furthermore, it looks at the measured datasets and contains a critical literature survey section.

Next, *Chapter 3* discusses the **Methodology**. Here, the design approach is summarised along with the software used.

Following, *Chapter 4,* exhibits the **Algorithm Implementations and Results**. The algorithms were implemented based on the relevant theory and methodology. Each sub-chapter corresponds to a different range alignment algorithm. The outcome of the simulations is also presented and analysed in this section.

In *Chapter 5 t*he **Discussion** of the results is found. A discussion of the results of the different algorithms on the CSIR dataset is shown using different blocks of data.

Lastly, *Chapter 6* presents the **Conclusion**. Using the results, conclusions were drawn indicating the level of success of the project as well as a summary of the findings.

2. Literature Review

2.1 Introduction

The following literature review covers the topics which are essential aspects of the project. Relevant theories and techniques are discussed as well as current implementations in the industry. Moreover, relevant history and research into the topics are discussed.

The review starts with a background in radar concepts followed by the theory relating to the signal processing of radar. Next, the review looks more specifically at ISAR concepts. Thereafter, the review unpacks many range alignment techniques that have been previously implemented by other researchers, along with their respective quality measures. Finally, a critical literature survey is done to assess previous work done in the field. A simple tree diagram of the structure of the review is shown in Fig 2.1 depicting this.

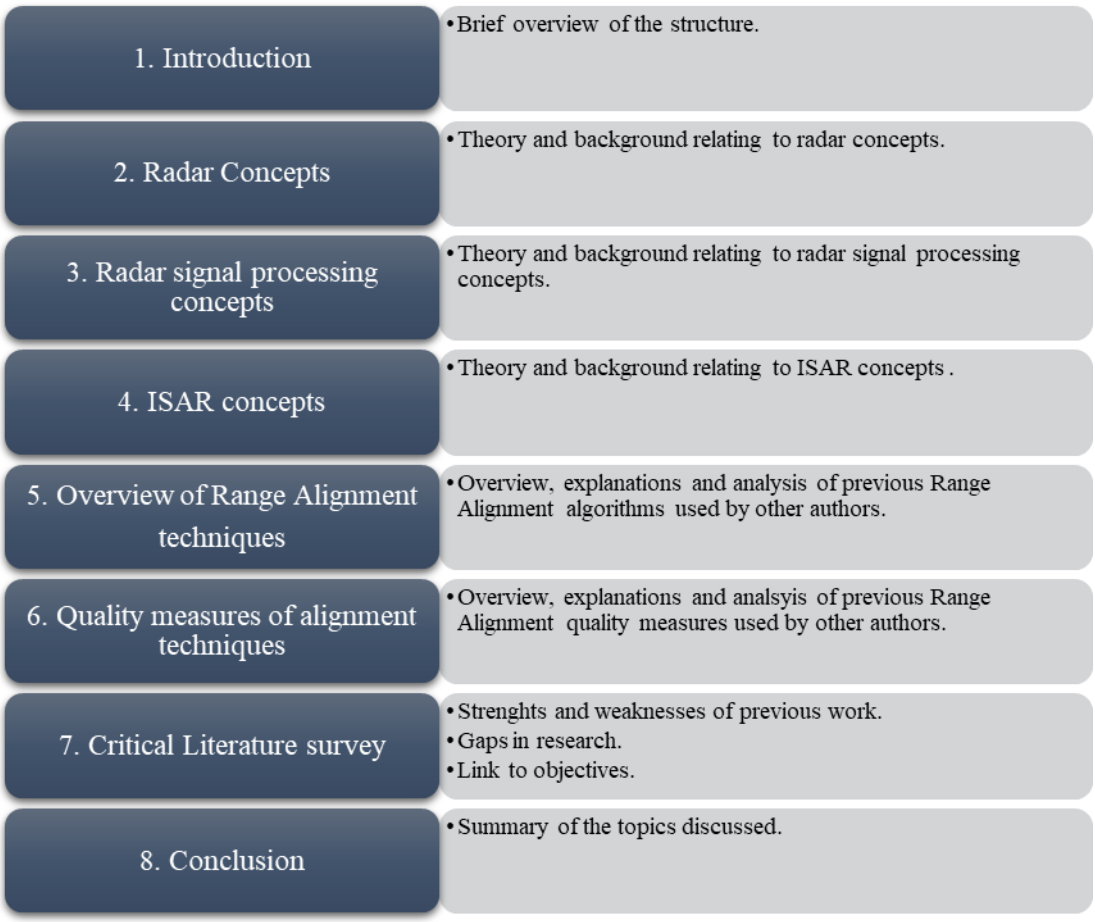

Figure 2.1 Literature Review Structure

2.2 Radar Concepts

2.2.1 Introduction to Radar

The term RADAR stands for Radio Detection and Ranging. It is a system used to detect the distance and velocity of targets relative to the system. The systems use radio waves to achieve this. A simple illustration of the radar process is shown in Fig 2.2. Here, it is seen that an antenna (through a transmitter) generates a pulse which is transmitted to the target. The target subsequently sends a reflected pulse("echo") which is received by the antenna (through a receiver). Some examples of radar include surveillance radars, airborne radars and instrumentation radars. [12]

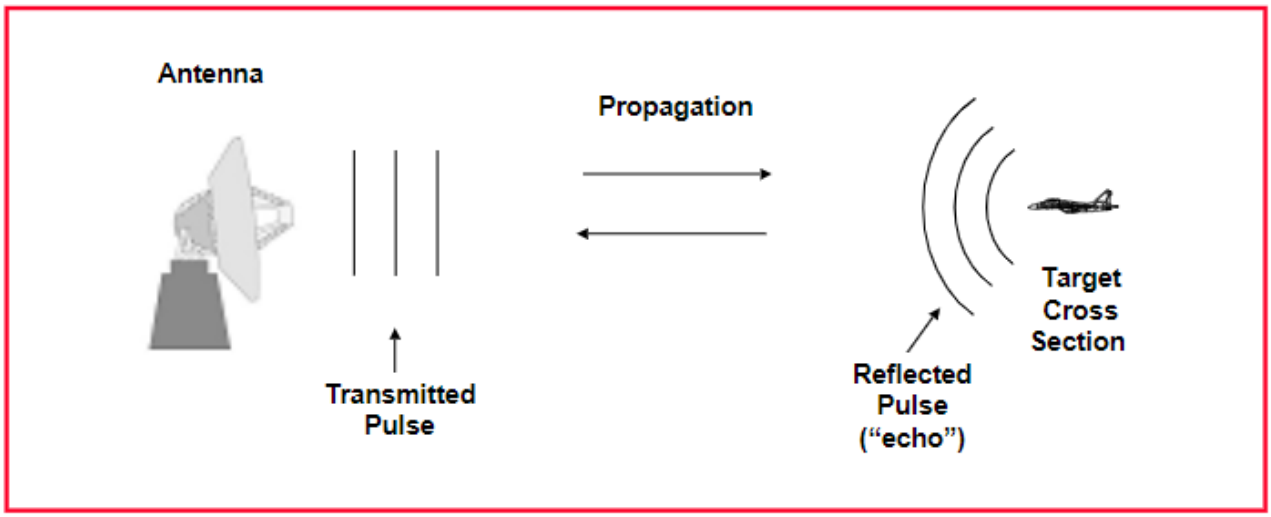

Figure 2.2 Radar process [12]

2.2.2 The Radar Concept

As mentioned earlier, a radar is a system that transmits radiofrequency (RF) electromagnetic waves towards a target region and receives electromagnetic waves from objects in the same region. The major subsystems in radar include an antenna, receiver, transmitter and signal processor. This can be seen in Fig 2.3. The transmitter generates the electromagnetic wave. The antenna takes in these electromagnetic waves and incorporates them into a propagation medium (usually air). The connection between the antenna and the transmitter is through a transmit/receive (T/R) device. The electromagnetic waves incite currents onto targets, which radiate into the environment. In this process, unintentional signals are created which are a result of other surfaces. These signals are known as clutter. The receiver receives the "reflected" electromagnetic waves picked up by the antenna. The part of the signal which was reflected off the target is applied to the receiver circuitry. The received RF signal is converted to an intermediate frequency (IF) and subsequently applied to an analogue-to-digital converter (ADC), before being sent to the signal processor. Detectors erase the carriers from modulated returned signals.[13]

The range to a target, R, can be expressed by the time in seconds for round-trip travel, T, and by the speed of light in metres per second, *c*. This is expressed in Equation 2.1 [13].

$$R = \frac{c\Delta T}{2} \tag{2.1}$$

It is important to note that received signals are subject to interference. Interference can be in the form of noise, clutter, electromagnetic interference and intentional jamming.

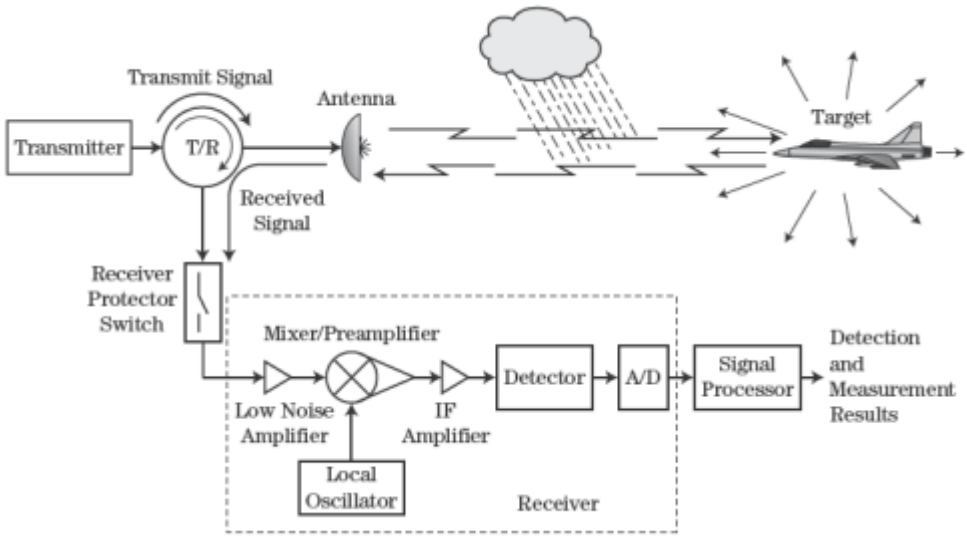

Figure 2.3 Radar transmission and reception [13]

2.2.3 The Physics of electromagnetic waves

Electromagnetic waves are field waves (electric and magnetic), which oscillate at a carrier frequency. These fields are described by Maxwell's equations [13].

<u>Wavelength, Frequency and phase of a sinusoidal signal</u>

The wavelength, λ, of a sinusoidal signal is the distance from any one point on a sinusoid to the first corresponding point. The period of a wave, *T*, is the time from any one point on a sinusoid to the first corresponding point, with the inverse of this being the frequency, *f*. Lastly, the phase is used to differentiate between waves. [13]

<u>Intensity and Polarisation</u>

The power per unit area of a wave is known as its intensity, *Q*. Moreover, the polarisation of an electromagnetic wave describes the motion and orientation of the electric field. [13]

<u>The Radar Equation</u>

A radar's ability to track a target is measured by the signal to noise ratio. One such equation comes from Richards et al. This is described in Equation 2.2. [14]

$$S/N = \frac{P_t\, G^2\, \lambda^2\, \sigma}{(4\pi)^3\, R^4\, K\, T_s\, B_n\, L} \tag{2.2}$$

With:

- S/N, the signal to noise ratio.
- P_t, the peak transmitter power.
- G, the transmitter gain.
- λ, the transmitter wavelength.
- σ, the radar cross section.
- R, the distance from the radar.
- k, Boltzman's constant
- T_s, the system noise.
- B_n, the noise bandwidth of the receiver.
- L, the total system losses.

2.2.4 *The bandwidth of electromagnetic waveforms*

The bandwidth of the waveform is a measure of its frequency change. The bandwidth size is directly related to the amount of information achievable from a target. That is, more bandwidth means more available information. Furthermore, a higher bandwidth implies improved range resolution. A smaller range resolution value is generally desirable. Fig 2.4 illustrates this effect [12]. The term range resolution is discussed later.

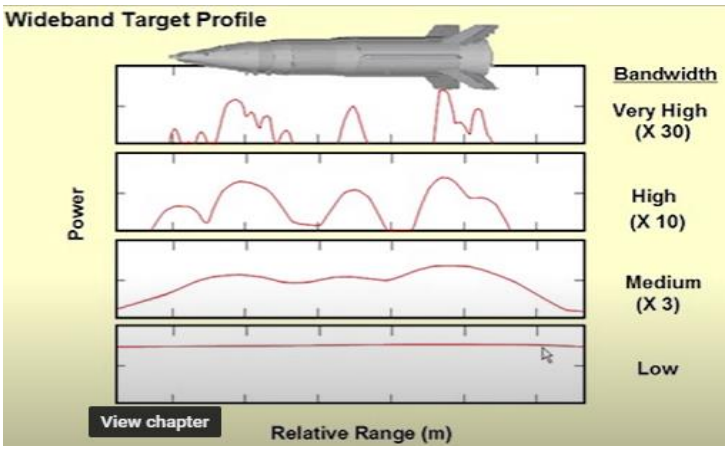

Figure 2.4 Effect of bandwidth on range resolution [12]

2.2.5 *Basic radar configurations and waveforms*

Monostatic and Bistatic configurations

The two basic radar antenna configurations are the monostatic configuration and the bistatic configuration. The former has the antenna acting as both a receiver and a transmitter, with the latter having separate antennas for transmitting and receiving. [13]

Continuous and pulsed waveforms

The two major classes of radar waveforms are continuous waveforms and pulsed waveforms. With continuous waveforms, the transmitter continuously transmits a signal, with the receiver operating as well.

Contrary, with pulsed waveforms, sequences of finite duration pulses are transmitted and the receiver operates only when the transmitter is "off". The width of the pulse together with the receive time (when the antenna is listening for echoes) is known as the pulse repetition interval (PRI). The inverse of the PRI is the pulse repetition frequency (PRF). [13]

Ambiguous range measurement can occur if the total travel time of the pulse is greater than the PRI. Conversely, the maximum range at which a target's range can be measured unambiguously is known as the *unambiguous range measurement,* R_{ua}. This is given by Equation 2.3, with *c* being the speed of light. [13]

$$R_{ua} = \frac{c}{2PRF} \tag{2.3}$$

2.2.6 *Range resolution*

Range resolution, δR, is a radar system's ability to differentiate targets which are on the same bearing but have different ranges. The width and shape of the wave's mainlobe response, govern this. To reiterate what was mentioned earlier, range resolution and bandwidth are inversely proportional to one another. Equation 2.4 which describes a formula for range resolution, highlights this relationship. Here, *k* is a degradation factor, *B is* the bandwidth, and *c is* the speed of light. [13]

An enhanced resolution refers to a decreased δR, while a reduced resolution refers to an increased δR.

$$\delta R = k\frac{c}{2B} \tag{2.4}$$

2.2.7 Pulse compression or matched filtering [for Pulse-Doppler Radars]

A *matched filter* is derived from the transmitting waveform and allows for accurate range measurement when used with pulses that are uncompressed. The filter improves the signal-to-noise ratio. This is done by reducing the spectral bandwidth of the noise in addition to reducing the noise of the wavelets' bandwidth. The filter also helps in the processing of pulse compression waveforms. [13]

2.2.8 Range concepts – pulse compression and waveforms [for Pulse-Doppler Radars]

Pulse compression waveforms are waves which decouple energy and resolution via interpulse or intrapulse modulation. Moreover, the *pulse compression* gain is the SNR of the output over the SNR before the filter. Linear frequency modulated forms are worth mentioning here. They are sinusoids that have linearly frequency changes over time. Pulse compression is achievable due to the frequency dependency of the propagation delay through dispersive filters. Pulse compression techniques give radars the ability to attain the energy of a long pulse, while simultaneously retaining the resolution of a short pulse. [13], [15]

2.2.9 Doppler concepts

<u>Introducing the Doppler effect</u>

The doppler effect is the change in frequency of a wave observed by a listener, who is moving relative to the source of the wave [12]. The difference between the transmitted frequency and the received frequency is known as the doppler frequency, f_d. A target's Doppler frequency is aliased into the interval [-PRF/2 +PRF/2]. This is the range of Doppler frequencies that can be observed unambiguously. For example, when the target's Doppler frequency is higher than the unambiguous frequency an incorrect velocity will be given. [13]

<u>Doppler resolution</u>

The smallest difference in the Doppler shift of targets, with equal amplitude responses, which makes them reliably distinguishable, is known as the Doppler resolution The pulses are considered resolved if they are spaced by the single pulse bandwidth. This is determined by the coherent processing interval (CPI). A longer pulse train leads to a finer Doppler resolution. [13]

<u>Multiple pulses</u>

Radars use phase information from pulse-to-pulse to estimate the speed of a moving object. Therefore, Pulse-Doppler and frequency-modulated continuous waveforms (FMCW) radar need to transmit multiple pulses to estimate the Doppler frequency of the target. Moreover, the required processing for multiple pulses is a way of coherent integration which improves target detection. [13]

<u>Range-Doppler map</u>

A range-doppler map is a visual representation displaying Doppler frequencies on the x-axis and their corresponding range on the y-axis. [13]

2.3 Radar Signal Processing Concepts

2.3.1 Sampling the radar's received signal

A pulse is characterised by its amplitude, A, and its phase, θ, which forms the complex amplitude, $Ae^{j\theta}$. Assuming that is the transmitted signal, the received signal will be a shifted version with a new amplitude A'. A coherent detector is important for radar signal processing as this configuration splits incoming signals into two. The output of a single channel is not sufficient to identify both the amplitude and the phase as there are

multiple combinations of A' and θ that will produce the same output. Furthermore, the detector cannot differentiate between negative and positive phase shifts. [13]

2.3.2 Range bins

A range bin is one index of the range vector and is calculated by Equation 2.5, where the sampling frequency, f_s, is equal to the bandwidth, B. [13]

$$range\ bin = \frac{1}{B} \tag{2.5}$$

2.3.3 Radar data matrix: fast time vs slow time

When a radar transmits pulses in a CPI, a set of range bins are measured for the respective pulses. These corresponding values are stored in a data matrix. Since PRF is far lower than the sampling rate in the range, the pulse number axis is known as "slow time". Consequently, the range is called the "fast time". [13]

2.3.4 Measuring Doppler with multiple pulses

Pulse-Doppler signal processing(spatial doppler) needs to be applied to the baseband received signal, to estimate the Doppler frequency of the target. This is usually a Fast-Fourier transform (FFT). The processing is applied to the slow time dimension, to estimate the Doppler frequency, as the range bin(fast time) can stay constant. [13]

2.3.5 High Resolution Radar (HRR)

There have been many advancements in developing radars which operate at high centre frequencies and increased bandwidths, whilst retaining phase stability. Namely, the specialised group is known as High Resolution Radar. Radar resolution contains both range resolution, as well as angular resolution. [4], [5]

2.3.6 Radar Imaging

A specific goal of radar imaging is creating a picture of a target illustrating its physical features, making it recognisable in comparison to an optical image of the target. Optical images and images from radar have many differences. Due to its long-range capability, its all-weather capability and its all-time (day or night) capability, radar images have many advantages.

Carl Wiley, in 1951, stated that Doppler frequencies in backscattered signals from targets could be used for radar imaging [16]. He believed that if there was a relative speed between a target and a radar, components of the target would have different speeds relative to the antenna. Accurate analysis of the Doppler frequency using Fourier Transforms, modern spectral estimation and time-frequency renditions [17] will permit the creation of detailed images of target objects.

This is the basis of coherent radar imaging, explicitly Synthetic Aperture Radar (SAR) and Inverse SAR (ISAR), which are more advantageous over non-coherent imaging, for instance, amplitude-only tomography.

Fig 2.5 depicts the trajectory of the work covered in the project. The focus, as highlighted, is range bin alignment.

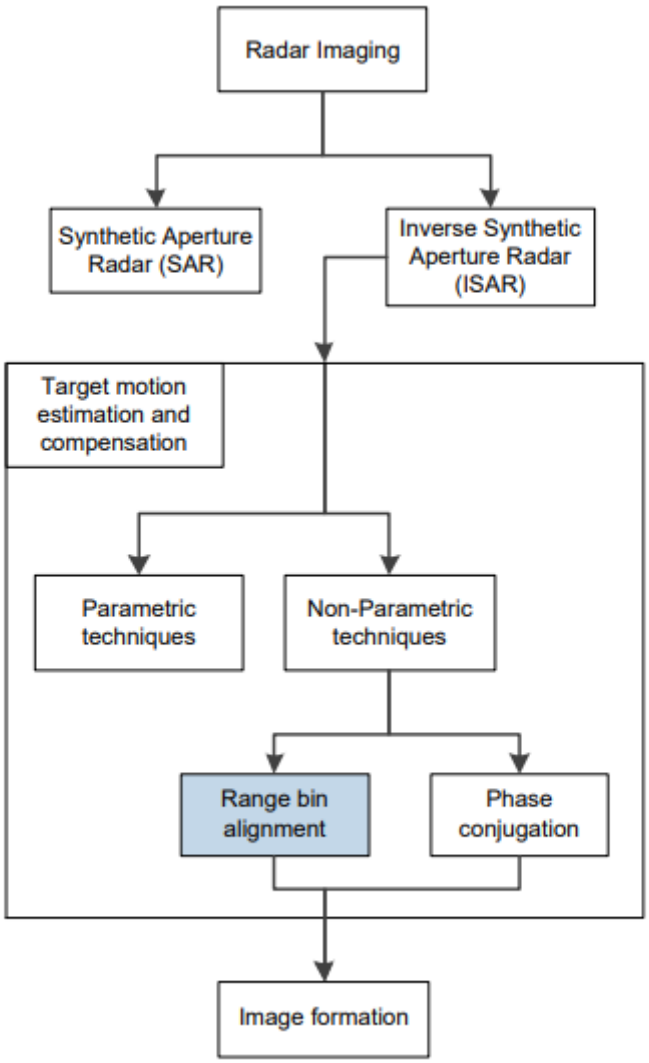

Figure 2.5 Trajectory of the research [4]

2.3.7 Synthetic Aperture Radar (SAR)

SAR involves a radar which is fixed on a moving platform, with the beams of the antenna illuminating the surface of a target. Data is acquired and subsequently processed to form a detailed SAR image. [4]

Some examples of SAR are [16] :

- Imaging of landscapes
- Detection of geological structures
- Military reconnaissance
- Ice Studies
- Oceanography

2.3.8 Inverse Synthetic Aperture Radar (ISAR)

ISAR processing is similar to SAR processing, but with ISAR, the radar remains stationary while the target is moving. Another difference between ISAR and SAR is the target's cooperativity. Fig 2.6 depicts an image of a ship with its ISAR image [18]. [4]

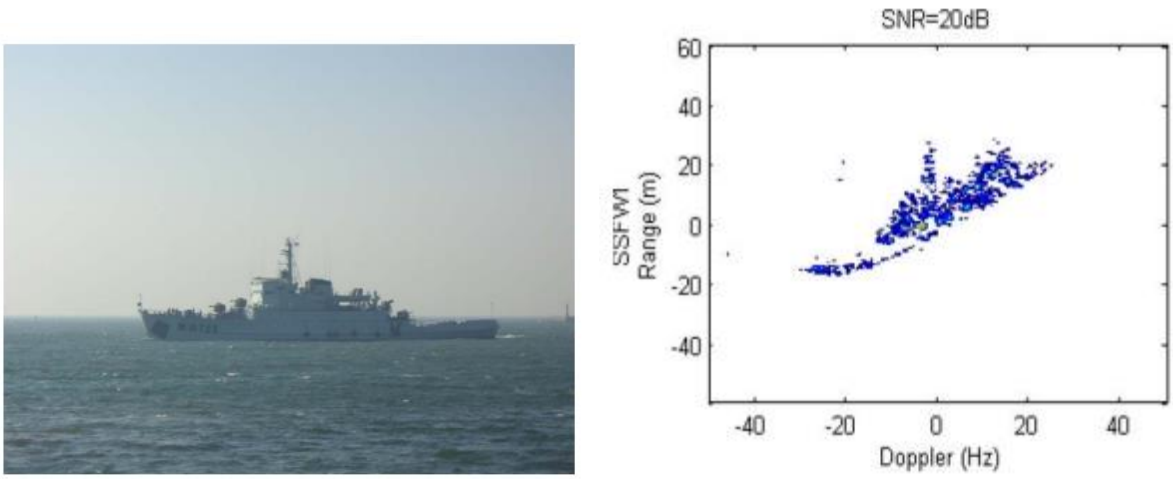

Figure 2.6 A ship with its ISAR image [18]

The cooperativity is judged by the details available regarding both translational motion as well as rotational motion. The translational motion (which blurs the ISAR image) can be determined by tracking and the rotational motion by sensors. For non-cooperative targets, the rotational motion cannot be determined. One problem found with non-cooperative targets, specifically marine vessels, is that external factors including the roll and pitch caused by waves cause undesirable movements. [4]

The rotational movement of targets relative to radars creates a synthetic aperture which is used to construct radar images. A rotation vector is formed by the roll, pitch and yaw and influences the orientation of the ISAR image. This is illustrated in Fig 2.7 by Ozdemir [19]. [4]

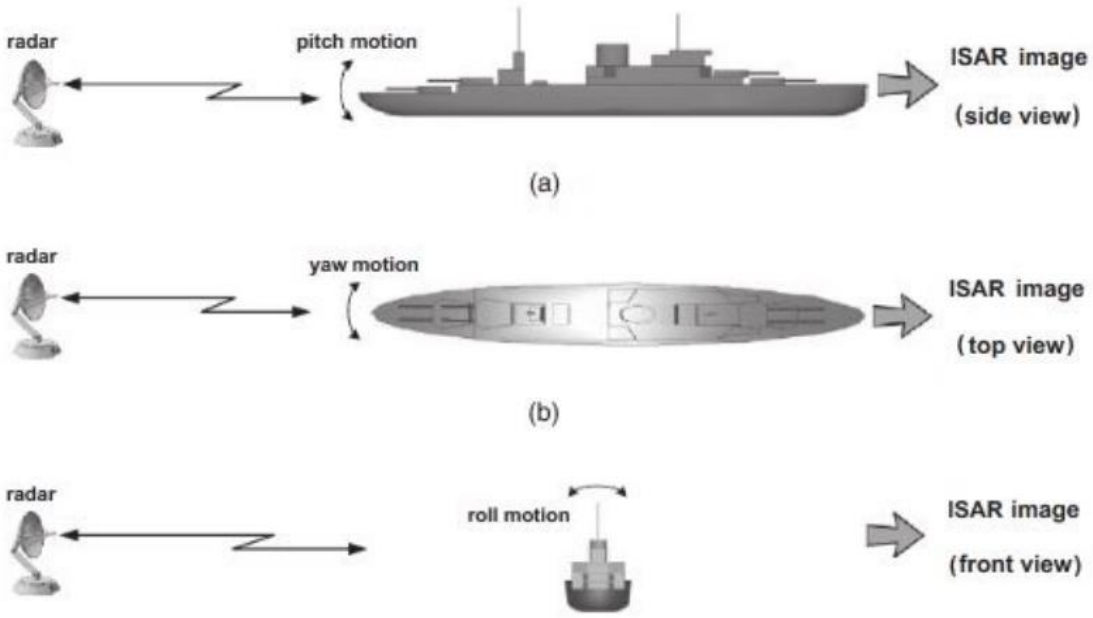

Figure 2.7 How pitch, yaw and roll affect the orientation [19]

2.3.9 Motion Compensation and Autofocus

Motion compensation techniques, as well as autofocusing techniques, have been created to determine the motion of targets as they are required to construct focussed images. The techniques are split into parametric and non-parametric categories. [4]

The target's radial motion causes misalignment of range profiles and also introduces a phase error in the scatterers. Therefore, many non-parametric motion compensation techniques consist of two steps, which are range alignment and phase conjugation [20].

2.3.10 Target Feature Extraction

Aligned high range resolution (HRR) profiles are also required for a classification known as target feature extraction. An average profile is created from aligned profiles, which results in a better SNR for improved identification. An average profile contains more distinct peaks for better feature clarity. The accuracy of the alignment is crucial as misalignment would cause peaks to spread in the average profile. [4]

2.4 Inverse Synthetic Aperture Radar Concepts

2.4.1 Detailed introduction to ISAR

For radar imagining a high resolution is required. Fine range resolution is achievable by selecting wide bandwidths. Fine cross-range resolution radar, on the other hand, requires a large antenna aperture. These large antennas are not physically realisable and therefore SAR gives a small antenna aperture the ability to synthesise a larger aperture. The cross-range resolution refers to the radar's ability to resolve scatterers in the cross-range dimension. The cross-range dimension is perpendicular to the down-range or slant-range dimension of the radar. To reiterate what was mentioned earlier, with SAR, the assumption is that the target is stationary with radar moving. Contrary, the hypothesis of the target moving while the radar remains stationary is known as ISAR. [21]

One theory suggests that relative motion depends on the location of the coordinate system. With SAR the reference system would be placed on the target and conversely, for ISAR it would be placed on the radar. This concept is shown in Fig 2.8. In the figure, a spotlight SAR configuration is converted to an ISAR one, by changing the reference system. [21]

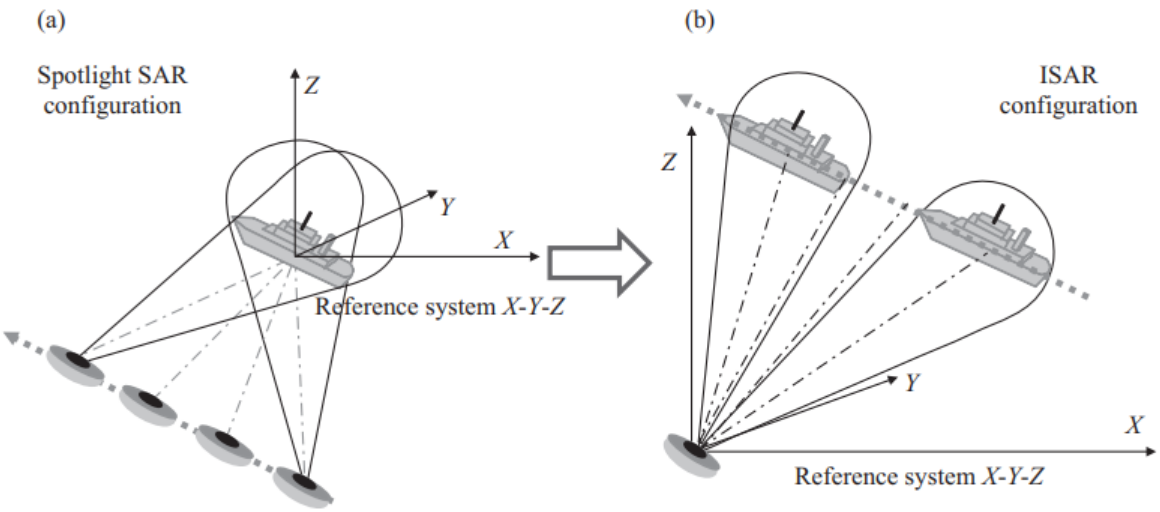

Figure 2.8 a) Spotlight SAR configuration to b) an ISAR configuration [21]

A standard motion compensation procedure is shown in Fig 2.9. The range tracking method keeps scatterers in their range bins. Doppler tracking by correcting the phase produces constant frequency shifts. Thus, after compensation (motion) the target's scatterers appear to move with a constant velocity. Cross-correlation is commonly used for range tracking. The method fins unaligned range bins and performs a range alignment with respect to a reference profile. The Doppler tracking follows using phase compensation methods. [21]

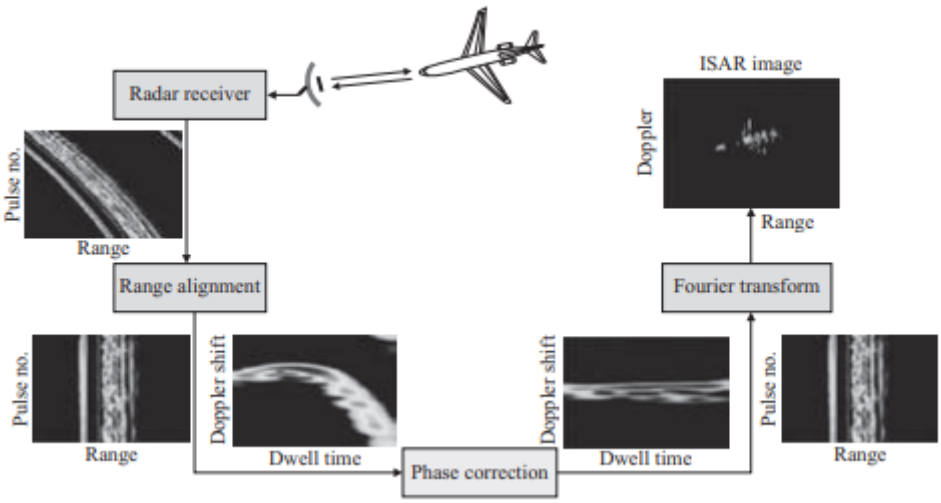

Figure 2.9 Motion compensation procedure for ISAR imaging [21]

2.4.2 Waveforms used to obtain high range resolution

To achieve high bandwidth, multifrequency signals or modulated continuous waveform signals should be used. These include stepped-frequency signals, linear frequency modulated (LFM) signals and trains of modulated pulses. For accurate Doppler frequency measurement and to avoid Doppler anomalies, the PRF should be sufficiently high. [21]

<u>LFM pulse waveform</u>

LFM (or chirp) waveforms are often used in radars. An LFM pulse waveform is one in which the carrier frequency changes linearly in a single pulse. The shape of the pulse is determined by a windowing function, such as the Gaussian window function. [21]

<u>FMCW waveform</u>

Another solution to achieve high bandwidth is the use of an FMCW waveform. These included triangular modulation and sawtooth modulation. [21]

<u>*Stepped Frequency Continuous Wave waveform*</u>

This is the waveform used in the research. It can be described as a sequence of pulses which are coherent and continuous waves, where the frequency of each pulse increases by a fixed step of Δf. Furthermore, the pulses have a fixed width and they are transmitted at a PRF.[5], [21]

A specific type of processing is done on the received signal to generate a high range resolution profile. That is, an IFFT is applied to the received echoes of N pulses to obtain one high range resolution profile.

2.4.3 Range alignment vs phase adjustment

Translational motion effects from targets can be compensated for by aligning the range profiles, which keep the returned signals of the scatterer in the same range bin. [21]

A phase adjustment process, namely fine motion compensation is used to remove phase drifts resulting from range alignment and to create linear phase functions at bins where the target is found. [21]

2.4.4 ISAR motion compensation

To reiterate what was mentioned earlier, cross-correlation can be used for range alignment. Cross-correlation is performed between a range profile and a selected reference profile. The resulting cross-correlation peak is

used to determine the number of shifts (range bin shifts) a profile is away from the reference profile. Shifting the profile back by this estimated number of bins aligns the profiles. The previous step is repeated for every range profile to align a dominant scatterer. Other algorithms include global range alignment, minimizing the entropy of an averaged range profile, and Hough transforms. [21]

2.4.5 Effect of Coherent Processing Interval Window Length (CPIWL) on ISAR images

The CPIWL value affects the ISAR images in the following way. An increase in the CPIWL increases the resolution of the image but decreases the focus. Conversely, a decrease in the CPIWL decreases the resolution but increases the focus of the image. [21]

2.5 Overview of range alignment techniques

As discussed there many range alignment techniques that have been researched and implemented. The following chapter analyses and describes these techniques, as well as highlights their strengths and weaknesses. The majority of the techniques come from work done by Van Rensburg [4].

2.5.1 Peak alignment

This technique works under the assumption that there is a dominant scatterer in the data which is then used as a reference for alignment. The algorithm aligns the peak of profiles adjacent to each other to form aligned profiles. The peak represents the return gathered from a dominant scatterer. [4]

It is the simplest range alignment technique and requires minimal effort for implementation. Misalignment is still apparent in this technique due to unrealistic assumptions. The first unrealistic assumption is that there is a single dominant scatterer in the data and the second is that the largest amplitude returned is a representation of the dominant scatterer. Target fluctuations can thus cause misalignment. Furthermore, the dominant scatterer returns an apparent vibration, which is caused by restricting the range bin shifts to being integers. The target's return sits between two range bins and this can lead to the returns folding over to appear as a vibration. Interpolating the shifts required to sub-integer values can mitigate this problem. [4]

2.5.2 Envelope correlation

The next technique to be discussed is the envelope correlation technique. This is widely used for range bin alignment. It works by finding the number of shifts, τ, which is required to achieve the maximum cross-correlation between a profile to be aligned, denoted P_m, and a reference profile, denoted R_m. [4]

The cross correlation, given by X_m, which is a result of P_m being shifted by a varying τ_m, is calculated by Equation 2.6 [9].

$$X_m(\tau_m) = \sum_{n=1}^{N} R_m(n).P_m(n-\tau_m) \tag{2.6}$$

The technique is manipulated as follows:

Correlation of adjacent profiles

With this version, $\hat{P}_{m-1}$ replaces R_m in Equation 2.6, indicating that the reference profile is the previously aligned profile. This gives rise to Equation 2.7. [4]

$$X_m(\tau_m) = \sum_{n=1}^{N} \hat{P}_{m-1}(n).P_m(n-\tau_m) \tag{2.7}$$

The cross correlation is calculated for each profile. The bin shift which produces the highest cross correlation is used to align the m profiles. For now, only integer bin shifts are considered. [4]

This method is considered more accurate than the peak alignment and presents an improved smoothness. A problem relating to this technique arises from using preceding aligned profiles as references. This is a propagating error embedded in the alignment vector throughout the entire aligned data. [4]

Non-coherent averaging of profiles to create a reference profile

This technique uses the non-coherent average of all the aligned profile envelopes, preceding the profile to be aligned, as the reference profile for cross correlation. Using the non-coherent average is simpler than exponentially weighted averages, which is discussed later. [4]

The reference profile denoted as R_m, is defined in Equation 2.8, where *m* is the profile number and *n* is the range bin number [9].

$$R_m(n) = \frac{\sum_{i=1}^{m} \hat{P}_i(n)}{m} \tag{2.8}$$

Exponentially weighted reference profile

This technique is similar to the previous non-coherent averaging technique. However, this time exponential weighting is used to create an average reference profile. A moving filter, given by Equation 2.9 is used to explain the technique. In the equation, W_m is the filter weight, γ_m is the filter gain and *k* is the exponential factor between 0 and 1. Recall, that *m* is the profile number.

$$W_m = k\gamma_m + (1-k)W_{m-1} \tag{2.9}$$

The changing filter weights are applied to the different profiles to diminish the effect of previous older profiles on the determined reference profile. The reference profile, R_m, is given by Equation 2.10.

$$R_m(n) = \frac{\sum_{i=1}^{m} W_i.\hat{P}_i(n)}{m} \tag{2.10}$$

Sliding window averaging

Due to data possibly having changing characteristics, the window length of the previously measured filter can greatly affect the alignment. Therefore, a sliding window is implemented to mitigate the effects of data with changing characteristics. A parametric sweep can be done to find the ideal window. [4]

Improved alignment, particularly of later profiles is apparent, compared to the previous techniques. This is confirmed by Van Rensburg [4]. The alignment is degraded by vibration as a result of using integer bin shifts. [4]

2.5.3 The spectral domain phase difference

This method described in Chen [22], relies on a few assumptions:

- A constant phase change between profiles.
- A negligible phase variation due to changes in aspect angle.

- The dominant scatterer's range bin migration is less than a single bin per profile [23].

The steps to implement this method are as follows [4]:
1. For each profile, estimate the phase of its Fourier transform.
2. Calculate the difference in phase of profiles adjacent to each other.
3. Calculate the magnitude of the Inverse Fourier Transform (IFT) of the determined phase difference.
4. The peak magnitude's location determined in step 3 indicates the required range bin shift for alignment.

When the assumptions hold, the technique proves to be very useful. In Van Rensburg's work [4], high-velocity targets are considered, which cause many range bin shifts for each profile. Therefore, the technique did not result in satisfactory range alignment. [4]

2.5.4 Minimum entropy of the average range profile

The technique is similar to the cross-correlation techniques. The only difference is that the cost function of this method is the entropy, H_m, as opposed to the cross correlation, X_m, used earlier. H_m is described by Equation 2.11.[4]

$$H_m(\tau_m) = -\sum_{n=1}^{N} R_m(n, \tau_m)\, ln\, R_m(n, \tau_m) \tag{2.11}$$

According to Xi [24], this technique produces fewer errors due to scintillation effects than the correlation methods. In Van Rensburg's study [4], a degradation of alignment is seen, particularly in the profiles towards the end of the data. This is due to averaging over many profiles and "smoothening" the reference.

With the entropy as the cost function, the algorithms mentioned earlier are adapted to include this change. These include the adjacent reference profile method, the non-coherent averaging of the aligned profiles as a reference profile method, and the sliding window averaging method. [4]

2.5.5 Sub-integer range bin alignment

This alignment method, implemented by Munoz-Ferreras and Perez-Matinez [9], is argued to produce better range alignment than the previously discussed techniques (as well as the Global method which is discussed next) in that particular study. The research was done on both simulated and real data. [4]

Robustness against target fluctuations, noise, error accumulation and vibration effects, is apparent. The cross-correlation, $X(\tau_m)$, is calculated by using a reference profile, R_m, as described by Equation 2.12. [9]

$$R_m(n) = \frac{m}{m+1}\, R_{m-1}(n) + \frac{1}{m+1} P_m(n) \tag{2.12}$$

To acquire sub-integer shifts, the method uses a multiplication in the frequency domain, with a phase ramp. The Fourier transform's shift property produces $P_m(n - \tau_m)$, the shifted profile, described by Equation 2.13. The Fourier transform is approximated by the FFT. [4]

$$P_m(n - \tau_m) = IFFT\{e^{j\left(\frac{2\pi}{N}\right)\tau_m n}\, FFT\{P_m(n)\}\} \tag{2.13}$$

In Equation 2.13, *n* is a vector $[0,1 \ldots, \mathrm{N}-1]^T$ and *N* is the total number of bins for each profile.

The optimal shift, $\hat{\tau}_m$, relates to the τ_m which produces the highest cross-correlation. The optimal shift is used in Equation 2.14 to create the aligned profile, $\hat{P}_m$. [4]

$$\hat{P}_m(n) = P_m(n - \hat{\tau}_m) \tag{2.14}$$

The steps followed in the algorithm are presented in Appendix A.

Claims of improved robustness in [9], are justified as there is no limiting of the allowed range bin shifts between profiles. However, this could also result in undesirable results as the algorithm could lock on to the wrong scatterers. Moreover, in [4] it is evident that degradation of alignment occurs in the later profiles. This is due to the validity of the reference profile being compromised. The reference profile should sufficiently represent profiles which are close to the profile to be aligned. However, this is not the case when averaging profiles. A solution to this could be to use a sliding window. [4]

Another implementation for sub-integer shifts is using Haywood's ISAR motion compensation algorithm [25] as discussed in [5]. The algorithm consists of three stages, namely radial motion compensation, adaptive beamforming and doppler processing. The sub-integer shifts or delays are fitted to the HRR profiles by multiplying them, element-wise, by a phase shift vector in the frequency domain. [5] A more mathematical definition for Haywood's algorithm is found in Appendix A.

2.5.6 Hough transform

The Hough transform is a technique which uses feature extraction. It is used in computer vision as well as digital image processing and image analysis. The technique's objective is to identify imperfect instances of targets within a class. Filtered data is usually obtained by discarding data which is smaller than a selected threshold of the peak in an image. [4]

As stated in [4], the Hough Transform technique has improved alignment performance in an environment with a high clutter, as opposed to cross-correlation methods. This makes it ideal for applications such as surface movement control (E.g at airport terminals). [4]

Due to mismatches between the radial velocity and the real velocity of a target, misalignments can occur. [4]

2.5.7 Global Method

The global range alignment method is an optimization algorithm designed to align profiles in a way that maximises the contrast, *C*, of the sum envelope. The contrast *C* is given by Equation 2.15, where *S(n)* is the sum envelope, *n* is the profile number, and *N* is the total profiles. [4], [17]

$$C = \sum_{n=0}^{N-1} S(n)^2 \tag{2.15}$$

The sum envelope is calculated for changing shifts which are applied to the present profile. The contrast determines if the iterations are causing an enhancement or degradation of the range alignment. A better contrast signifies a more enhanced alignment and vice versa. [4]

The steps are determined by using the contrast history throughout all of the iterations. A polynomial model is used to calculate the required shifts for range bin alignment. A flow diagram of the technique is presented in Appendix B. [4]

The technique in [4] has significant computational efficiency as opposed to the original global alignment method in Wang's work [17].

2.5.8 Other range alignment techniques

Scatter-point referencing is another technique used for ranged alignment and is worth mentioning. [26]

2.6 Quality measures of alignment techniques

The following chapter presents techniques used to quantify the effectiveness of the alignment algorithms of chapter 2.5. These measures of performance are essential for validating the research done and assessing the quality of the work. The measure to be described are as follows:

- Sum Envelope Contrast
- Sum Envelope Entropy
- Global Envelope Correlation
- The variance of the peak location
- Mean squared envelope difference
- Burst Derivative

2.6.1 Sum Envelope Contrast

The Sum envelope *S* is given by Equation 2.16, where *n* is the range bin number and *m* is the profile's number. Furthermore, M is the total number of profiles and *p(m,n)* is denoted as the amplitude sample in the nth range bin of the mth range profile. [17]

$$S(n) = \sum_{m=1}^{M} |p(m,n)| \tag{2.16}$$

The first measure to be discussed is the sum envelope contrast technique. The sum envelope contrast is described by Equation 2.17 [17].

$$C = \sum_{n=1}^{N} S(n)^2 \tag{2.17}$$

It is evident that using a dataset with more range bins will result in a higher contrast value. This will lead to incorrectly favouring these datasets. Therefore, the contrast is divided by the number of range bins to avoid this error. [4]

For readability, the contrast value is converted to decibels (dB) using Equation 2.18.

$$C\ in\ dB = 10.\log_{10}(C) \tag{2.18}$$

2.6.2 Sum Envelope Entropy

The entropy relates to the standard deviation (fluctuation) as a result of the misalignment between the range profiles. Larger standard deviations indicate that there is a lower probability of determining the position of

dominant scatterers based on where the peaks are. Conversely, a lower standard deviation indicates a better probability of estimating the position of scatterers. [4]

To showcase the effect that the standard deviation has on the entropy value, a Sinc function with various widths is presented in Fig 2.10 [4]

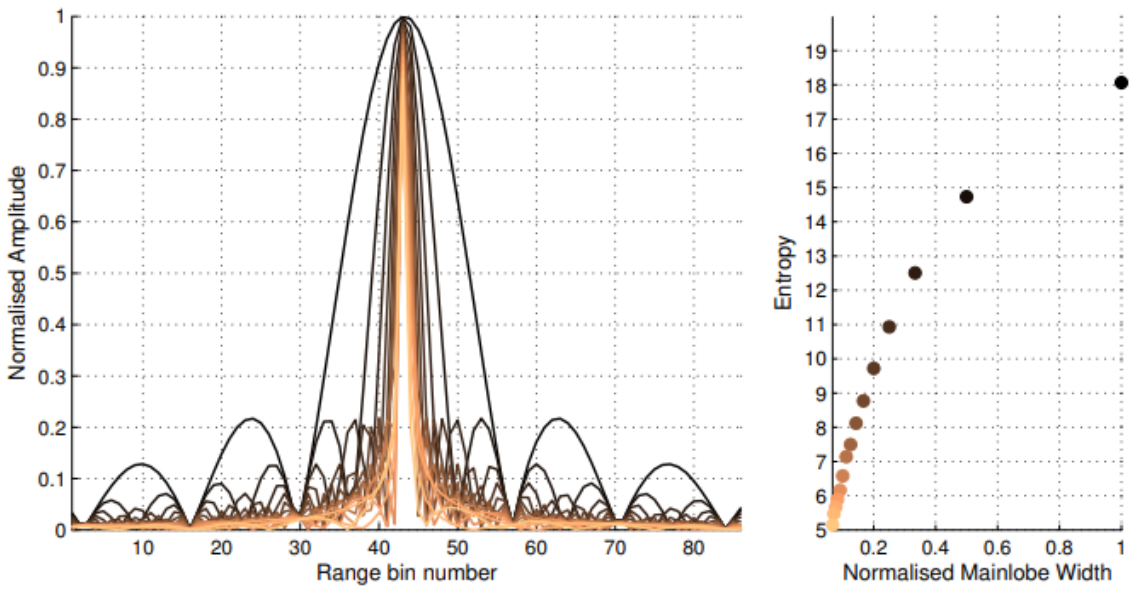

Figure 2.10 Effect of standard deviation on the entropy value [4]

When using the sum envelope for the calculation, the misalignment between profiles causes the standard deviation of the average profile to increase, therefore increasing the uncertainty of the scatterers' position. This leads to increased entropy. Fig 2.11 illustrates this concept by using a shifted copy of a Sinc function, to calculate the sum envelope as well as the entropy. [4]

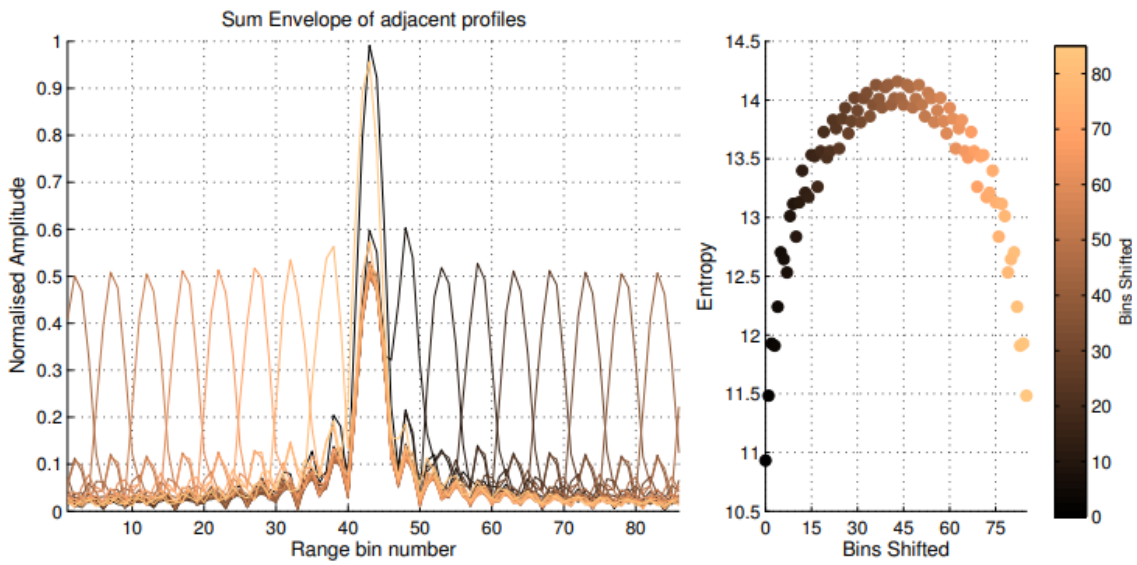

Figure 2.11 Using a shifted Sinc function to highlight the influence of misalignment [4]

The sum entropy, *H*, is calculated using Equation 2.19. [4] The derivation for Equation 2.19 can be found in Appendix C.

$$H = -\sum_{n=1}^{N} S(n) \ln S(n) \tag{2.19}$$

Similarly to the contrast value in the previous section, the entropy value needs to be dived by the number of range bins, *N*. This normalisation will prevent favouring datasets with more range bins. [4]
Using Equation 2.18, and replacing *C* with *H*, the entropy in dB can be calculated.

2.6.3 Global Envelope Correlation

A commonly used cost function for range alignment techniques is correlation. The global envelope correlation method is described by Wang [17] as per Equation 2.20. In the equation, $X(m,l)$ is the envelope correlation of the profiles m and l described in Equation 2.21. $\emptyset(m,l)$ is a weighting function given by Equation 2.22. [4]

$$G = \sum_{m=1}^{M-1} \sum_{l=m+1}^{M} \emptyset(m,l) X(m,l) \tag{2.20}$$

$$X(m,l) = \sum_{n=1}^{N} |p(m,n)||p(l,n)| \tag{2.21}$$

$$\emptyset(m,l) = \exp\left[-\left(\frac{l-m}{\delta}\right)^2\right] \tag{2.22}$$

In Wang [17], it is unclear whether δ is fixed for the entire operation or not. Van Rensburg [4] assumes it to be fixed.

2.6.4 The variance of the peak location

In an ideal scenario, the location of dominant scatterers in aligned profiles should be zero. The variance quality measure is used under two assumptions: [4]

a) The data has one dominant scatterer
b) The scatterers return is always the peak return

The method could be described as the cost function for the peak alignment algorithm. Equation 2.23 describes the peak location variance, $v(n_p)$. [4]

$$v[n_p(m)] = \frac{1}{M} \sum_{m=0}^{M-1} n_p(m)^2 - \left[\frac{1}{M} \sum_{m=0}^{M-1} n_p(m)\right]^2 \tag{2.23}$$

Target fluctuations effects can adversely affect the validity of this quality measure. However, it can still be used. [4]

2.6.5 Mean squared envelope difference

This measure is based on the fact that two perfectly aligned identical profiles should have an envelope difference of zero across all range bins. Misalignment or amplitude deviations between profiles that are next to each other will increase the mean squared difference. The mean squared envelope difference, *D*, is calculated by Equation 2.24. [4]

$$D = \left[\sum_{n=1}^{N} \sum_{m=2}^{M} (p_{m-1,n} - p_{m,n})^2\right]^{1/2} \tag{2.24}$$

The measure is susceptible to producing incorrect results when anomalies, like target fluctuations, are present. [4]

2.6.6 Burst Derivative

The burst derivative is determined by using the reflectivity of the target in the frequency domain, thereby eliminating the IFFT required in Image contrast Based Autofocus and Image entropy Based Autofocus. This results in increased computational efficiency. The approach was first presented by Bocker and Jones [27] and further analysed in Son [23]. [4]

The burst derivative is given by Equation 2.25 as follows: [27]

$$B(\hat{v},\hat{a},\hat{j}\,) = \sum_{n=0}^{N-1}\sum_{m=0}^{M-1} \left|\frac{\partial}{\partial \mathrm{m}}\hat{P}(m,n;\hat{v},\hat{a},\hat{j})\right| \tag{2.25}$$

In the equation, $\hat{P}(m,n;\hat{v},\hat{a},\hat{j})$ is the sample which is compensated. This is in n^{th} range bin of the mth profile. The radial velocity is given by $\hat{v}$, the acceleration by $\hat{a}$ and the jerk by $\hat{j}$. [4]

2.7 Critical Literature Survey

2.7.1 Strengths and weaknesses of the literature

The literature discussed in this chapter provided an extensive understanding of the concepts of radar and its processing. This information is sufficient for comprehension of the specific objective of the report, that is, range alignment for ISAR imaging. The literature in the discussion here refers mainly to the textbooks [21] and [13].

Furthermore, the literature, especially by Van Rensburg [4], has presented an adequate amount of range alignment algorithms. The functionality of the algorithms as well as their derivations are explicitly explored. Furthermore, the strengths and weaknesses of these algorithms are clear and concise.

The above paragraph can be said for the alignment measures as well. In Van Rensburg's work [4] as well as in Wang's [17], the range alignment quality measurement algorithms are clearly explained.

Weaknesses in the literature include a lack of clearly defined processing steps to clarify how the algorithms and quality measures were implemented to ensure the validity of the given results. This is particularly for Van Rensburg [4] and Zyweck [5].

2.7.2 Gaps in the literature and topics out of the scope

A gap in the literature is that when a new range alignment algorithm is published, results are typically shown for a single radar dataset. Little or no literature exists where multiple range algorithms are applied to different datasets to assess the algorithm's robustness and to report on both quantitative measures as well as qualitative measures.

Another gap is that the literature has a lack of agreement on a suitable criterion that should be used to assess the performance of range alignment algorithms. Although the quality measures are presented, a concrete criteria hierarchy is not evident.

2.7.3 Link to Objectives

With the range alignment algorithms in the literature reviewed, the report can continue by showing the implementation of some of these algorithms on measured datasets. More specifically, the algorithms were implemented on different datasets and the performance was compared. This covered the first gap in the literature. Next, the range alignment measures were implemented and adapted to suit the different datasets used, and criteria for best performance were developed, to fill in the second gap in the research.

2.8 Conclusion

The literature review covered major topics that are essential to system design. Relevant theories are discussed as well as current implementations in the industry. Furthermore, research into the topics was analysed. Topics included radar concepts, radar signal processing concepts, ISAR concepts, range alignment techniques, and quality measurement techniques. A major gap in the review is due to the range alignment techniques not being compared using a variety of datasets.

3. Methodology

3.1 Overview

This chapter gives an overview of the plan of action for the project. First, the measured datasets used in the project are looked at. Next, the range alignment algorithms that were implemented in the project are identified. Subsequently, the quality measures used are stated. The penultimate discussion relates to the testing of the range algorithms on different blocks of data. Finally, the plots used in the report are described.

3.2 The Measured datasets and loading them into MATLAB

Two datasets were used to carry out the project. The first is known as the "Spanish Dataset" and the second as the "CSIR" dataset. Both datasets relate to maritime vessels. The Spanish dataset is smaller and tends to be better for testing and reliability as opposed to the CSIR dataset. These datasets are discussed in more detail below.

3.2.1 *Spanish Dataset*

An image of this maritime vessel is shown in Fig 3.1. The ship is known as the Altera Vessel and its data is the same used in Munoz-Ferreras and Perez-Martinez [28]. The dataset consists of 636 profiles, each with 601 range bins.

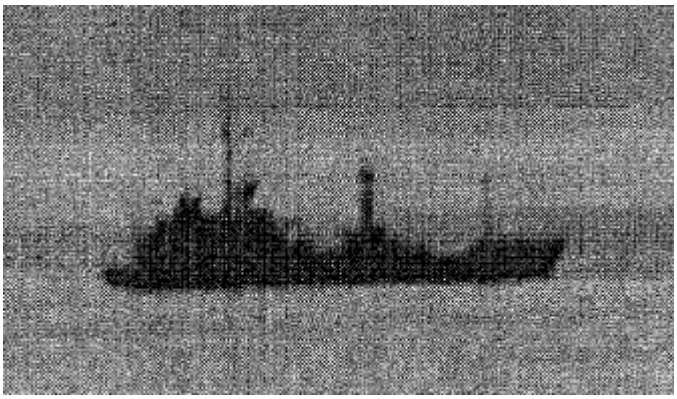

Figure 3.1 Image of the Altera vessel [28]

The radar used to gather the data of the vessel was a millimetre-wave Linear Frequency Modulated Continuous Waveform (LFMCW) radar. The parameters of the radar are shown in Table 3.1 while Fig 3.2 depicts the transmitted ramp waveform. [28]

Table 3.1 Radar parameters

Parameter	Value
Central frequency (f_0)	28.5 GHz
Bandwidth (∇f)	1 GHz
PRF	500 Hz
β	0.2 ms

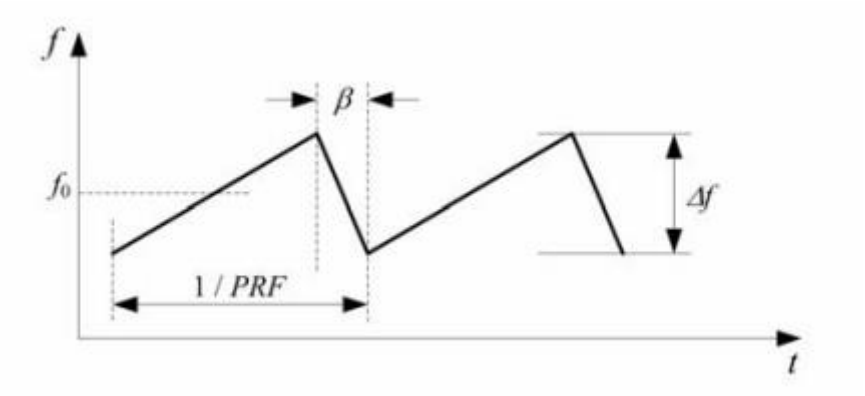

Figure 3.2 Transmitted waveform

Choosing a good length of data to analyse is important. This is done as follows where the CPI is chosen to be approximately 0.5s justified by the literature in Martorella [3] and Abdul Gaffar [8] :

$$Length\ of\ profiles = PRF * CPI$$
$$Length\ of\ profiles = 500Hz * 0.5s$$
$$Length\ of\ profiles = 250$$

To make the profile length a factor of two the following operation is done:

$$2^x = 250$$
$$x = 7.97\ (nearest\ integer\ is\ 8)$$
$$Length\ of\ profiles = 2^8 = 256\ (closest\ power\ of\ 2)$$

This dataset is generally used for testing purposes and is therefore used first, before moving onto the CSIR dataset.

3.2.2 CSIR Dataset

An image of this maritime vessel is shown in Fig 3.3. The ship is known as the Zayaan Vessel and its data is the same used in Abdul Gaffar et al [29]. The commercial fishing boat is 9m in length, and 3m in width and has a mast with height [3.5m 7m]. The dataset consists of 4473 profiles each with 96 range bins. [29]

Figure 3.3 Image of the Zayaan Vessel

The radar used to gather the data of the vessel was an experimental X-band Pulse-Doppler radar. The parameters of the radar are shown in Table 3.2. Stepped frequency waveforms were used to obtain high range resolution profiles (HRR profiles). [29]

Table 3.2 Parameters of the X-band radar

Parameter	Value
Central frequency (f_0)	~10 GHz
Bandwidth (∇f)	10 MHz
PRF	175 Hz

Once more, choosing a good length of data to analyse is important. This is done as follows where the CPI is chosen to be approximately 0.5s, again justified by Martorella [3] and Abdul Gaffar [8] :

$$Length\ of\ profiles = PRF * CPI$$
$$Length\ of\ profiles = 175Hz * 0.5s$$
$$Length\ of\ profiles = 87.5$$

To make the profile length a factor of two the following operation is done:

$$2^x = 87.5$$
$$x = 6.45\ (nearest\ integer\ is\ 6)$$
$$Length\ of\ profiles = 2^6 = 64\ (closest\ power\ of\ 2)$$

The interval chosen, where this length of profiles is used, affects the results of the algorithms. This is due to certain blocks of profiles being better than others. Also, wrapping of the profiles is evident in certain profile blocks. This is depicted in Fig 3.4, where the interval [900 964] is chosen.

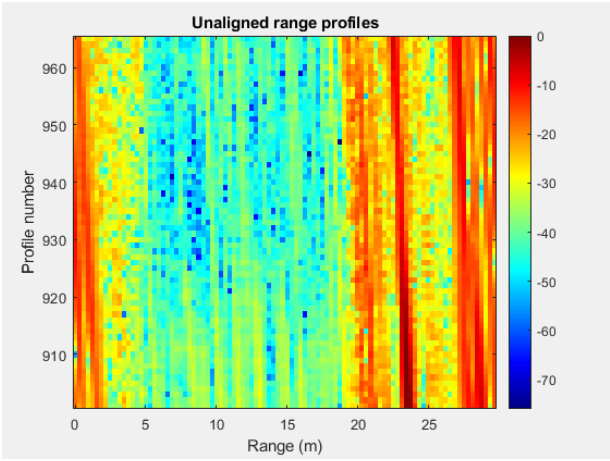

Figure 3.4 Wrapping of profiles [900 964]

3.3 Method for integer shift range alignment algorithms

The simulations and implementations of these algorithms as well as those in chapter 3.4, were performed on ***MATLAB R2021a***.

First, the integer shift envelope correlation algorithms were used. These are the simplest to implement apart from the peak alignment. The peak alignment, although simpler, would result in worse results.

The first algorithm implemented was the Single reference profile (envelope correlation method). This method is simple to implement. A single reference profile is chosen which is used in aligning every other unaligned profile.

The next algorithm used was the Adjacent reference profile envelope correlation algorithm. This algorithm is an improvement on the previous one as the reference profile is continually changed. This means that when aligning a profile, the preceding profile which had just been aligned is used, making the reference profile as updated as it can be.

Next, the Non-coherent Cumulative Average Reference Profile (envelope correlation) alignment algorithm was implemented. Using an average of all the aligned profiles preceding a profile to be aligned is advantageous in that errors produced by a minority of profiles will be filtered out. Therefore, an improvement in this regard was expected over the previous algorithm.

Lastly, the Sliding-Window Average reference profile (envelope correlation) alignment algorithm was used. This algorithm refines the previously discussed one. Here instead of using the average of all preceding algorithms, a sliding window is used where only a select amount of previously aligned profiles are used. In this way, the average unaligned profile is more up to date and the chance of error propagation is reduced.

3.4 Method for sub-integer shift range alignment algorithms

This method is similar to the above methods for the integer shift algorithms. The range alignment algorithms take place in the same order as in chapter 3.3 with the only difference being that the sub-integer versions of the algorithms are used. The order is as follows:

1. Single reference profile (envelope correlation method) alignment algorithm [Sub-integer shift]
2. Adjacent reference profile (envelope correlation) alignment algorithm [Sub-integer shift]
3. Non-coherent Cumulative Average Reference Profile (envelope correlation) alignment algorithm [Sub-integer shift]
4. Sliding-Window Average reference profile (envelope correlation) alignment algorithm [Sub-integer shift]

For the sub-integer shift algorithms to be used their counterpart integer shift algorithms were first implemented to calculate the shifts required for each algorithm. With the shifts required per profile determined for all the profiles, a low order polynomial curve was fitted to the set of integer shifts. This resulted in a set of sub-integer shifts for every profile. The previously aligned profiles (by integer shift methods) were once more “aligned” but now using the sub-integer shifts.

3.5 Method for the quality measures

The two quality measures that were explored are the contrast [4] and the entropy [4], [17]. These measures were chosen for both their simplicity and reliability. They are also well detailed in the literature and are less prone to target fluctuations as is apparent in the other methods. Although these measures can favour larger and different datasets this can be accounted for by dividing the values attained by the size of the datasets as well as normalising the data.

Before the contrast and entropy can be attained the sum envelope was calculated (using Equation 2.16) as its value was needed for both measures.

3.5.1 Contrast

Using Equation 2.17, the contrast was calculated. Here the MATLAB *sum* function was used. The value was subsequently converted to the logarithmic scale using Equation 2.18.

3.5.2 Entropy

Next, the entropy was calculated using Equation 2.19. The MATLAB *sum* function was used once more.

3.5.3 Qualitative measure

It is important to note that the range alignment algorithms were also analysed simply by looking at the HRR profiles and seeing how well they were aligned.

3.6 Testing across the different datasets

The algorithms described above were used across both the Spanish dataset as well as the CSIR dataset. The results for each algorithm are shown under the same sub-chapter. A comparison of the performance of each algorithm on the different datasets is given as well. The results include both the visual results as well as the quality measures such as the contrast and the entropy.

Within the CSIR dataset, different blocks of profiles were also compared. This is because the dataset has a large variation among different blocks of profiles.

3.7 Plotting the HRR profiles and bin shifts

Three types of plots are presented in the results. These are the HRR profile plots, the bin shift plots and lastly the quality measure comparison plots.

3.7.1 HRR profile plots

The HRR plots give a qualitative measure of how well the profiles were aligned. The plots have a stipulated range on its x-axis and the profile number on the y-axis, showing how the scatterers of each profile were distributed across the range bins. A colour bar is used to visually highlight dominant scatterers and the magnitude of the remaining scatterers. The amplitudes of the profiles were plotted using their magnitude on a logarithmic (dB) scale.

3.7.2 Bin shift plots

These figures plot the profile number against their required shift for alignment. The profile number is on the x-axis with the required bin shift on the y-axis. They usually form a staircase shape indicating profiles closer together usually were not different enough to require “integer” shifts.

With the sub-integer shift algorithms, the bin shift plots are shown with a fitted polynomial, to represent those sub-integer shifts.

3.7.3 Quality measure comparison plots

These plots are used to show how using different blocks of data (in the CSIR dataset) affects the resulting contrast and entropy. Therefore, the plots have the blocks on the x-axis and the contrast/entropy (in dB) on the y-axis.

4. Algorithm Implementations and Results

4.1 Introduction and structure of the chapter

The following chapter describes the high-level processing steps of all the discussed algorithms identified in Chapter 3. For each algorithm, the results of the implementations are shown for both measured datasets, that is, the Spanish dataset as well as the CSIR dataset. The results include the unaligned and range aligned HRR profiles plots, bin shift plots and the contrast and entropy values.

Firstly, the steps to calculate the contrast and entropy values of the HRR profiles are discussed. Thereafter, the range alignment algorithms [4] are presented in this order:

1. Single Reference Profile envelope correlation Alignment (Integer shift)
2. Adjacent Reference Profile Alignment (Integer shift) [4]
3. Non-coherent Cumulative Average Reference Profile Alignment (Integer shift) [4], [9]
4. Sliding-Window Average Reference Profile Alignment (Integer shift) [4]
5. Single Reference Profile envelope correlation Alignment (Sub-integer shift) [4], [5], [9], [25]
6. Adjacent Reference Profile Alignment (Sub-integer shift) [4], [5], [9], [25]
7. Non-coherent Cumulative Average Reference Profile Alignment (Sub-integer shift) [4], [5], [9], [25]
8. Sliding-Window Average Reference Profile Alignment (Sub-integer shift) [4], [5], [9], [20]

The structure of how each range alignment algorithm is presented in this chapter is shown in Fig 4.1.

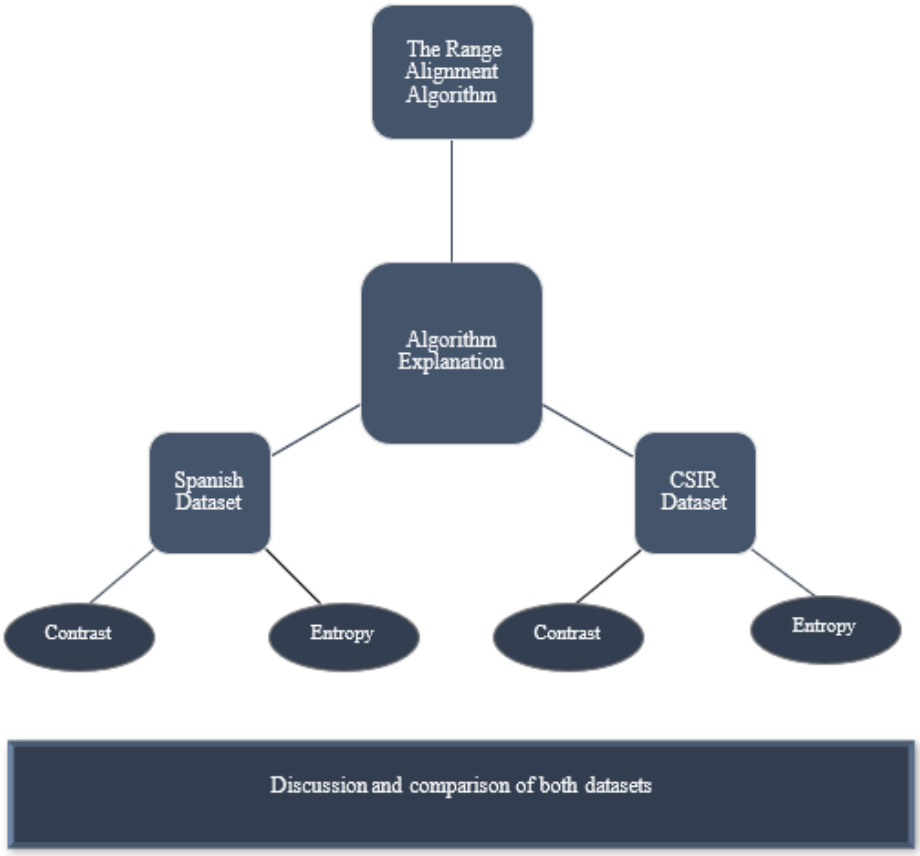

Figure 4.1 Structure of algorithm presentation

The unaligned profile plots for each dataset are shown in Fig 4.2 and Fig 4.3. The profile block 1:256 for the Spanish dataset and the profile block 1536:1599 were chosen for analysis as there was no wrapping of the profiles here. The lengths of these blocks were chosen as per the reasons in Chapter 3. The term unaligned HRR profiles refer to the radar data before any range alignment was applied.

Spanish Dataset

The HRR plot for profiles 1:256 is shown in Fig 4.2. The profiles are clearly unaligned as is evident by the linear migration of scatterers across the profiles. Furthermore, it can be seen that there exist multiple dominant scatterers indicated by the deep red coloured pixels scattered among different range bins. The qualitative measures which are the contrast and entropy are shown in Table 4.1. A higher contrast value is expected after alignment as this is indicative of a higher cross-correlation. A lower contrast was expected after alignment as this would be an indication of a lower variance between profiles.

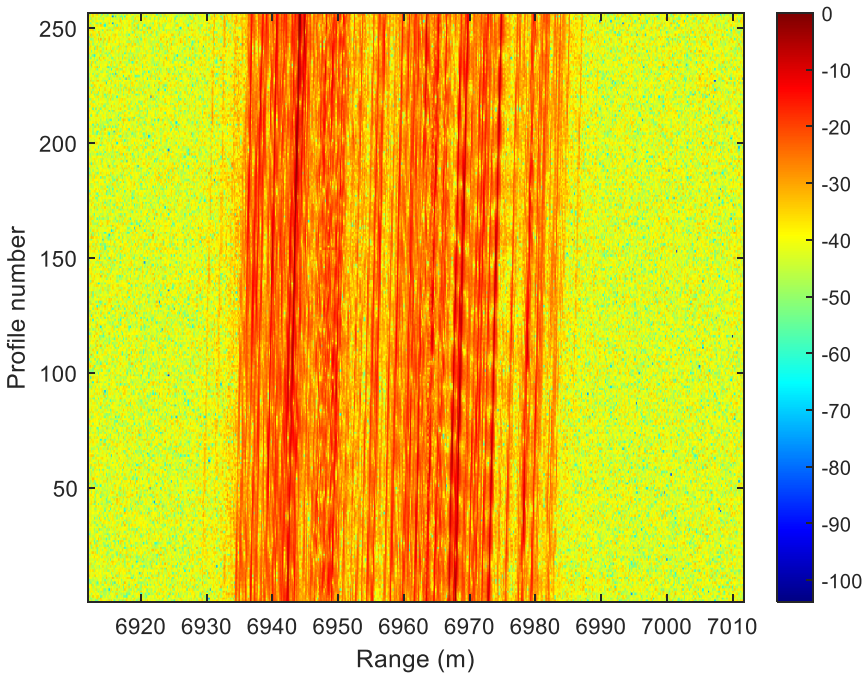

Figure 4.2 HRR unaligned profiles 1:256

Table 4.1 Table showing the contrast and entropy values in dB

Contrast (dB)	Entropy (dB)
-25.4775	-9.6308

CSIR Dataset

The HRR plot for profiles 1536:1599 is shown in Fig 4.3. Once more it is clear that the profiles are unaligned due to the linear migration of scatterers through the HRR profiles. The dominant scatterer indicated by the deep red colour does not remain in the same range bin throughout the HRR profiles. The contrast and entropy for these unaligned HRR profiles are shown in Table 4.2.

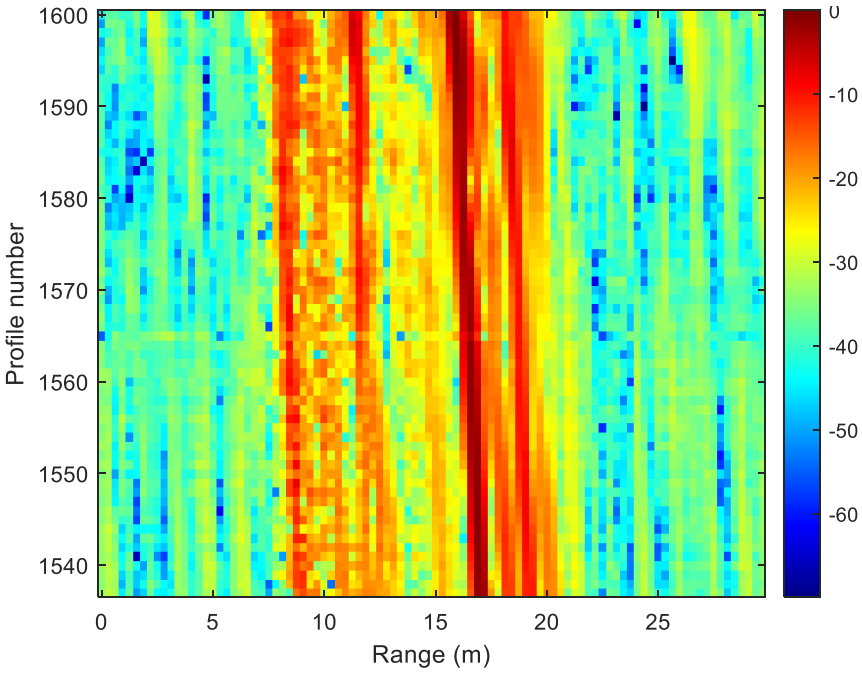

Figure 4.3 HRR unaligned profiles 1536:1599

Table 4.2 Table showing the contrast and entropy values in dB

Contrast (dB)	Entropy (dB)
-18.6563	-8.5985

4.2 Contrast and Entropy techniques

The equations used to calculate the contrast and the entropy values are discussed in this section. The first step is to calculate the sum envelope, *S(n)*, using Equation 2.16 [17]. These measures were chosen for analysis as per the reasons presented in Chapter 3.

This was implemented in MATLAB by summing up all the columns of the absolute values of the HRR profiles array. The HRR profiles consisted of a 2-dimensional array with the rows representing the profile number and the columns representing the range bins. In this way, a single row was outputted with each column being the total value of the columns of all the rows. An example code snippet is shown in Fig 4.4 for clarity. Note that the sum envelope was divided by the number of profiles for a fair comparison of the value across datasets of different sizes.

```
sum_unalign=sum(abs(HRR_profiles_normalised))/number_of_profiles;
```

Figure 4.4 Code snippet to calculate the sum envelope S(n)

With the sum envelope now available the contrast could be calculated using Equation 2.17. The column values of the single row of values (*S(n)*), were now squared and then summed up. This resulted in a single value known as the contrast. Fig 4.5 depicts an example code snippet of the algorithm. Note that the contrast was divided by the number of range bins for a fair comparison of the value across datasets of different sizes.

```
Contrast_unalign = sum(sum_unalign.^2,2)/number_of_range_bins
```

Figure 4.5 Code Snippet to calculate the contrast

Similarly, the entropy could be calculated using Equation 2.19. The column values of the single row of values (*S(n)*) were now multiplied with the logarithm (base 10) of themselves, before being summed up. The result

was multiplied by -1 and the outcome of this was a single value known as the entropy. Fig 4.6 depicts an example code snippet of the algorithm. Note that the entropy was divided by the number of range bins for a fair comparison of the value across datasets of different sizes. When profiles are aligned well, prominent peaks appear in average profiles, thus providing smaller variances. This would result in a smaller entropy value. Therefore, a smaller entropy value is an indication of better alignment. As mentioned before, both the contrast and entropy values are dependent on the data, therefore normalisation was used to fairly compare values across different datasets.

```
Entropy_unalign =-(sum(sum_unalign.*log(sum_unalign),2))/number_of_range_bins
```

Figure 4.6 Code snippet to calculate the entropy

For more readability, both the contrast and entropy values were converted to the logarithmic (dB) scale. This was done by simply taking the logarithm (base 10) of the above-calculated values, and multiplying them by 10. This was shown previously by Equation 2.18. An example code snippet is given in Fig 4.7.

```
Contrast_unalign_db=10*log10(Contrast_unalign)
Entropy_unalign_db =10*log10(Entropy_unalign)
```

Figure 4.7 Code snippet to show the conversion to dB scale

4.3 Single Reference Profile envelope correlation Alignment (Integer shift)

This is the first algorithm explored and is based on theory in [4]. This algorithm is based on the cross-correlation given by Equation 2.6. The algorithm is explained by the flow chart in Fig 4.8.

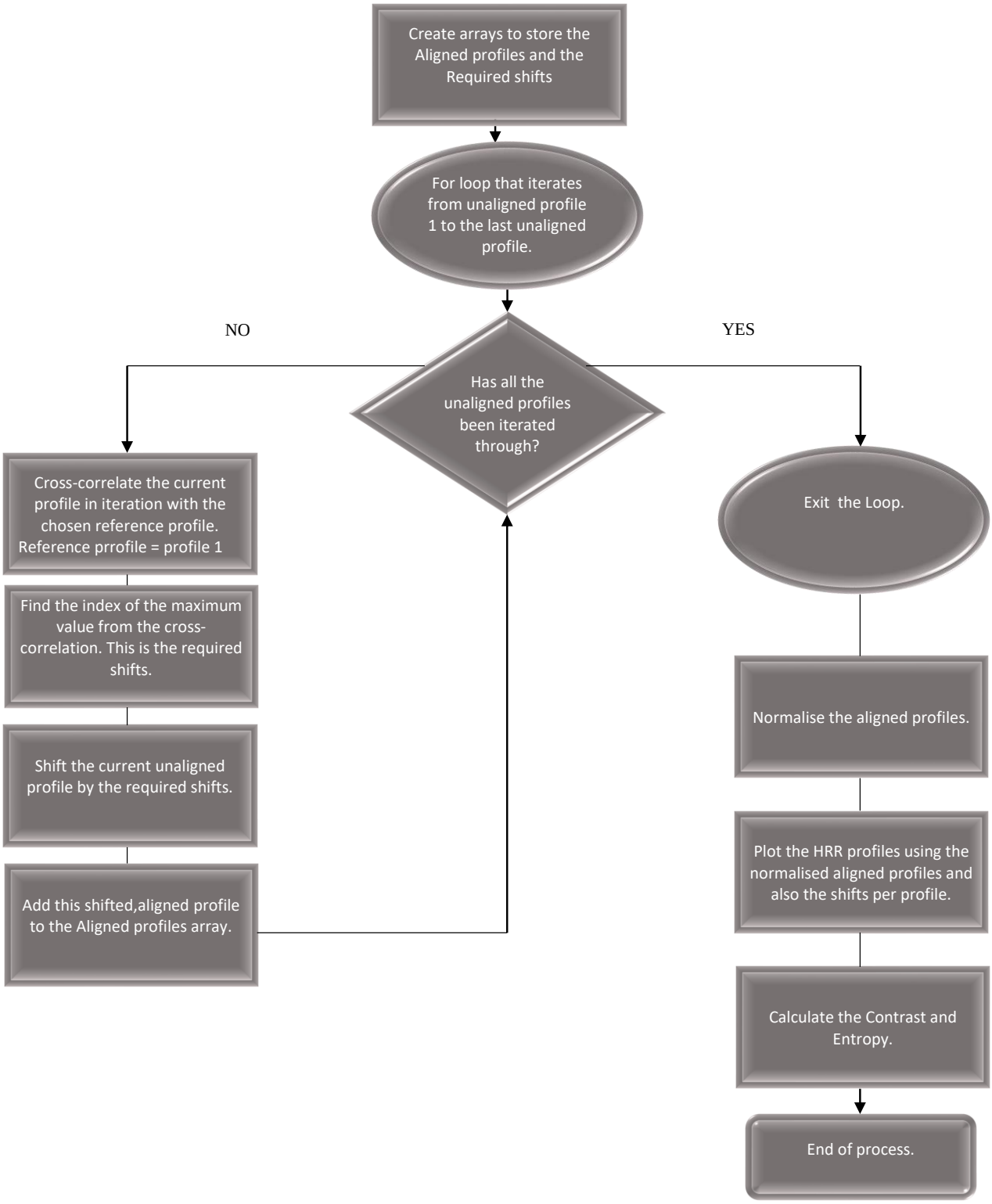

Figure 4.8 Single reference profile (integer) process

4.3.1 Spanish Dataset

The resulting range aligned HRR profiles for the Spanish Dataset are shown in Fig 4.9. Profile 1 was chosen as the reference profile, although another profile could be chosen as the reference profile. It is clear from the range aligned HRR profile plot that alignment has taken place. There is less migration of scatterers across range bins than in the unaligned HRR profiles. The integer shifts in the aligned profiles, cause the image to appear to have periodic jumps. This is due to a limitation of the technique only being able to implement integer shifts when in reality scatterers migrate by non-integer shifts from profile to profile. The qualitative measures of alignment were supported by the quantitative measures as shown in Table 4.3.

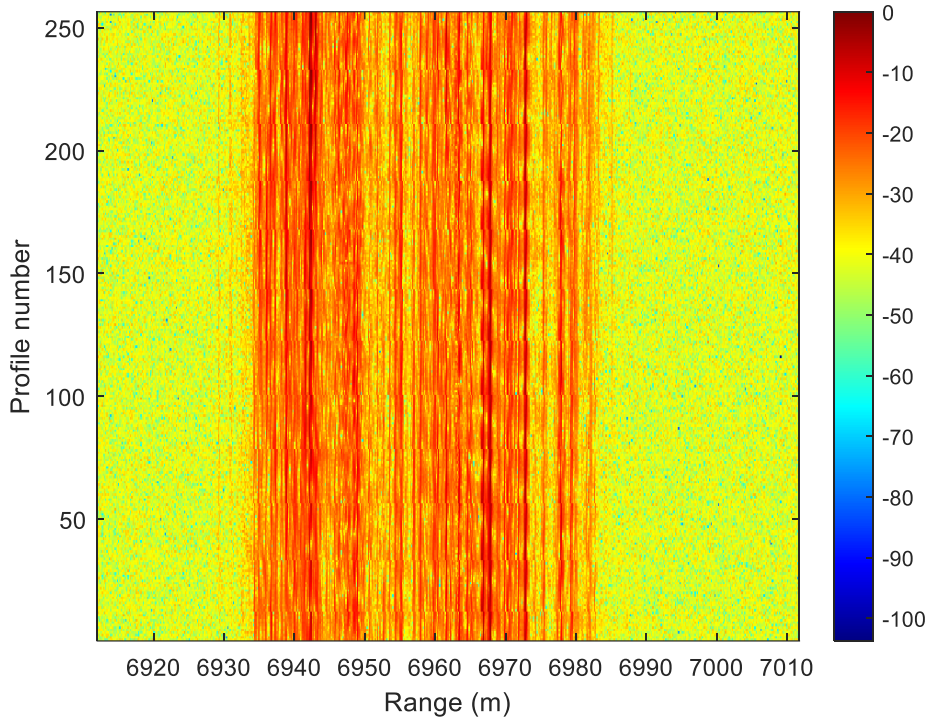

Figure 4.9 HRR profiles plot of the envelope correlation single reference profile algorithm

Table 4.3 Table showing the contrast and entropy values in dB

Contrast (dB)	Entropy (dB)
-23.7674	-9.8700

The contrast value had an increase of 6.705% when compared to the unaligned profiles. This was expected because as the dominant scatterers are aligned to the same range bin, the cross-correlation increases and this increases the sum envelope and subsequently the contrast.

The entropy value had a decrease of 2.484% when compared to the unaligned profiles. As a reminder, a smaller entropy value represents better alignment. This was expected as with all the profiles aligning to a single profile, the standard deviation would decrease.

Furthermore, the number of shifts that each unaligned profile underwent is displayed in Fig 4.10. The staircase shape was expected since profiles closer together require the same number of integer shifts as they are similar. Also, the steps relate to the jumps in integer shift values seen in the HRR profiles plot.

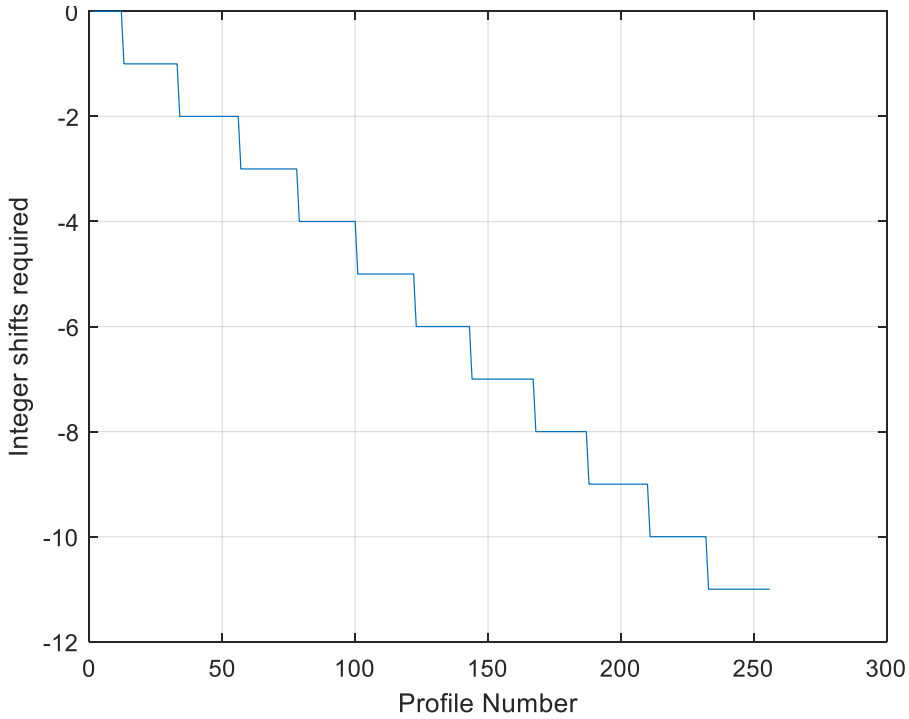

Figure 4.10 Plot of the bin shifts per profile for alignment

4.3.2 CSIR Dataset

The resulting range aligned HRR profiles for the CSIR Dataset are shown in Fig 4.11. Again, Profile 1 was chosen as the reference profile. It is clear from the HRR profiles plot, that alignment has taken place. In this dataset as well, there was less migration of scatterers across range bins than in the unaligned HRR profiles. Again, the qualitative measures of alignment were supported by the quantitative measures as shown in Table 4.3.

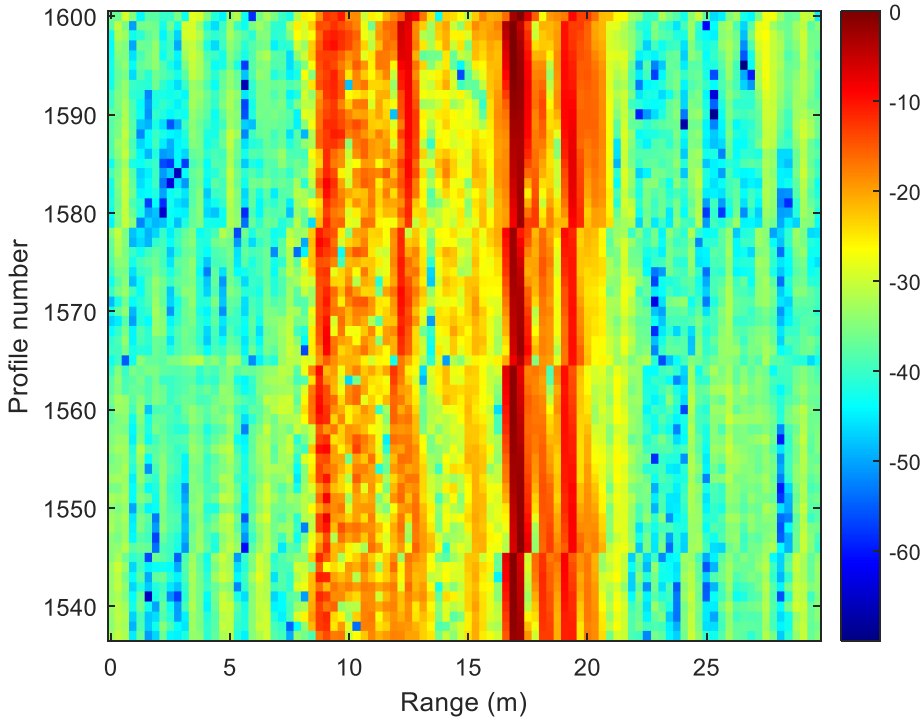

Figure 4.11 HRR profiles plot of the envelope correlation single reference profile algorithm

Table 4.4 Table showing the contrast and entropy values in dB

Contrast (dB)	Entropy (dB)
-17.5035	-8.8335

The contrast value had an increase of 6.179% when compared to the unaligned profiles. This was expected, as aligned dominant scatterers increase the contrast.

The entropy value had a decrease of 2.733% when compared to the unaligned profiles. This was desirable and indicates less variation among the profiles.

The number of shifts that each unaligned profile underwent is displayed in Fig 4.10. The staircase shape was expected since profiles closer together require the same number of integer shifts as they are similar. Moreover, the increased plateaus are due to a smaller block of profiles (64) used as compared to the Spanish dataset.

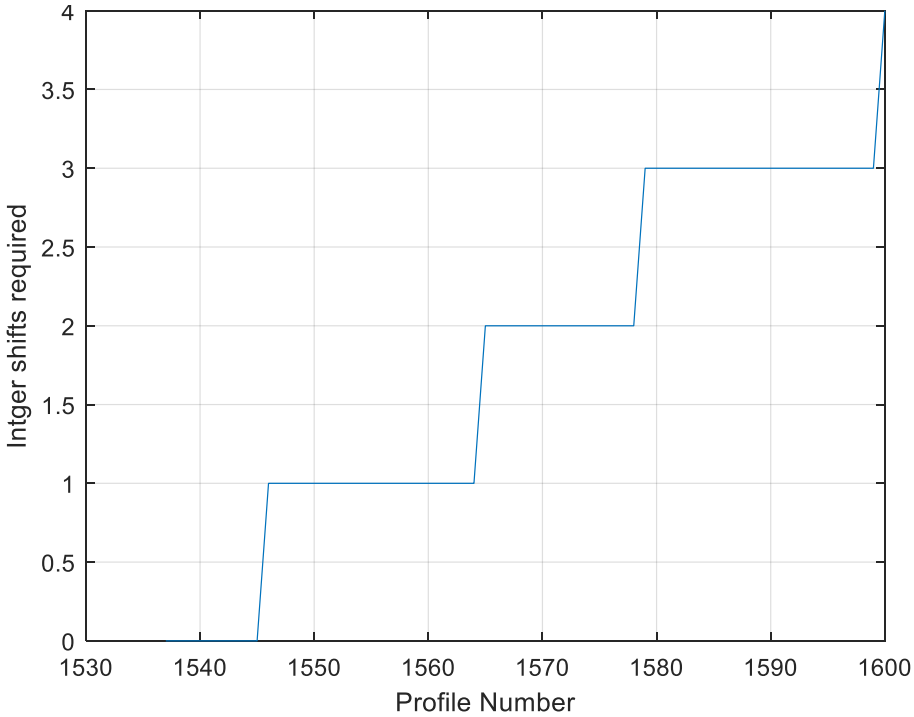

Figure 4.12 Plot of the integer bin shifts per profile for alignment

4.3.3 Discussion and comparison of both datasets

The alignment technique achieved a 6.705% improvement in the contrast value in the Spanish dataset and a 6.179% improvement in the CSIR dataset. This resulted in the Spanish dataset having a contrast of -23.7674dB and the CSIR dataset having a higher contrast of -17.5035dB. With each dataset (Spanish and CSIR) having an inherently different contrast and entropy value, the comparison is not straightforward. The unaligned Spanish dataset had a lower contrast value than the CSIR dataset and this is consistent with the contrast of the respective aligned profiles. The difference in percentage improvement was also very small, with the Spanish dataset being slightly better. This could be due to a lower contrast value having a larger room for improvement.

The alignment technique achieved a 2.484% improvement (decrease) in the entropy value in the Spanish dataset and a 2.733% improvement in the CSIR dataset. This resulted in the Spanish dataset having an entropy of -9.8700dB and the CSIR dataset having a higher entropy of -8.8335dB. Again, with each dataset having an inherently different entropy value, the comparison is not straightforward. The unaligned Spanish dataset had a lower entropy value (desirable) than the CSIR dataset and this is consistent with the entropy of the respective aligned profiles. The difference in percentage improvement once more was very small, with the CSIR dataset

being slightly better. This could be due to a higher entropy value having a larger room for improvement. Furthermore, with the Spanish dataset, the block chosen to analyse the dataset was larger (256) than the one chosen with the CSIR dataset (64). Aligning more profiles may show a worse variance than aligning fewer profiles.

In terms of a qualitative comparison, it is clear from the HRR profiles plots that the algorithm improved the alignment of the profiles of both datasets. The Spanish dataset appeared to be aligned better than the CSIR dataset visually. However, this could be due to the Spanish dataset having had a larger block of profiles, making the jumps in shifts less apparent.

4.4 Adjacent Reference Profile Alignment (Integer shift)

This is the second algorithm explored and is based on theory in [4]. This algorithm is based on the adjacent reference profile cross-correlation given by Equation 2.7. The algorithm is explained by the flow chart in Fig 4.13.

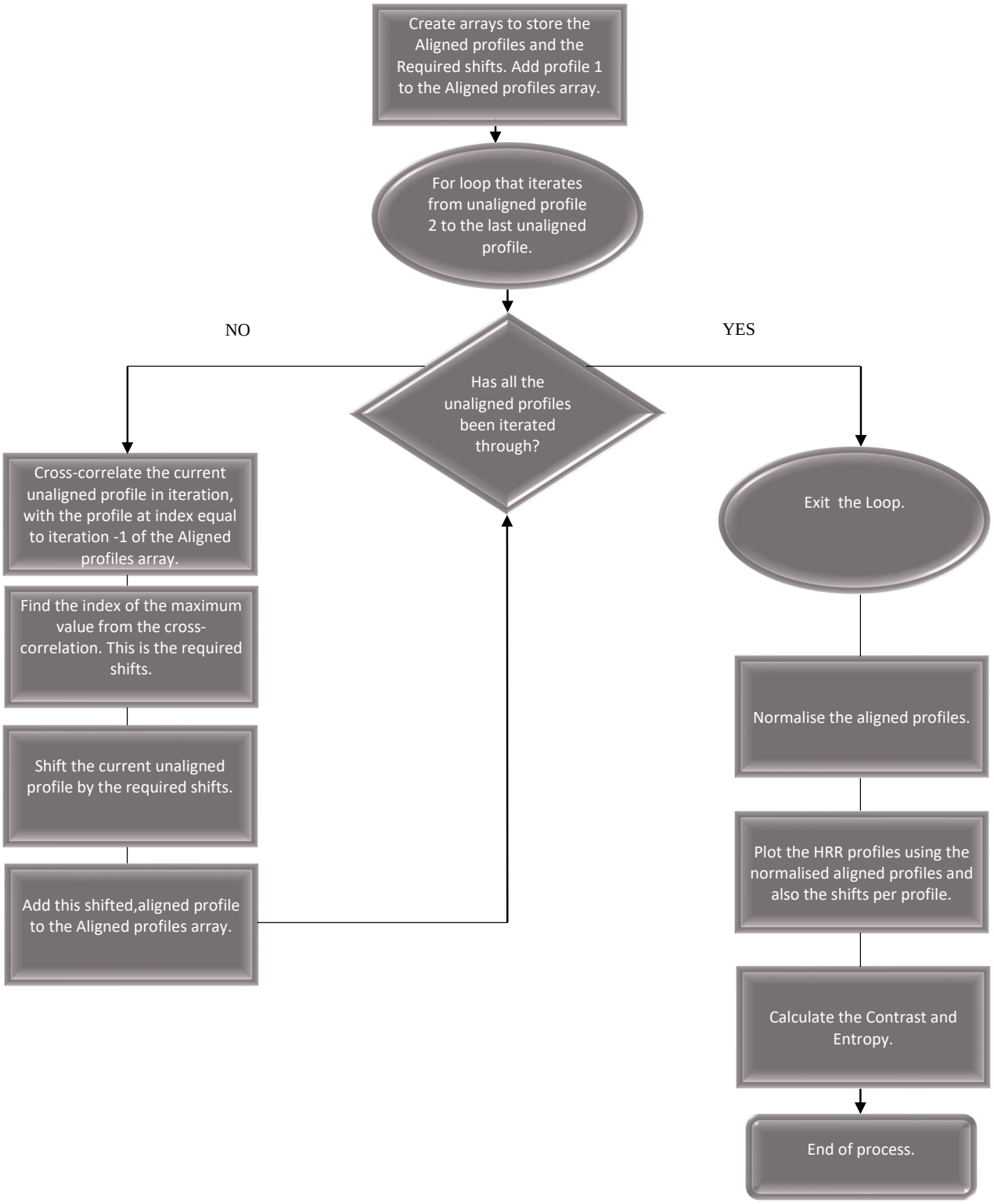

Figure 4.13 Single reference profile (integer) process

4.4.1 Spanish Dataset

The resulting HRR profiles for the Spanish Dataset are shown in Fig 4.14. It is clear from the HRR profiles plot, that no alignment took place. The profiles appear to be the same as the unaligned profiles. This was justified by the quantitative measures as well, given in Table 4.5.

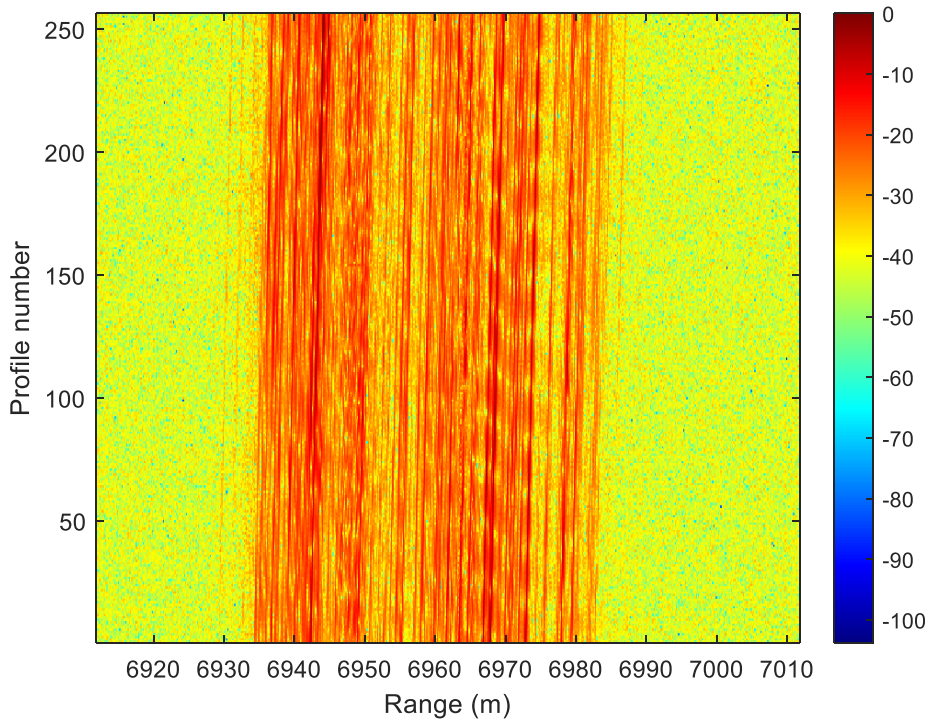

Figure 4.14 HRR profiles plot of the envelope correlation adjacent reference profile algorithm

Table 4.5 Table showing the contrast and entropy values in dB

Contrast (dB)	Entropy (dB)
-25.4775	-9.6308

The contrast value had no increase when compared to the unaligned profiles and the entropy value had no decrease when compared to the unaligned profiles.

The number of integer shifts that each unaligned profile underwent is displayed in Fig 4.15. A flat line indicates no shifts took place, and therefore no alignment.

<u>Why did alignment not take place?</u>

The reason alignment did not take place is due to adjacent profiles being too similar to one another. This is depicted in Fig 4.16 when profile 1 and profile 2 (any two adjacent profiles would depict this) are plotted over each other. They are too similar in dimension for any shift to be warranted and this propagates throughout the dataset. The plateaus of the staircase shifts seen earlier are due to this same reason.

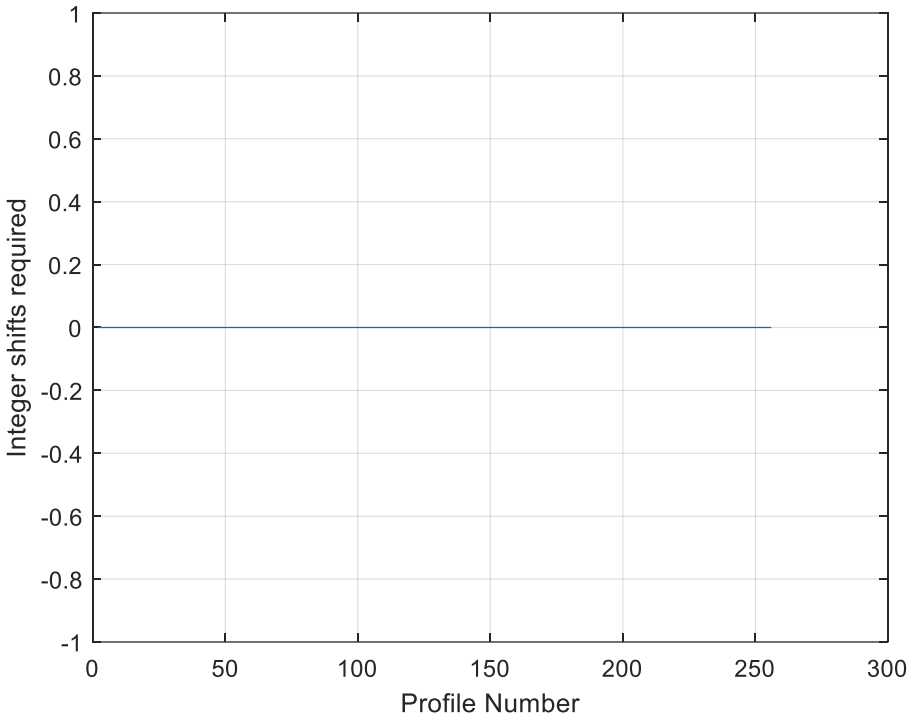

Figure 4.15 Plot of the integer bin shifts per profile for alignment

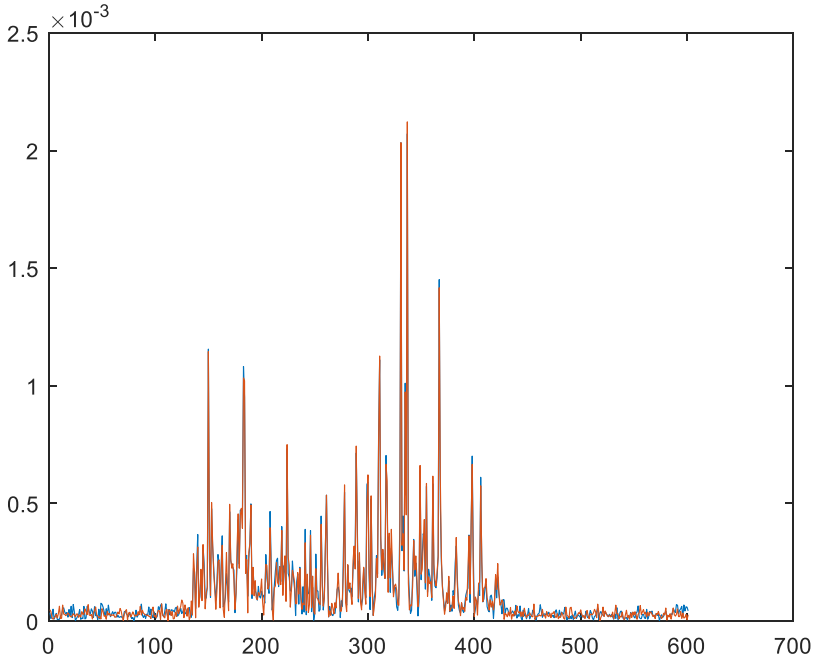

Figure 4.16 Plot of profile 1 and profile 2 to show similarities

4.4.2 CSIR Dataset

As with the Spanish dataset, no alignment took place here for the same reasons discussed. The resulting HRR profiles for the CSIR Dataset are shown in Fig 4.17. with the quantitative measures given in Table 4.6.

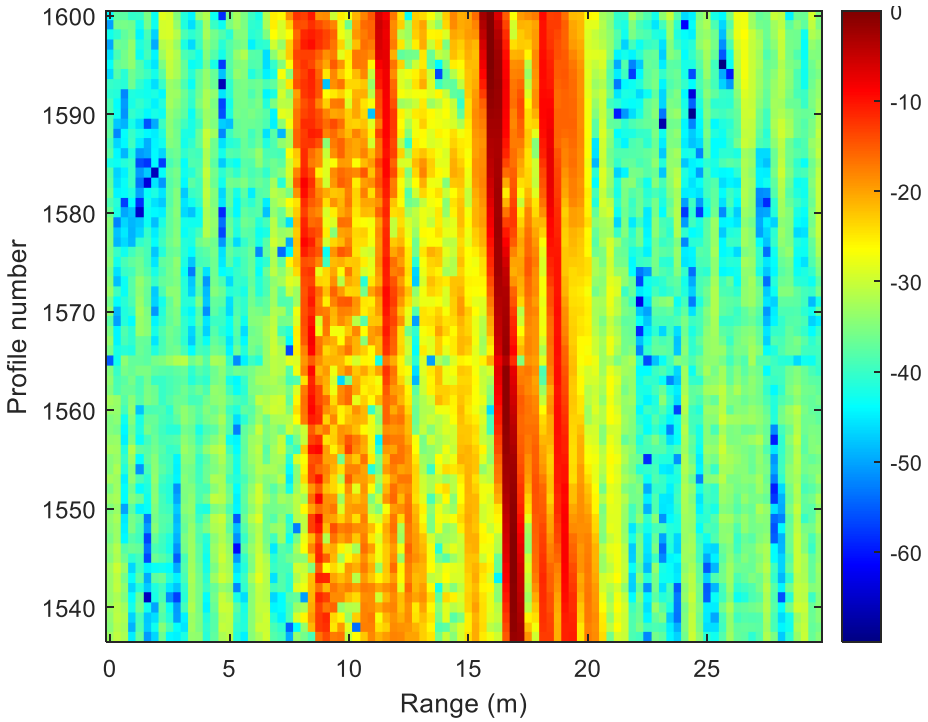

Figure 4.17 HRR profiles plot of the envelope correlation adjacent reference profile algorithm

Table 4.6 Table showing the contrast and entropy values in dB

Contrast (dB)	Entropy (dB)
-18.6563	-8.5985

As expected, the contrast and entropy values are unchanged when compared with the values of the unaligned profiles. A flat line in Fig 4.18 indicates that no shifts took place, and therefore no alignment.

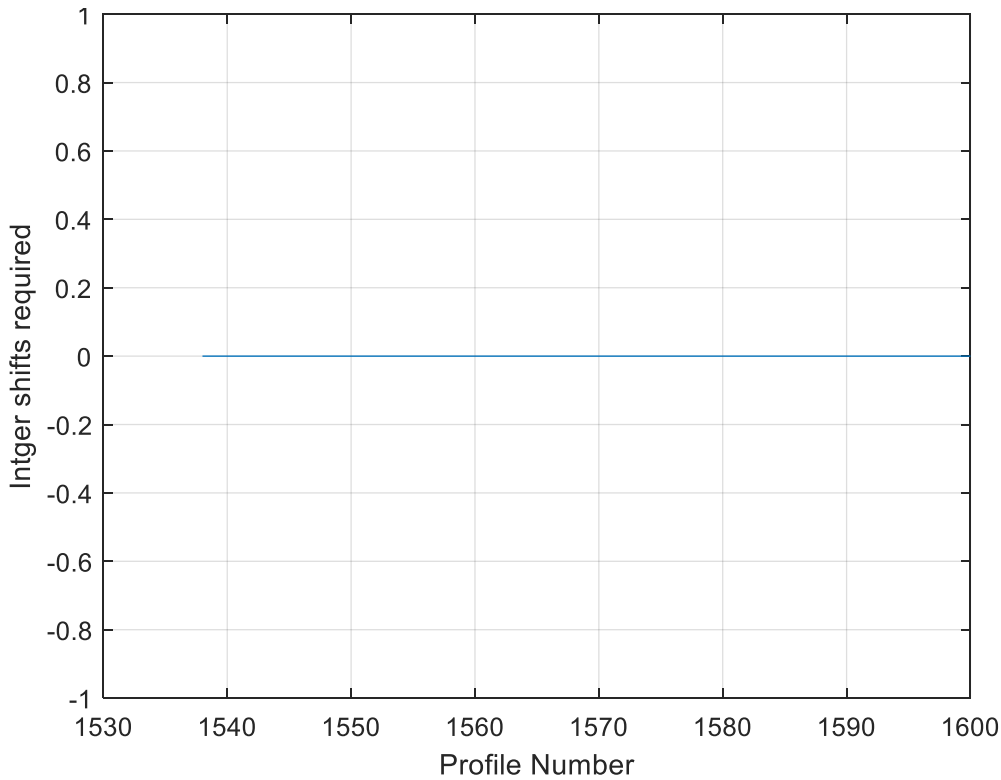

Figure 4.18 Plot of the integer bin shifts per profile for alignment

Why did alignment not take place?

Alignment did not take place for the same reason as discussed in the Spanish dataset. Adjacent profiles are too similar to one another in this dataset as well. This is depicted in Fig 4.19 when profile 1 and profile 2 are plotted over each other.

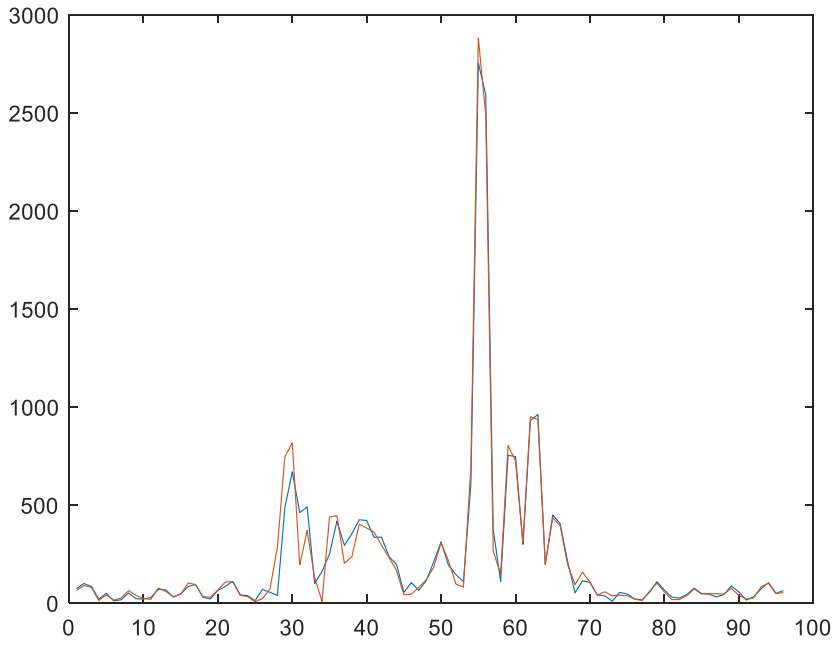

Figure 4.19 Plot of profile 1 and profile 2 to show similarities

4.4.3 Discussion and comparison of both datasets

As no alignment takes place in both datasets, a discussion is not required.

4.5 Non-coherent Cumulative Average Reference Profile Alignment (Integer shift)

This is the third algorithm explored and is based on theory in [4]. This algorithm is based on the reference profile given by Equation 2.8. The algorithm is explained by the flow chart in Fig 4.20.

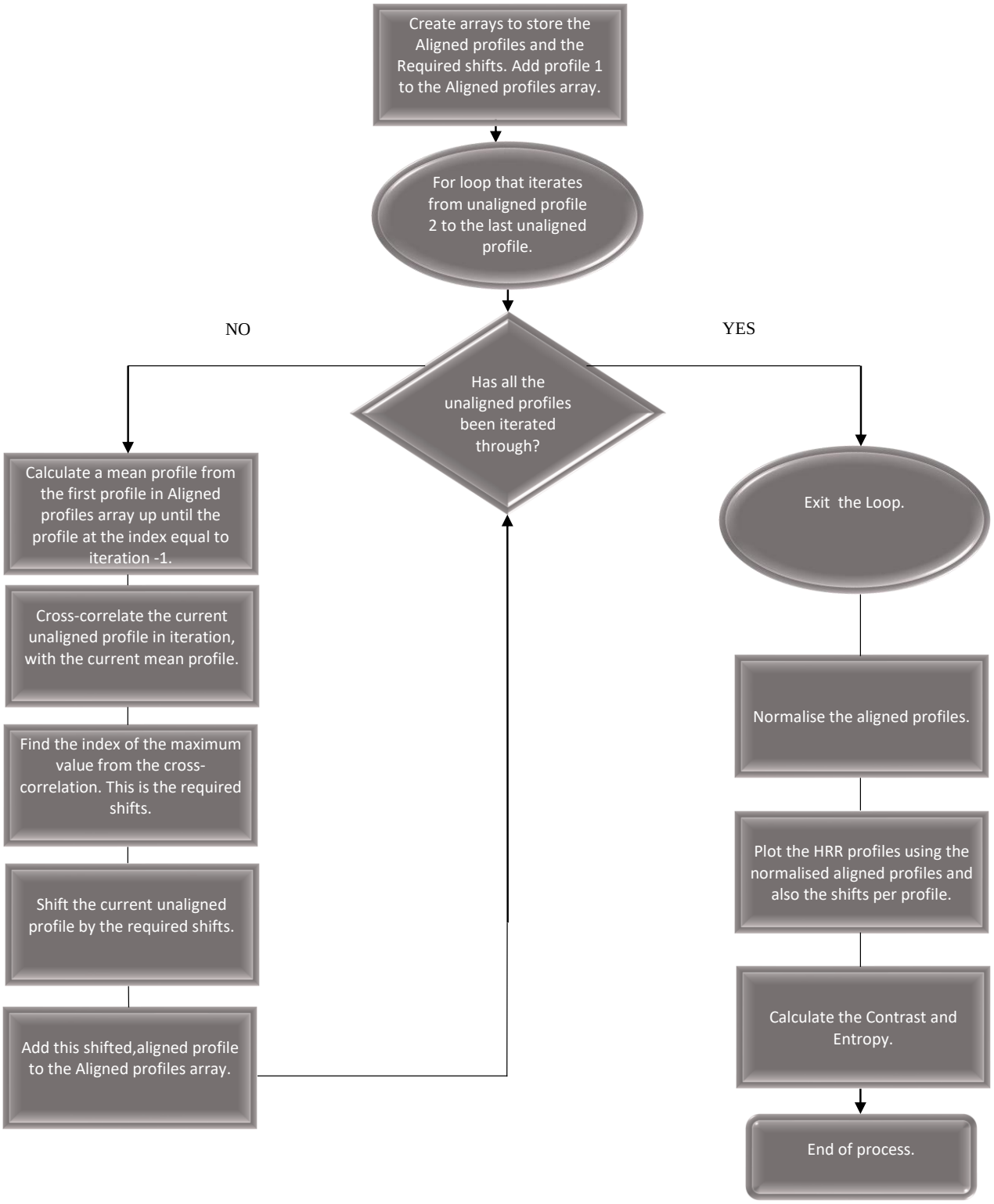

Figure 4.20 Cumulative average reference profile (integer) process

4.5.1 Spanish Dataset

The resulting range aligned HRR profiles for the Spanish Dataset is shown in Fig 4.21. The reference profile, as aforementioned, was the cumulative average of all the preceding profiles to the profile to be aligned. It is clear from the range aligned HRR profiles plot that alignment had taken place. There is less migration of scatterers across range bins than in the unaligned HRR profiles. Also, dominant deep red scatterers (at a range of ~6968m) appear to be aligned although they are broken as opposed to being solid. This is due to a limitation of the technique only being able to implement integer shifts when in reality scatterers migrate by non-integer shifts from profile to profile.

Visually it is very difficult to see if there is an improvement on the single reference algorithm. However, the scatterer line at approximately 6942m and from profiles [150 256] appears to be less black (lighter) than the same scatterer in the single reference profile HRR profiles plot (Fig 4.9). This indicates a weaker alignment based on the colour bar. The qualitative measures of alignment were supported by the quantitative measures, given in Table 4.7.

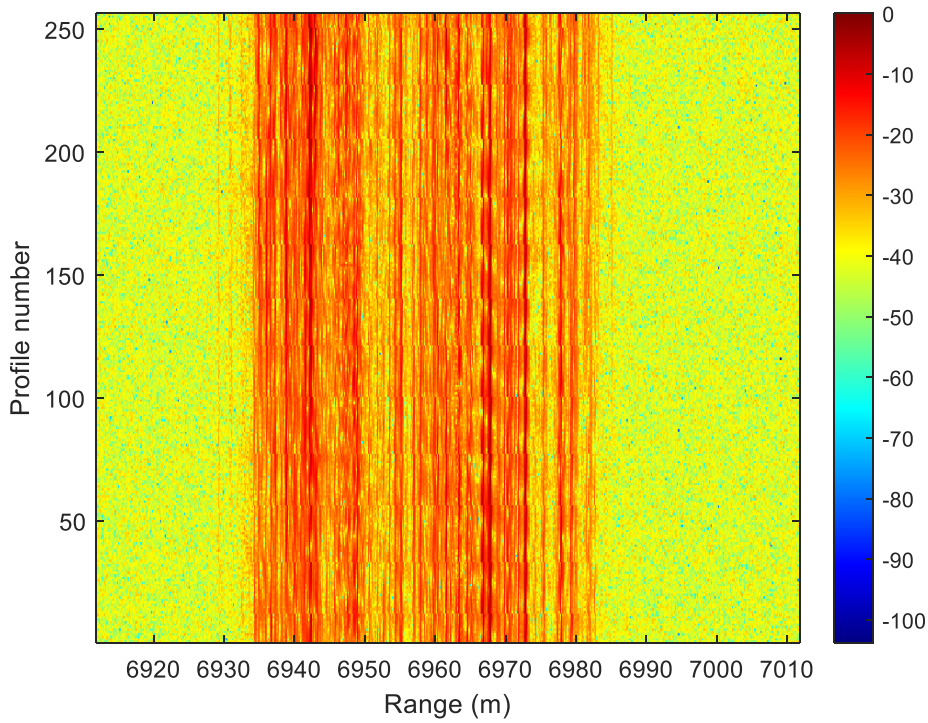

Figure 4.21 HRR profiles plot of the envelope correlation cumulative average reference profile algorithm

Table 4.7 Table showing the contrast and entropy values in dB

Contrast (dB)	Entropy (dB)
-23.7982	-9.8643

The contrast value had an increase of 6.584% when compared to the unaligned profiles, indicating more aligned profiles. This is 0.121% lower than the improvement from the single profile reference alignment algorithm. This was a very small difference.

The entropy value had a decrease (desirable) of 2.425% when compared to the unaligned profiles, indicative of a lower variance among profiles. This is 0.059% worse than the improvement from the single profile reference alignment algorithm. Again, this was a small difference.

Furthermore, the number of integer shifts that each unaligned profile underwent is displayed in Fig 4.22. The staircase shape was expected since it is an integer shift algorithm.

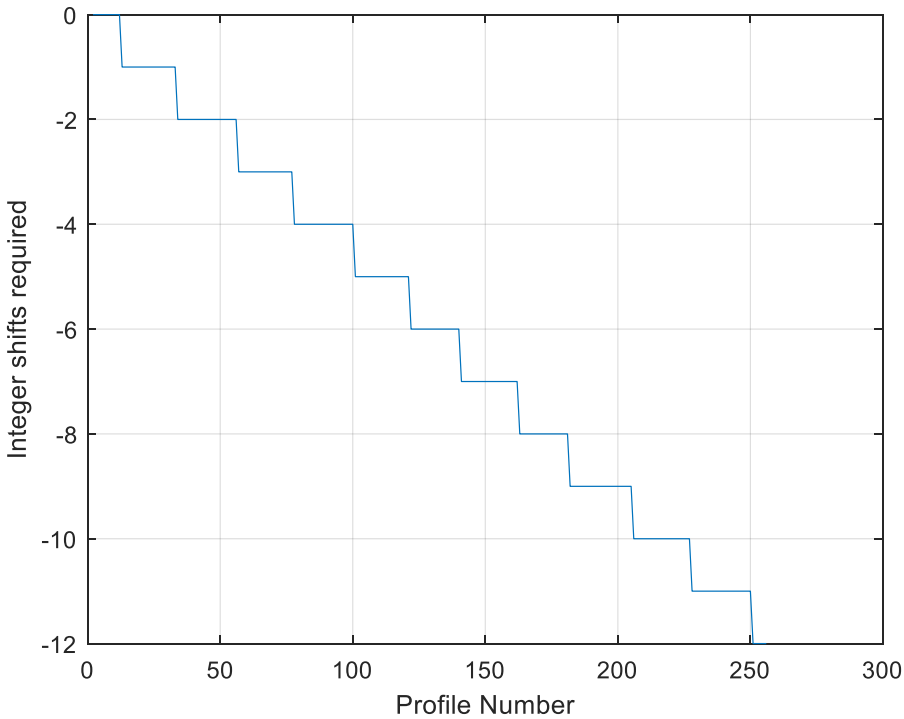

Figure 4.22 Plot of the integer bin shifts per profile for alignment

4.5.2 CSIR Dataset

The resulting range aligned HRR profiles for the CSIR Dataset are shown in Fig 4.23. It is clear from the HRR profiles plot, that alignment had taken place. There is less migration of scatterers across range bins than in the unaligned HRR profiles. Also, dominant deep red scatterers (at a range of ~17m) appear to be aligned although they are broken as opposed to being solid. This is due to a limitation of the technique only being able to implement integer shifts when in reality scatterers migrate by non-integer shifts from profile to profile.

Using the scatterers at ~8m it appears that the single reference algorithm had a better alignment (the same scatterer was straighter in that HRR profile represented by Fig 4.11). Furthermore, the HRR profiles plot in Fig 4.23 appears to have a lower change in shifts. The quantitative measures of contrast and entropy values are given in Table 4.8.

Table 4.8 Table showing the contrast and entropy values in dB

Contrast (dB)	Entropy (dB)
-17.5369	-8.8279

The value contrast had an increase of 6% when compared to the unaligned profiles, indicating more aligned profiles. This is 0.179% lower than the improvement from the single profile reference alignment algorithm.

The entropy value had a decrease (desirable) of 2.668% when compared to the unaligned profiles, indicative of a lower variance among profiles. This is 0.105% worse than the improvement from the single profile reference alignment algorithm.

Furthermore, the number of integer shifts that each unaligned profile underwent is displayed in Fig 4.24. Again, the staircase shape was expected since it is an integer shift algorithm. It is evident that a lower change in integer shifts required occurs than in the single reference profile alignment algorithm in Fig 4.12. This is based on the lower number of steep inclines seen (1 less).

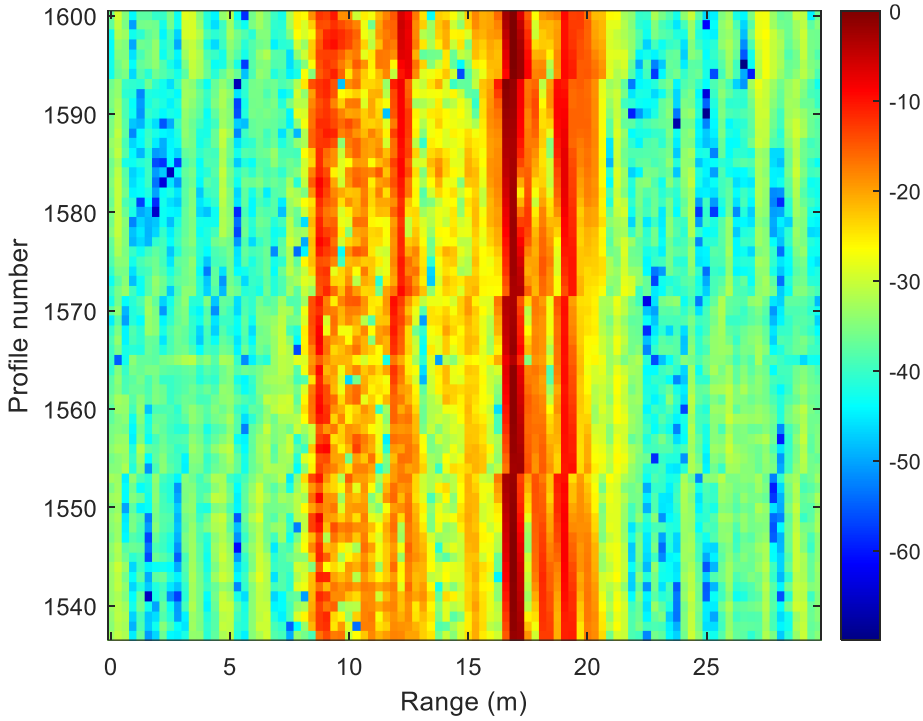

Figure 4.23 HRR profiles plot of the envelope correlation cumulative average reference profile algorithm

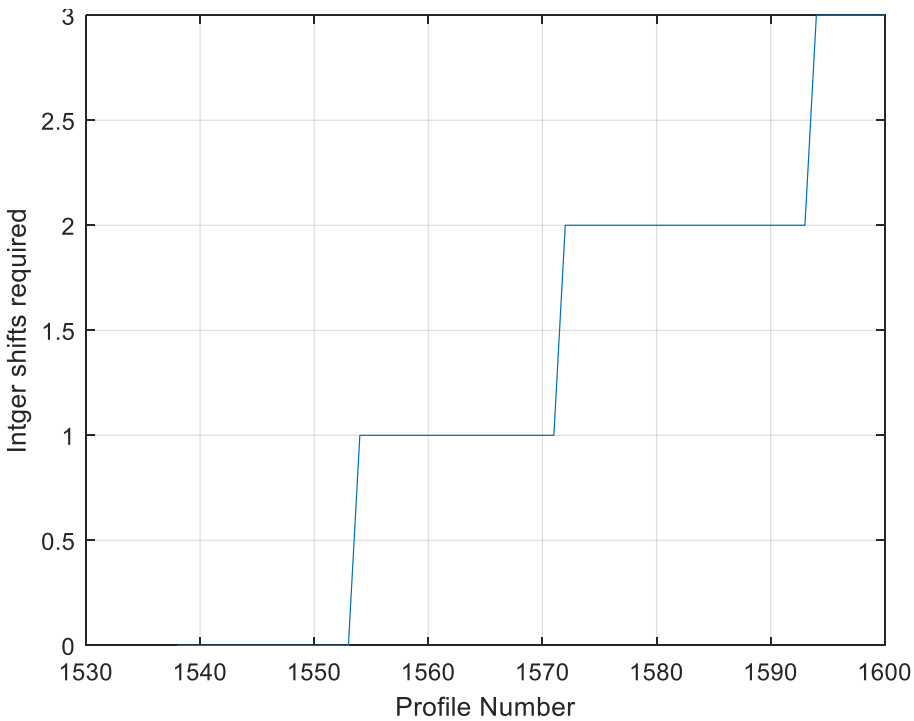

Figure 4.24 *Plot of the integer bin shifts per profile for alignment*

4.5.3 Discussion and comparison of both datasets

The technique improved the alignment of the profiles for both datasets in comparison with the unaligned profiles. This was both qualitatively and quantitatively justified. However, the technique performed worse than

the single reference profile technique for both datasets, with it being slightly more noticeable on the CSIR dataset.

A reason for the worsening of alignment in this algorithm compared to using the single reference profile algorithm could have been due to the continuously changing reference of the moving average, as opposed to having a single fixed reference, which all of the profiles align to.

4.6 Sliding-Window Average Reference Profile Alignment (Integer shift)

This is the final Integer shift algorithm explored and is based on theory in [4], relating to a sliding window averaging of the reference profile. The algorithm is explained by the flow chart in Fig 4.25.

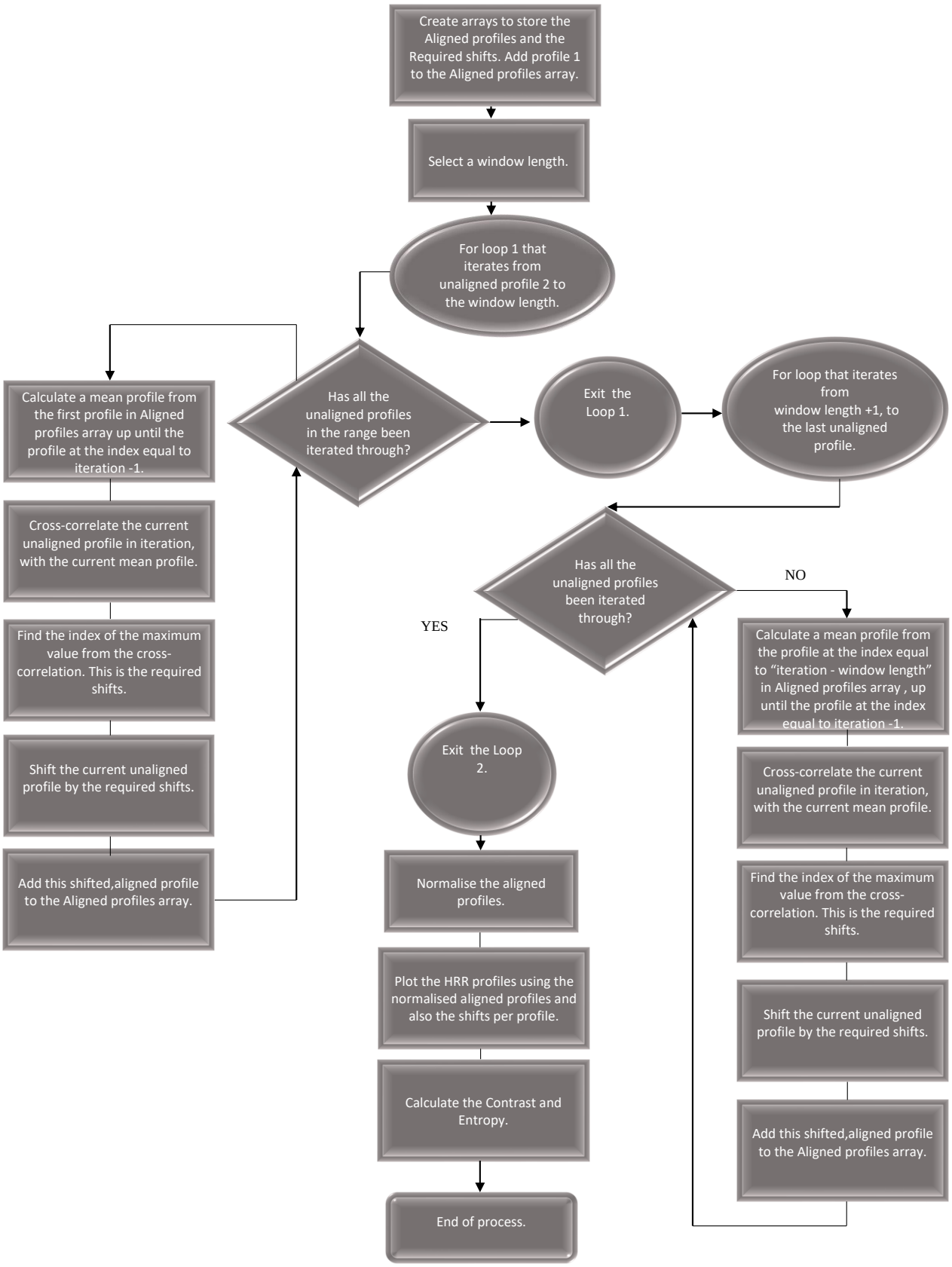

Figure 4.25 Sliding window average reference profile (integer) process

How to get the sliding window

The sliding window was chosen by testing every possible window in the length of the profiles and finding the one which resulted in the highest combined contrast and entropy. The entire algorithm was put through a for loop where the sliding window used in each iteration ranged from [1:number_of_profiles]. At the extremes, a sliding window of 1 is simply the adjacent reference profile algorithm and a sliding window equal to the number of profiles is simply the non-coherent cumulative averaging algorithm.

The combined value for the contrast and entropy was calculated as follows. First, the values were normalised. Next, the contrast was added to the inverse of the entropy(noting that a lower entropy is better). Due to this, it is evident that the contrast and entropy are given the same weighting.

The siding window for the Spanish dataset was chosen as 42 profiles, and for the CSIR dataset, it was chosen as 22 profiles.

4.6.1 Spanish Dataset

The resulting range aligned HRR profiles for the Spanish Dataset is shown in Fig 4.26. A sliding window of 42 profiles resulted in the best performance. It is clear from the range aligned HRR profiles plot, that alignment had taken place as there is less migration of scatterers across range bins than in the unaligned HRR profiles. Also, dominant deep red scatterers (at a range of ~6972m) appear to be aligned although they are broken as opposed to being solid (as expected).

The scatterer at a range of ~6968m appears to be darker (more black) than the same scatterer in the single reference profile HRR profiles plot in Fig 4.9. This indicates a stronger alignment based on the colour bar. Therefore, qualitatively this technique was better than the cumulative averaging method. The contrast and entropy values of Fig 4.26 are presented in Table 4.9.

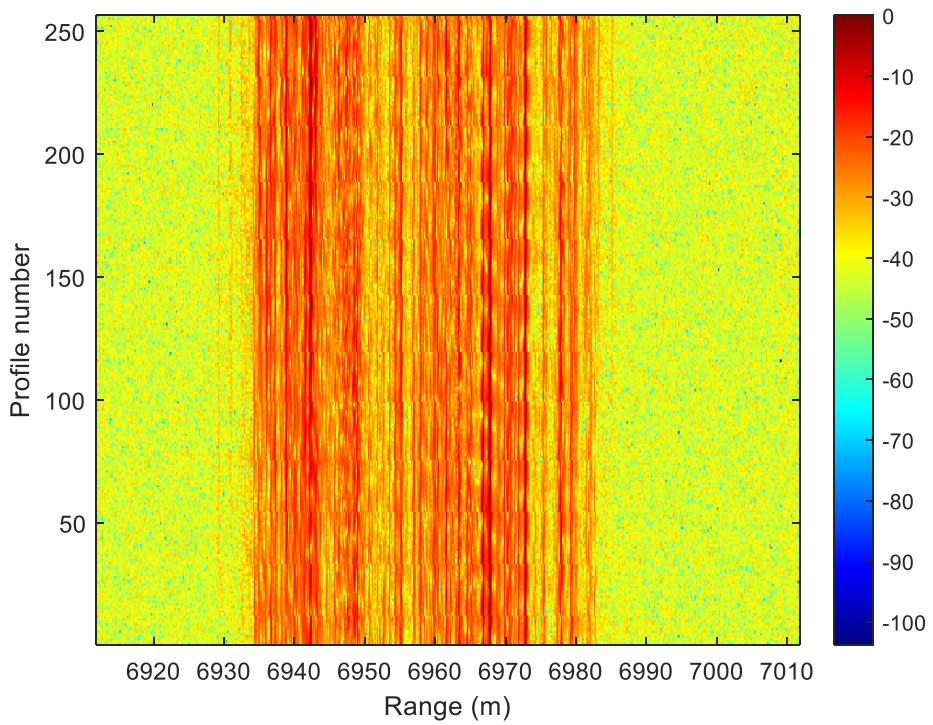

Figure 4.26 HRR profiles plot of the envelope correlation sliding window average reference profile algorithm

Table 4.9 Table showing the contrast and entropy values in dB

Contrast (dB)	Entropy (dB)
-23.7613	-9.8699

The contrast value had an increase of 6.729% when compared to the unaligned profiles, indicating better-aligned profiles. This is 0.024% higher than the improvement from the single profile reference alignment algorithm. Subsequently, in terms of contrast, this algorithm was better than the cumulative averaging method.

The entropy value had a decrease (desirable) of 2.483% when compared to the unaligned profiles, indicative of a lower variance among profiles. This is 0.001% worse than the improvement from the single profile reference alignment algorithm, which is negligible. Subsequently, in terms of contrast, this algorithm was better than the cumulative averaging method.

Furthermore, the number of integer shifts that each unaligned profile underwent is displayed in Fig 4.27 with the expected staircase shape.

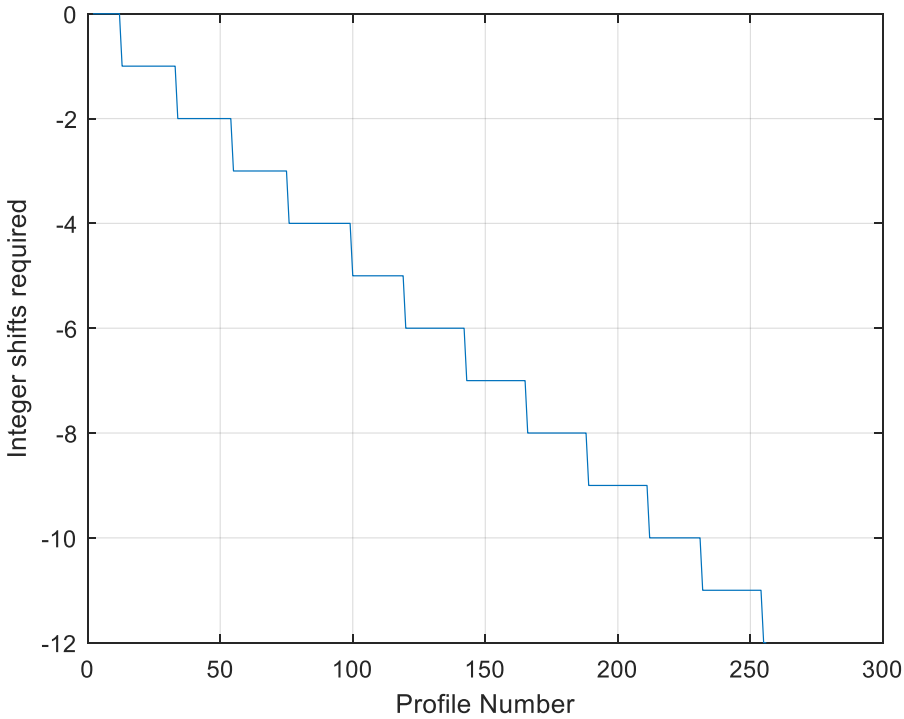

Figure 4.27 Plot of the integer bin shifts per profile for alignment

4.6.2 CSIR Dataset

The resulting range aligned HRR profiles for the Spanish Dataset is shown in Fig 4.28. A sliding window of 22 profiles resulted in the best performance. It is clear from the HRR profiles plot, that alignment had taken place as there is less migration of scatterers across range bins than in the unaligned HRR profiles. Also, from the plot, it is evident that the technique is trying to align the dominant scatterer at ~17m.

The HRR profiles in Fig 4.28 looks indistinguishable from the HRR profiles of the cumulative average reference profile in Fig 4.23. This was confirmed by the contrast and entropy values of Fig 4.28 which are presented in Table 4.10.

Table 4.10 Table showing the contrast and entropy values in dB

Contrast (dB)	Entropy (dB)
-17.5369	-8.8279

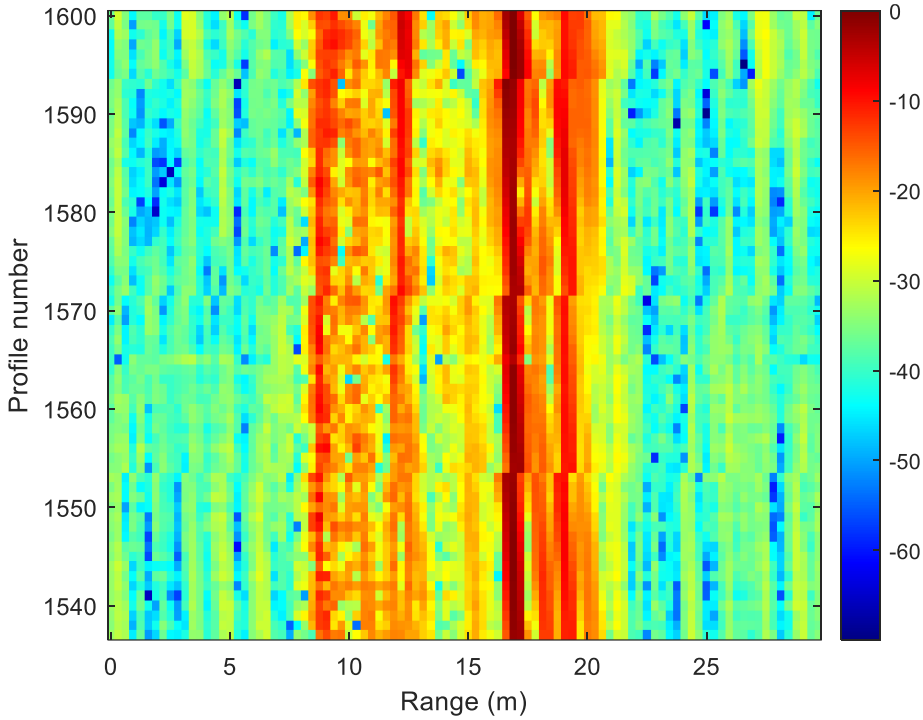

Figure 4.28 HRR profiles plot of the envelope correlation sliding window average reference profile algorithm

The contrast value had an increase of 6% when compared to the unaligned profiles. To reiterate, this is 0.179% lower than the improvement from the single profile reference alignment algorithm.

The entropy value had a decrease (desirable) of 2.668% when compared to the unaligned profiles, indicative of a lower variance among profiles. Similar to the cumulative averaging reference profile method, this is 0.105% worse than the improvement from the single profile reference alignment algorithm.

Furthermore, the number of integer shifts that each unaligned profile underwent is displayed in Fig 4.29 with the expected staircase shape.

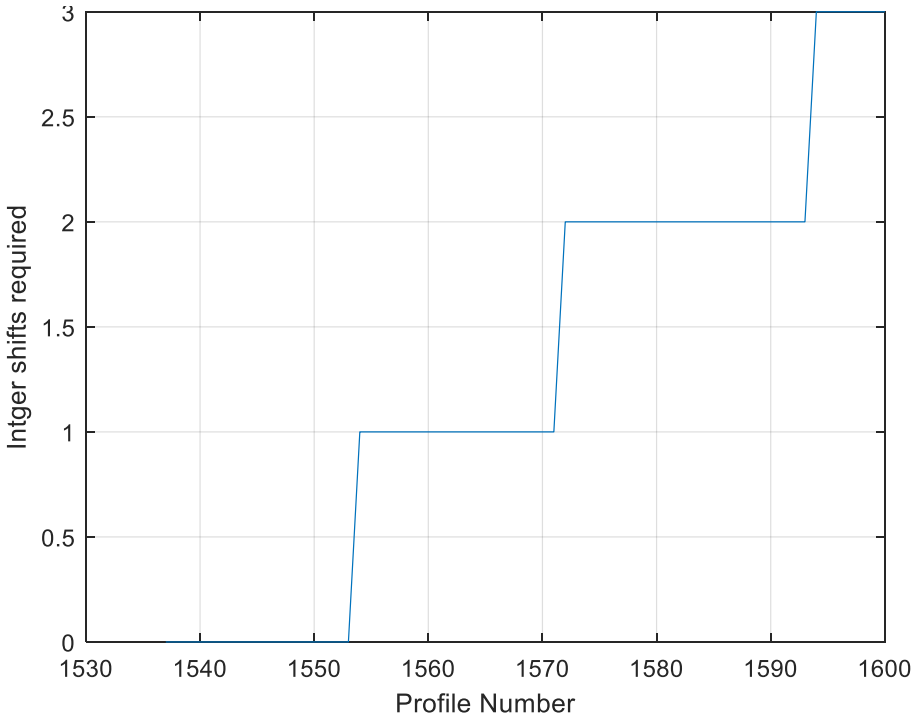

Figure 4.29 Plot of integer the bin shifts per profile for alignment

4.6.3 Discussion and comparison of both datasets

The technique improved the alignment of the profiles for both datasets in comparison with the unaligned profiles. This was both qualitatively and quantitatively justified.

However, the technique performed better than the single reference profile technique (integer shift) for the Spanish datasets, but worse on the CSIR dataset. This made it the best integer shift technique for the Spanish dataset. For the CSIR dataset, it was the tied worst integer shift technique with the cumulative averaging technique.

The similarities in the results of the technique, on the CSIR data, could have been due to the small block of profiles (64) used. This may have caused a sliding window average profile to be extremely similar to the cumulative average counterpart.

4.7 Overview of Sub-integer shift algorithms

All the sub-integer algorithms followed the same process after using their counterpart integer-shift algorithms. Therefore, it is only necessary to show the algorithm implementation for the general case as it allows for the understanding of all of them. This is depicted in Fig 4.30.

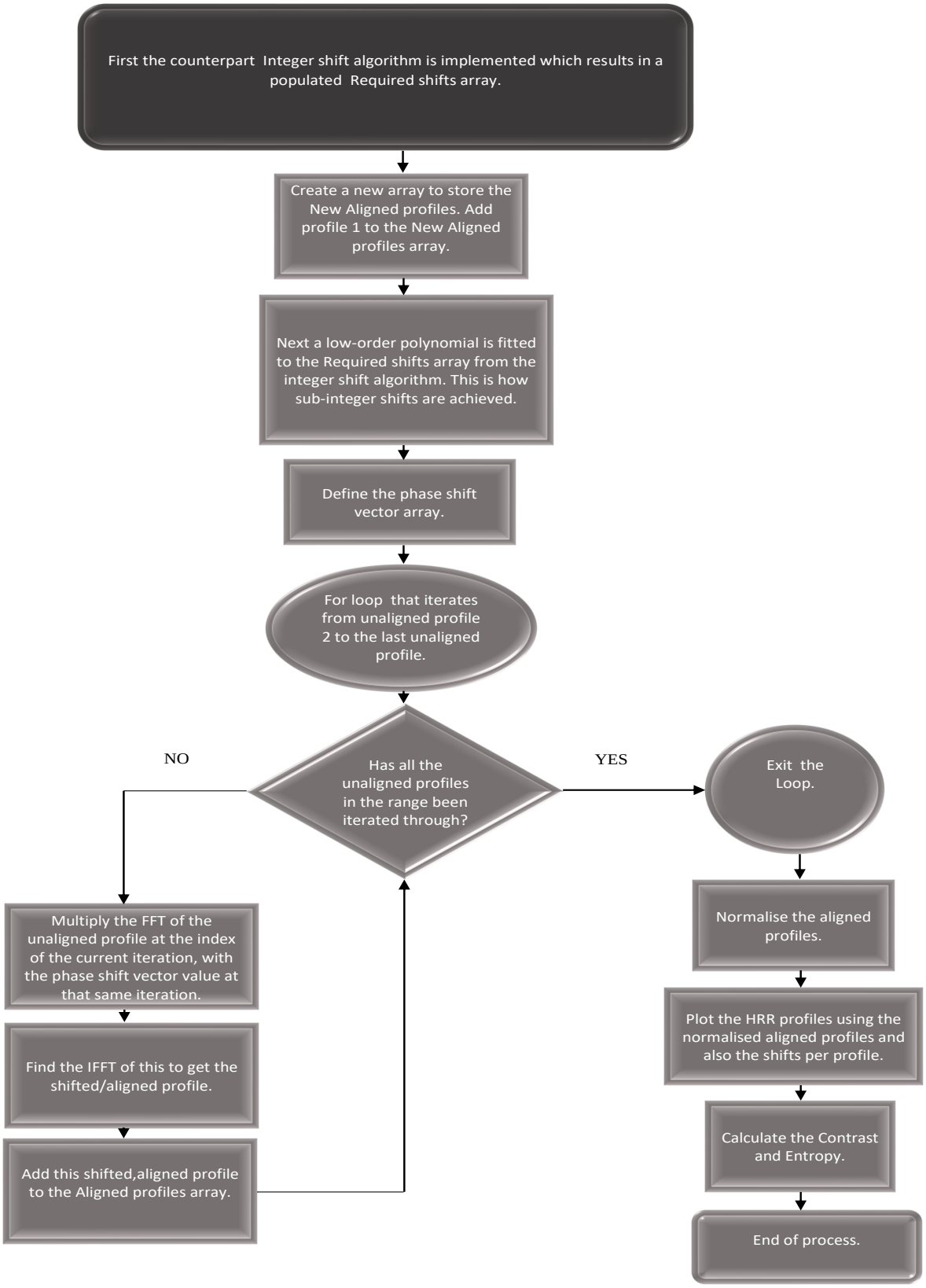

Figure 4.30 Sub-integer shift process

Phase shift vector

The phase shift vector was multiplied by the FFT of every unaligned profile. The phase shift vector changed with each iteration and was given by Equation 4.1. Note that the phase shift vector was for a single profile. A different phase shift vector was needed for each profile since each would require a slightly different non-integer bin shift. [5]

$$phase_shift_vector = e^{j2\pi . s_l . m/n} \tag{4.1}$$

Where:

- n is the total number of range bins.
- N is the total number of profiles.
- m = 0:1:(n-1)
- s_l is the delay for the lth profile. This can be an integer or a non-integer value.

Why low-order polynomial 1

To gather the s_l shifts, a low order polynomial was fitted to the integer shifts per profile calculated in the previous counterpart algorithms. For this project, a polynomial of order 1 was chosen. This is due to the maritime vessels not having sudden movements and therefore having less abrupt required shift changes between profiles.

4.8 Single Reference Profile envelope correlation Alignment (Sub-integer shift)

4.8.1 Spanish Dataset

The resulting range aligned HRR profiles for the Spanish Dataset are shown in Fig 4.31. As in the integer shift version of this algorithm, profile 1 was chosen as the reference profile. It is clear from the HRR profiles plot, that a better alignment had taken place here compared to the result of the counterpart algorithm in Fig 4.9. There is less migration of scatterers across range bins than in Fig 4.9. Also, there are no periodic jumps in shifts as seen previously, as this is remedied by using sub-integer shifts. A clear example of this visually improved alignment can be seen in the scatterer at ~6972m. The dominant scatterer here appears to be aligned well with there being a solid black line. Visually, this HRR profile plot looks the best aligned. The contrast and entropy values of Fig 4.31 are presented in Table 4.11.

Table 4.11 Table showing the contrast and entropy values in dB

Contrast (dB)	Entropy (dB)
-22.8357	-9.7278

The contrast value had an increase of 10.362% when compared to the unaligned profiles, indicating better-aligned profiles. This is a much better increase than all of the preceding algorithms.

The entropy value had a decrease (desirable) of 1.007% when compared to the unaligned profiles, pointing to a lower variance among profiles. This decrease, however, is lower than every other preceding algorithm (apart from the adjacent reference profile algorithm).

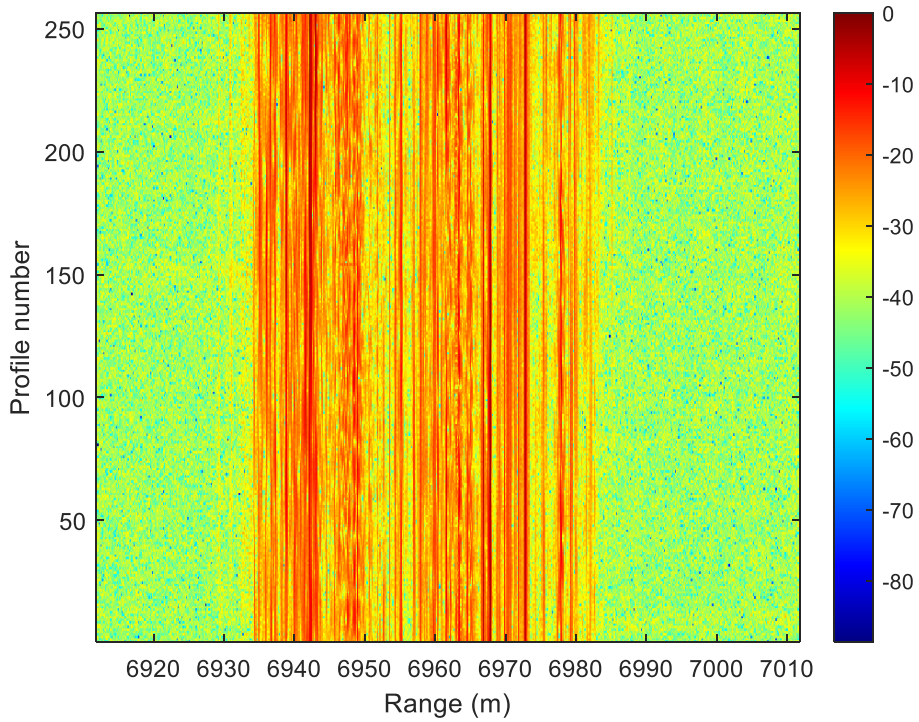

Figure 4.31 HRR profiles plot of the envelope correlation single reference profile algorithm (sub-integer shift)

Furthermore, the number of sub-integer shifts that each unaligned profile underwent is displayed in Fig 4.32. The linear red line indicates the first order fitted polynomial fitter to the integer shifts, creating the sub-integer shifts. The negative gradient was expected in accordance with the staircase shape.

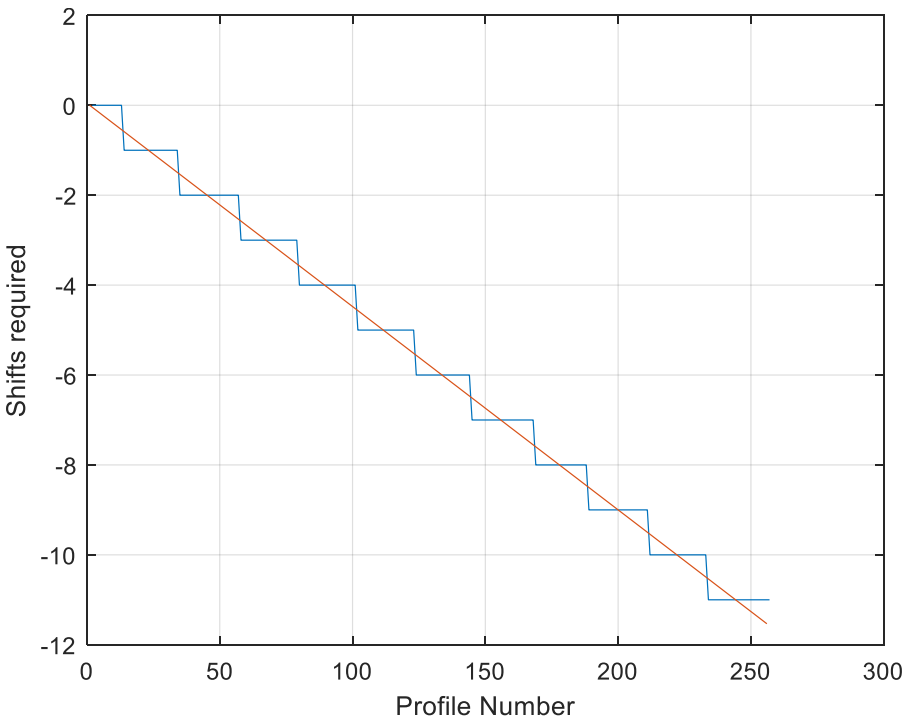

Figure 4.32 Plot of the bin shifts per profile for alignment with a first order polynomial

4.8.2 CSIR Dataset

The resulting range aligned HRR profiles for the CSIR Dataset are shown in Fig 4.33. As in the integer shift version of this algorithm, profile 1 was chosen as the reference profile. It is clear from the HRR profile plot that a better alignment had taken place here compared to the result of the counterpart algorithm in Fig 4.11.

There is less migration of scatterers across range bins than in Fig 4.11. Similarly to the Spanish dataset result, there are no periodic jumps in shifts as seen previously as this is remedied by using sub-integer shifts. A clear example of this visually improved alignment can be seen in the scatterer at ~16m. The dominant scatterer here appears to be aligned well with there being a solid deep red line. Visually, these HRR profiles look the best aligned for the CSIR dataset. The contrast and entropy values of Fig 4.33 are shown in Table 4.12.

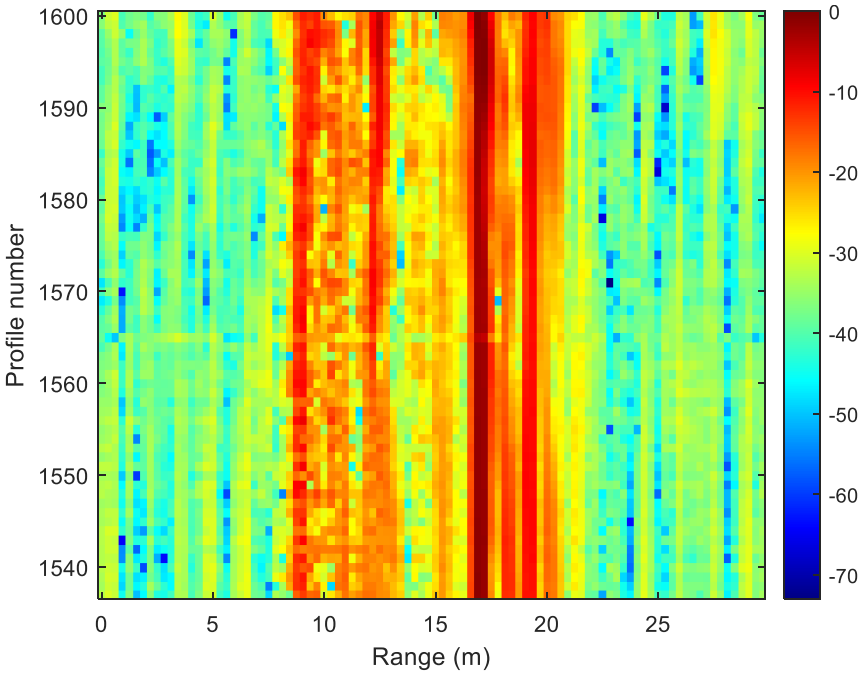

Figure 4.33 HRR profiles plot of the envelope correlation single reference profile algorithm (sub-integer shift)

Table 4.12 Table showing the contrast and entropy values in dB

Contrast (dB)	Entropy (dB)
-16.7817	-8.7455

The contrast value had an increase (desirable) of 10.048% when compared to the unaligned profiles. As with the Spanish dataset, this is a much better increase than all of the preceding algorithms.

The entropy value had a decrease (desirable) of 1.71% when compared to the unaligned profiles. This decrease, however, is lower than every other preceding algorithm (apart from the adjacent reference profile algorithm). This is consistent with the results from the Spanish dataset.

Furthermore, the number of sub-integer shifts that each unaligned profile underwent is displayed in Fig 4.34. The linear red line indicates the first order polynomial fitted to the integer shifts, creating the sub-integer shifts. The positive gradient was expected based on the increasing staircase shape.

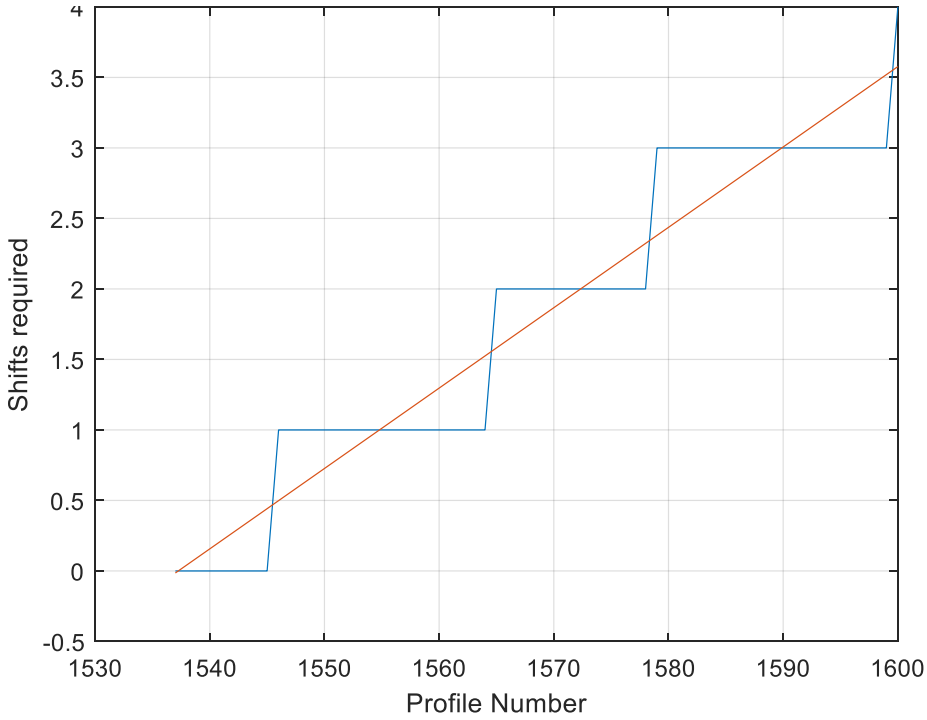

Figure 4.34 Plot of the bin shifts per profile for alignment with a first order polynomial

4.8.3 Discussion and comparison of both datasets

The technique improved the alignment of the profiles for both datasets in comparison with the unaligned profiles. This was very clear qualitatively as the profiles were visually more aligned. Furthermore, it was justified by the increases in contrast as well as the decrease in entropy, across both of the datasets.

Furthermore, from the HRR profiles plots, it appeared that this algorithm worked the best for alignment when compared to the preceding algorithms. This was justified by the highest improvement in contrast across all the preceding algorithms. However, the entropy improvement had been the worst when compared with the previous algorithms. These statements are consistent across both datasets.

The entropy indicator could be an anomaly for this algorithm. With an improvement in alignment, which is clear from the other measures, the reason the entropy does not improve more (as expected) is questionable. A possible explanation could be that due to the reference being a single profile; with sub-integer shifts a higher variance exists between profiles due to the profiles having dissimilar shifts.

4.9 Adjacent Reference Profile Alignment (Sub-integer shift)

This sub-chapter is only presented for completeness. With the procedures involved in the sub-integer shift algorithms, it is obvious that there would be no alignment resulting from using this algorithm. Specifically, this was due to the counterpart integer shift algorithm having no effect on alignment. To reiterate what was earlier said, the sub-integer shift algorithms were a result of fitting a polynomial onto the integer shifts required in those algorithms (integer shift). In sub-chapter 4.4, Fig 4.15 and Fig 4.18 show that there were zero shifts throughout the profiles. Therefore, fitting a polynomial to that flat horizontal line would have made no difference to the original shifts.

4.10 Non-coherent Cumulative Average Reference Profile Alignment (Sub-integer shift)

4.10.1 Spanish Dataset

The resulting range aligned HRR profiles for the Spanish dataset are shown in Fig 4.35. It is clear from the HRR profiles plot, that a better alignment had taken place here compared to the result of the counterpart algorithm in Fig 4.21. There is less migration of scatterers across range bins than in Fig 4.21. Also, there are no periodic jumps in shifts as seen previously, as this is remedied by the sub-integer shifts.

Visually the plot appears to be second only to the single reference profile (sub-integer shift), at this point. A clear example of this can be seen in the scatterer at ~6978m. The scatterer here is much less prominent (lighter) than the same one in Fig 4.31. The contrast and entropy values of Fig 4.35 are presented in Table 4.13.

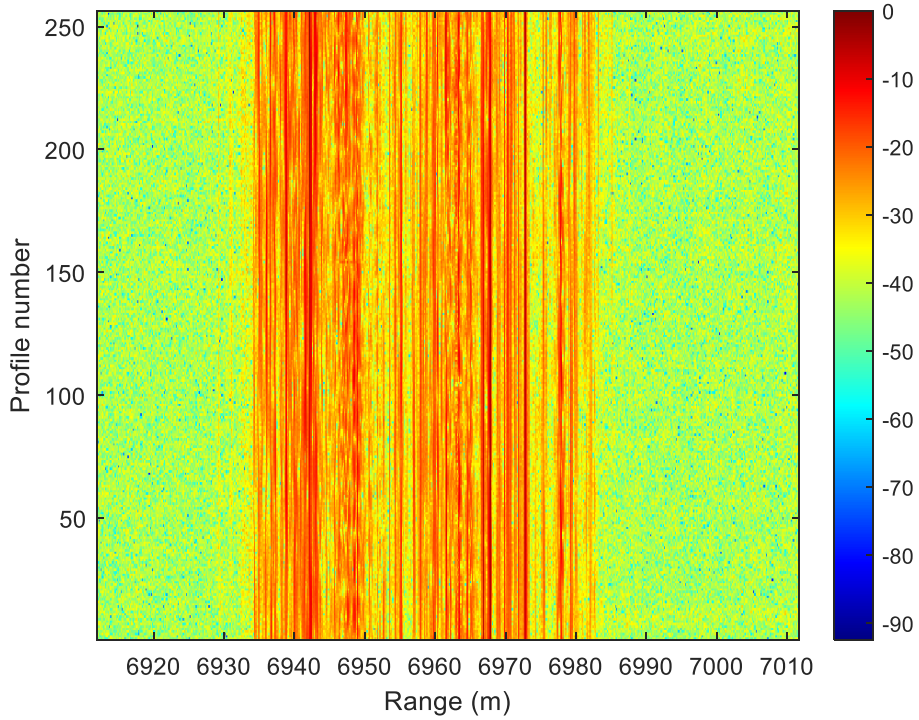

Figure 4.35 HRR profiles plot of the envelope correlation cumulative average reference profile algorithm (sub-integer shift)

Table 4.13 Table showing the contrast and entropy values in dB

Contrast (dB)	Entropy (dB)
-23.7364	-10.0138

The contrast value had an increase of 6.827% when compared to the unaligned profiles. This is a better improvement than all of the integer shift algorithms but worse than the single reference sub-integer shift algorithm.

The entropy value had a decrease (desirable) of 3.977% when compared to the unaligned profiles. This is the biggest decrease seen across all of the other algorithms making it the best in this regard.

Furthermore, the number of sub-integer shifts that each unaligned profile underwent is displayed in Fig 4.36. The linear red line indicates the first order polynomial fitted to the integer shifts, creating sub-integer shifts. The negative gradient was expected in accordance with the staircase shape.

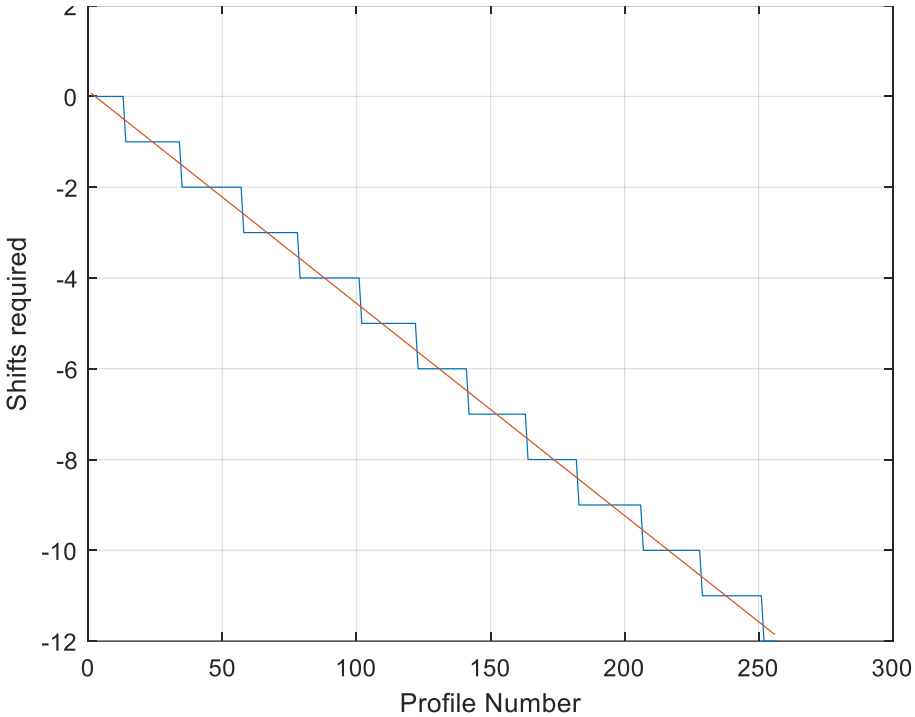

Figure 4.36 Plot of the bin shifts per profile for alignment with a first order polynomial

4.10.2 CSIR Dataset

The resulting range aligned HRR profiles for the CSIR dataset are shown in Fig 4.37. It is clear from the HRR profile plot, that a better alignment had taken place here compared to the result of the counterpart algorithm in Fig 4.23. There is less migration of scatterers across range bins than in Fig 4.23. Also, similarly to the Spanish dataset, there are no periodic jumps in shifts as seen previously as this is remedied by using sub-integer shifts.

As in the Spanish dataset, the plot appears to be second only to the single reference profile (sub-integer shift). A clear example of this can be seen in the scatterer at ~8m. At this range, the scatterer is a lighter shade of orange as compared to the same scatterer in Fig 4.33. Also, profile ~1565 appears to be less aligned in Fig 4.37 as opposed to in Fig 4.33. The contrast and entropy values of Fig 4.37 are presented in Table 4.14.

Table 4.14 Table showing the contrast and entropy values in dB

Contrast (dB)	Entropy (dB)
-17.2711	-8.8395

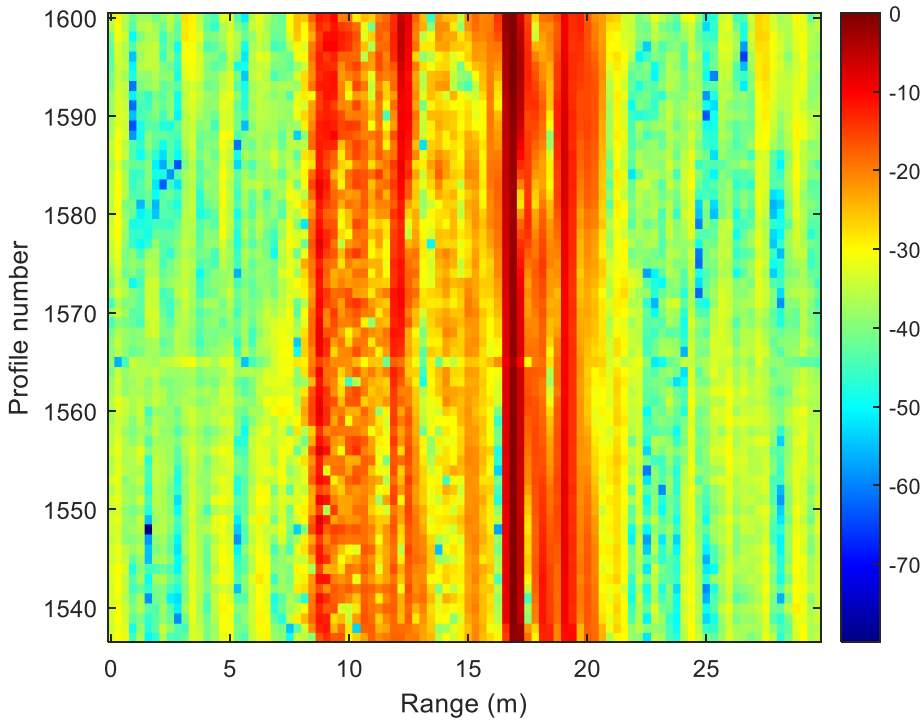

Figure 4.37 HRR profiles plot of the envelope correlation cumulative average reference profile algorithm (sub-integer shift)

The contrast value had an increase of 7.425% when compared to the unaligned profiles. This is a better improvement than all of the integer shift algorithms but worse than the single reference sub-integer shift algorithm.

The entropy value had an improvement of 2.803% when compared to the unaligned profiles. As with the Spanish dataset, this is the biggest decrease seen across all of the other algorithms making it the best in this regard.

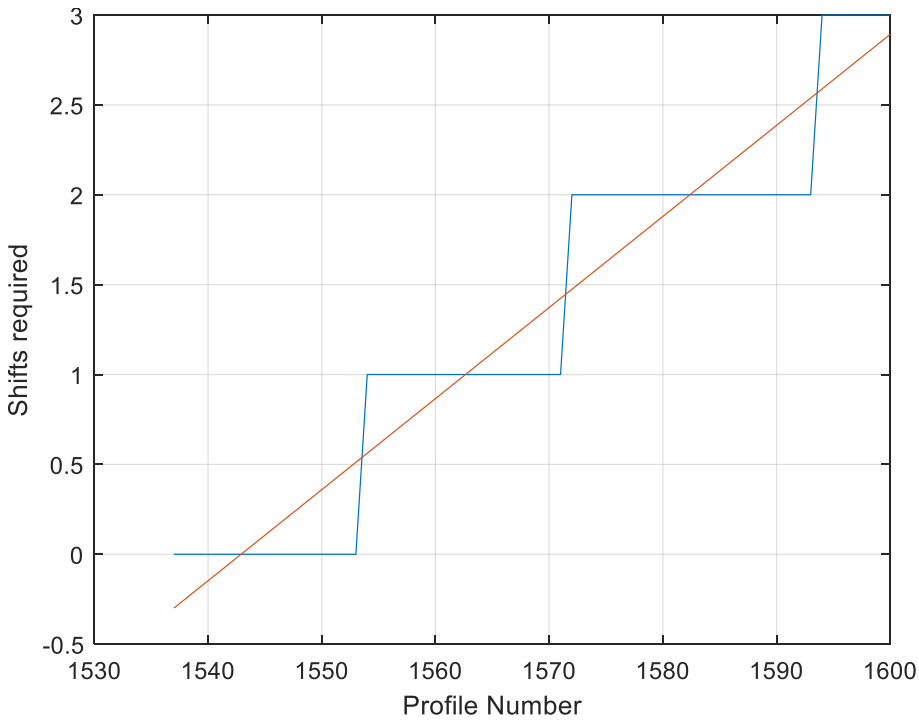

Figure 4.38 Plot of the bin shifts per profile for alignment with a first order polynomial

Furthermore, the number of sub-integer shifts that each unaligned profile underwent is displayed in Fig 4.38. The linear red line indicates the first order polynomial fitted to the integer shifts, creating the sub-integer shifts. The positive gradient was expected as it aligns with the staircase shape.

4.10.3 Discussion and comparison of both datasets

In terms of improvement when comparing the alignment with respect to the unaligned profiles, the same that was said for the other alignment algorithms (bar the adjacent reference profile algorithms) holds true.
The technique improved the alignment of the profiles for both datasets in comparison with the unaligned profiles. This was very clear qualitatively as the profiles were visually more aligned. Furthermore, it was justified by the increases in contrast as well as the decrease in entropy, across both of the datasets.

Furthermore, from the HRR profiles plots, it appeared that this algorithm performed second only to the single reference profile sub-integer algorithm. This is justified by the second highest improvement in contrast across all the preceding algorithms at this point. Strangely enough, the entropy had the best improvement seen. These statements are valid across both datasets.

The lowest (desirable) entropy values were seen here indicating that profiles aligned by this technique have the least variance, at this point.

4.11 Sliding-Window Average Reference Profile Alignment (Sub-integer shift)

4.11.1 Spanish Dataset

As mentioned earlier, a sliding window of 42 was chosen for the counterpart integer shift algorithm.
The resulting range aligned HRR profiles for the Spanish dataset is shown in Fig 4.39. It is clear from the HRR profile plot, that a better alignment had taken place here compared to the result of the counterpart algorithm in Fig 4.26. Here, there is less migration of scatterers across range bins than in Fig 4.26. Moreover, there are no periodic jumps in shifts which were seen previously.

Visually the plot appears to be better than the cumulative averaging (sub-integer) shift algorithm that was seen in the previous sub-chapter. An example of this can be seen in the scatterer at ~6968m. The scatterer here is much more prominent (darker) than the same one in Fig 4.35. However, using the same scatterer, visually it remains worse than the single reference profile algorithm in Fig 4.31. The contrast and entropy values of Fig 4.39 are shown in Table 4.15.

Table 4.15 Table showing the contrast and entropy values in dB

Contrast (dB)	Entropy (dB)
-23.1264	-9.8314

The contrast value had an increase of 9.221% when compared to the unaligned profiles. This is a better improvement than the cumulative averaging method but worse than the single reference profile method, justifying the qualitative measure.

The entropy value had a decrease (desirable) of 2.083% when compared to the unaligned profiles. This is the second lowest improvement (the first being the single reference sub-integer algorithm) bar the adjacent reference profile method.

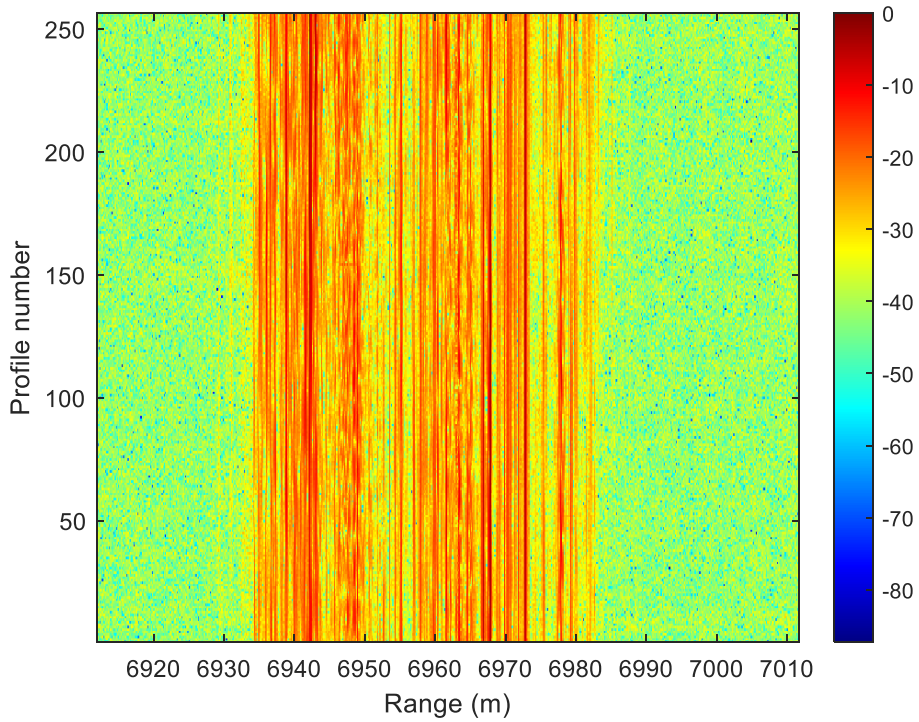

Figure 4.39 HRR profiles plot of the envelope correlation sliding window average reference profile algorithm (sub-integer shift)

Furthermore, the number of sub-integer shifts that each unaligned profile underwent is displayed in Fig 4.40. The linear red line indicates the first order polynomial fitted to the integer shifts, creating the sub-integer shifts. The negative gradient was expected due to the decreasing staircase shape.

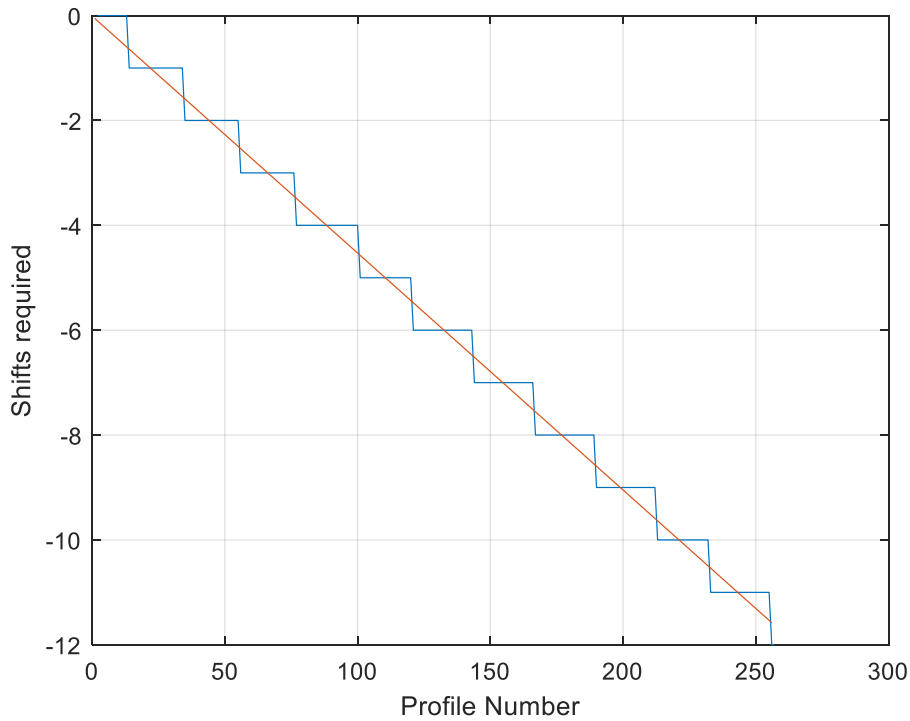

Figure 4.40 Plot of the bin shifts per profile for alignment with a first order polynomial

4.11.2 CSIR Dataset

As mentioned earlier, a sliding window of 22 was chosen for the counterpart integer shift algorithm.
The resulting range aligned HRR profiles for the CSIR dataset are shown in Fig 4.41. It is clear from the HRR profiles plot, that a better alignment had taken place here compared to the result of the counterpart algorithm

in Fig 4.28. There is less migration of scatterers across range bins than in Fig 4.28. Moreover, there are no periodic jumps in shifts which were seen previously.

Visually the plot appears to be indistinguishable from the cumulative averaging (sub-integer) shift algorithm that was seen in the previous sub-chapter. An example of this can be seen in the scatterer at ~16m. The scatterer here looks identical to the same one in Fig 4.37. (This was as expected because the cumulative averaging reference integer shift algorithm was identical to the sliding window averaging integer shift algorithm. This means the required integer shifts were the same, which is the sole dependency of the sub-integer shifts).
Using the same scatterer at ~16m, visually this algorithm remains worse than the HRR profiles plot of the single reference profile algorithm in Fig 4.33. These qualitative observations were supported by the quantitative measures in Table 4.16.

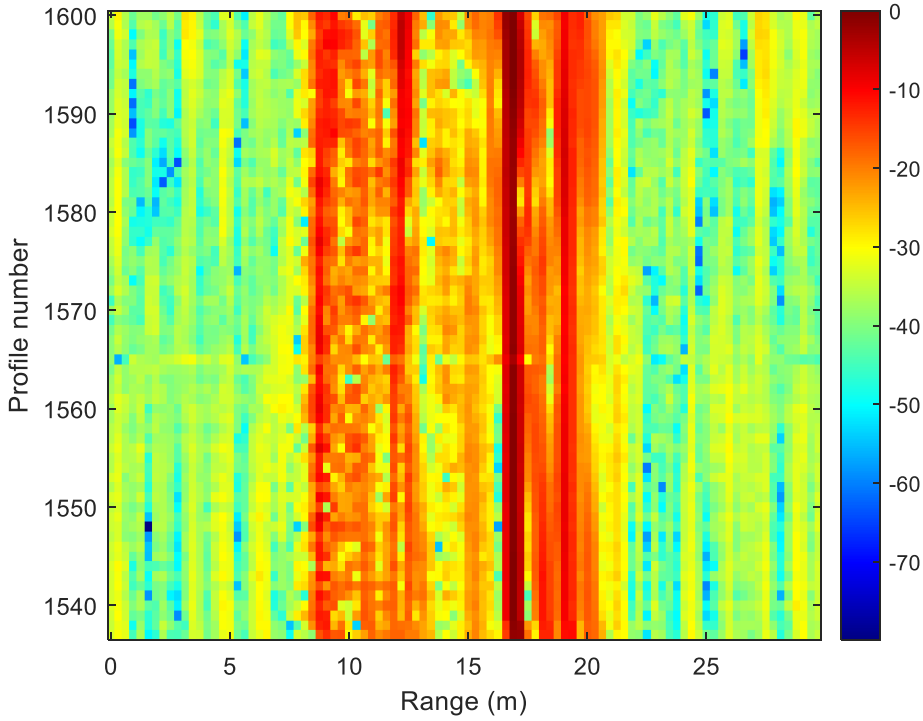

Figure 4.41 HRR profiles plot of the envelope correlation sliding window average reference profile algorithm (sub-integer shift)

Table 4.16 Table showing the contrast and entropy values in dB

Contrast (dB)	Entropy (dB)
-17.2711	-8.8395

The contrast value had an increase of 7.425% when compared to the unaligned profiles, which is the same as seen with the cumulative averaging method.

The entropy value had an improvement of 2.803% when compared to the unaligned profiles, which is the same as seen with the cumulative averaging method. This makes it the tied best algorithm in terms of entropy only, for this dataset.

Lastly, the number of sub-integer shifts that each unaligned profile underwent is displayed in Fig 4.42. The linear red line indicates the first order polynomial fitted to the integer shifts, creating the sub-integer shifts. The positive gradient agrees with the increasing staircase shape.

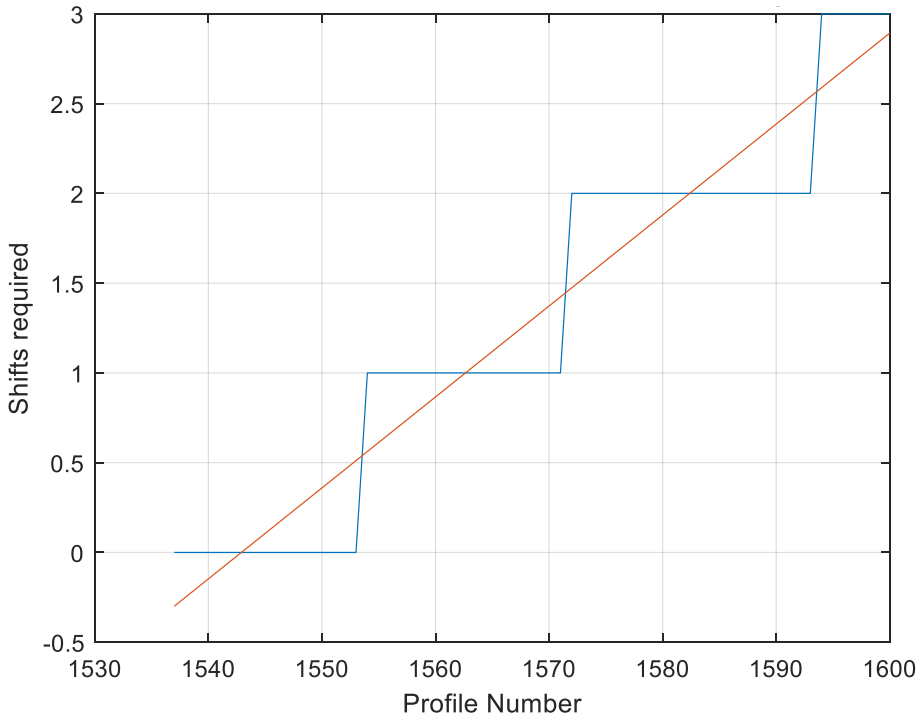

Figure 4.42 Plot of the bin shifts per profile for alignment with a first order polynomial

4.11.3 Discussion and comparison of both datasets

The technique too improved the alignment of the profiles for both datasets in comparison with the unaligned profiles. This was clear qualitatively as the profiles were visually more aligned. Furthermore, it was justified by the increases in contrast as well as the decrease in entropy, across both of the datasets.

For the Spanish dataset, this algorithm provided the second best alignment, second only to the single reference profile algorithm. It performed better than the cumulative averaging method on this dataset. This is further justified by it having the second highest contrast improvement. The improvement in entropy was the second worse (bar the adjacent reference profile algorithm). A reason for the second best alignment technique having the second worst entropy could have been due to the use of sub-integer shifts.

For the CSIR dataset, the algorithm performed the same as the cumulative averaging reference algorithm. This was expected due to them having identical integer shifts resulting from the first process in the respective algorithms.

5. Discussion of the algorithms on different blocks within a dataset

The performance of the algorithms across different datasets was explored in the previous chapter. However, it is worth noting that the performance can fluctuate within datasets themselves. An analysis in this could help with choosing the best blocks for alignment and also for fairly measuring the performance across various datasets. The following chapter looks into the performance of the algorithms on blocks within the Spanish dataset and CSIR dataset respectively.

5.1 Spanish Dataset intra-block performance

Only two blocks of data were available for analysis. These were blocks with profiles 1:256 and 257:513 respectively. The resulting performance of each data block, based on the quantitative measures, is shown in Table 5.1. The results were similar with the single reference profile sub-integer shift algorithm having the best (highest) contrast, and the cumulative averaging reference profile sub-integer shift algorithm having the best (lowest) entropy. The corresponding values are shown in bold in Table 5.1.

Table 5.1 Performance of the algorithms on different blocks

ALGORITHM	**CONTRAST (dB)**		**ENTROPY (dB)**	
Block	1:256	257:513	1:256	257:513
Integer Shifts				
Unaligned profiles	-25.4755	-26.1120	-9.6308	-9.8851
Single reference profile	-23.7674	-24.5325	-9.8700	-10.0841
Adjacent reference profile	-25.4755	-26.1120	-9.6308	-9.8851
Cumulative average reference profile	-23.7982	-24.5626	-9.8643	-10.0838
Sliding Window averaging reference (window =42)	-23.7613	-24.5380	-9.8699	-10.0849
Sub-Integer Shifts				
Single reference profile	**-22.8357**	**-24.2173**	-9.7278	-10.1074
Adjacent reference profile	-25.4755	-26.1120	-9.6308	-9.8851
Cumulative average reference profile	-23.7364	-24.4084	**-10.0138**	**-10.1582**
Sliding Window averaging reference (window =42)	-23.1264	-24.3845	-9.8314	-10.1562

5.2 CSIR Dataset intra-block performance

With over 4000 profiles and each block chosen to contain 64 of them, there were approximately 69 non-overlapping blocks available for analysis. The resulting performance of each data block, based on the quantitative measures, is presented in plots with quality measures on the y-axis and block numbers on the x-axis. They are split into the integer shift algorithms and sub-integer shift algorithms respectively.

Integer shift algorithms

The resulting contrast values when using the integer shift algorithms on different blocks of data can vary significantly. This is seen in Fig 5.1, where a legend is shown to distinguish the techniques. The contrast values ranged from -24dB to -15.5 dB but were normalised (divided by unaligned value) for readability. It is evident that the single reference algorithm produced the highest (desirable) contrast values, for most parts of the dataset. This relates to the red troughs, noting that a lower normalised value is a higher contrast value due to the negative signs of the values. Although there are many dominant troughs of the non-coherent cumulative averaging method, it is important to note that changing the sliding window could produce the same result or a better one for the sliding window(s-w avg) method.

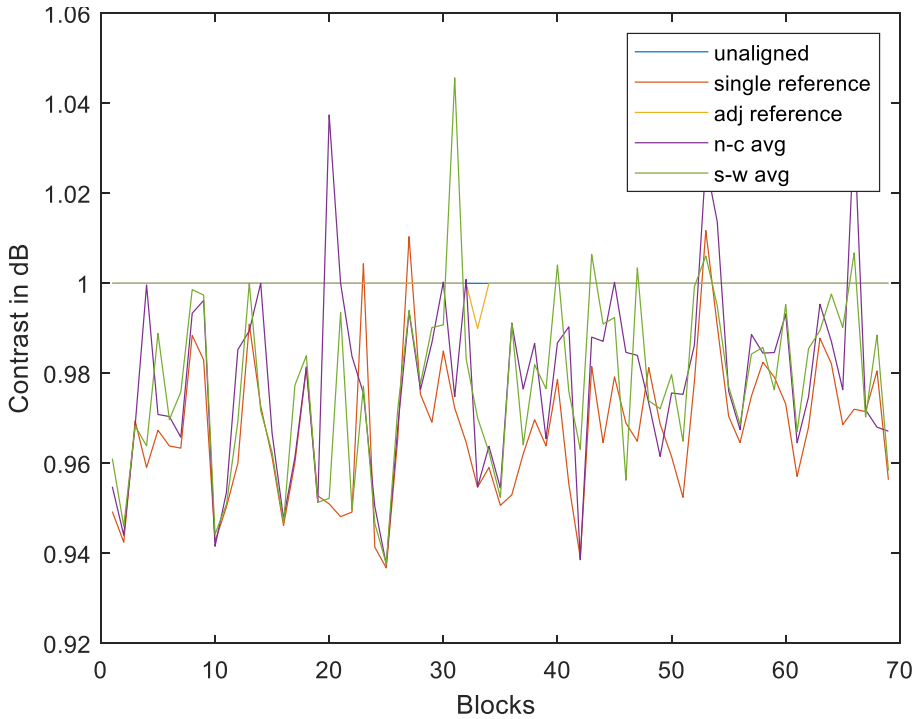

Figure 5.1 Plot of the block number vs normalised contrast (dB)

As with the contrast, the resulting entropy values when using the integer shift algorithms on different blocks of data can vary significantly. This is seen in Fig 5.2, where a legend is shown to distinguish the techniques. The entropy ranged from -10.4dB to -7.4 dB but was normalised (divided by unaligned value) for readability. Once more, it is apparent that the single profile reference algorithm produced the lowest (desirable) entropy values, for most parts of the dataset. . This relates to the red peaks, noting that a higher normalised value is a higher contrast value due to the negative signs of the values. Although there are many dominant peaks of the non-coherent cumulative averaging method, it is important to note that changing the sliding window could produce the same result or a better one for the former method. This is indicated by it having a lot of the lowest troughs.

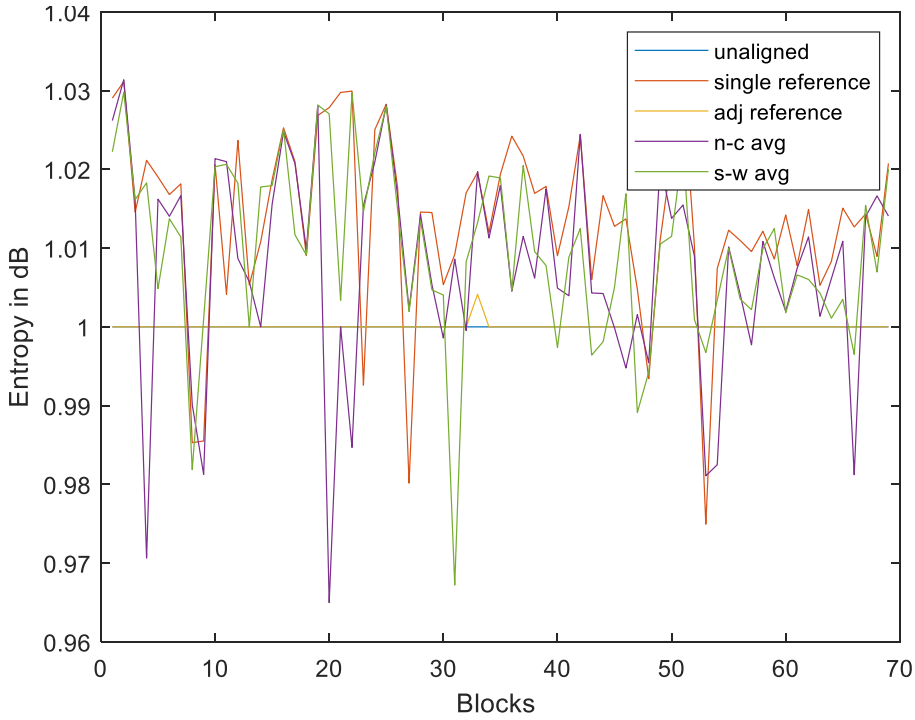

Figure 5.2 Plot of the block number vs normalised entropy (dB)

<u>Sub-integer shift algorithms</u>

The resulting contrast values when using the sub-integer shift algorithms on different blocks of data can vary significantly. This is seen in Fig 5.3, where a legend is shown to distinguish the techniques. The contrast ranged from -27.5dB to -15.5 dB but was normalised (divided by unaligned value) for readability. From the plot, it could be determined that different algorithms had the best performance, in terms of contrast, at different blocks. This is indicated by the different colour troughs being higher than others at certain blocks only.

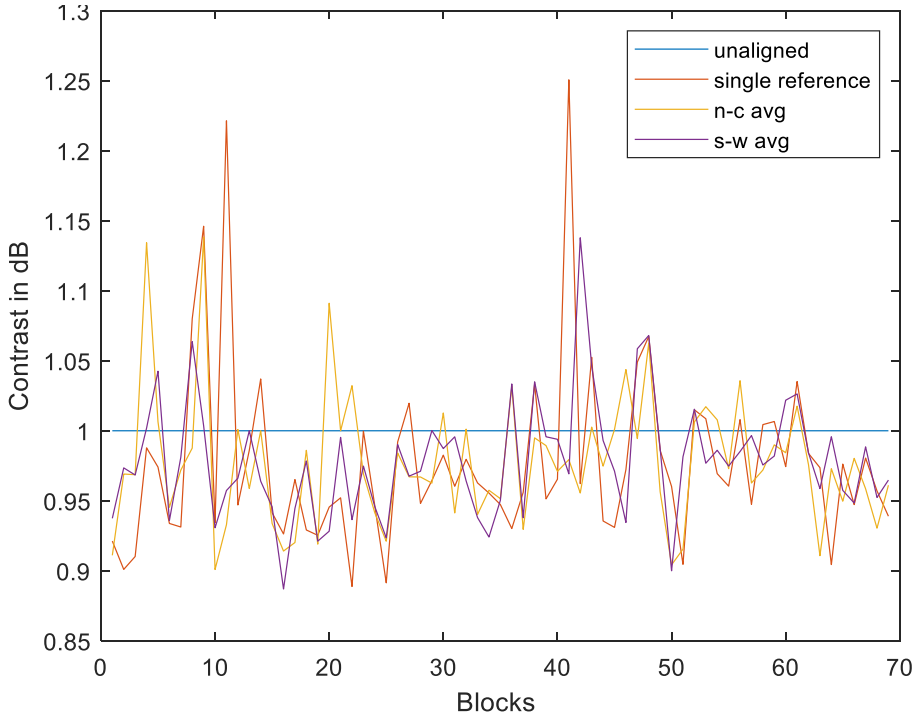

Figure 5.3 Plot of the block number vs normalised contrast (dB)

As with the contrast, the resulting entropy values when using the sub-integer shift algorithms on different blocks of data can vary significantly. This is seen in Fig 5.4, where a legend is shown to distinguish the

techniques. The entropy ranged from -10.4dB to -7.4 dB but was normalised (divided by unaligned value) for readability. Again, it is apparent that different algorithms had the best performance, in terms of entropy, at different blocks. This is indicated by the different colour peaks being higher than others at certain blocks only.

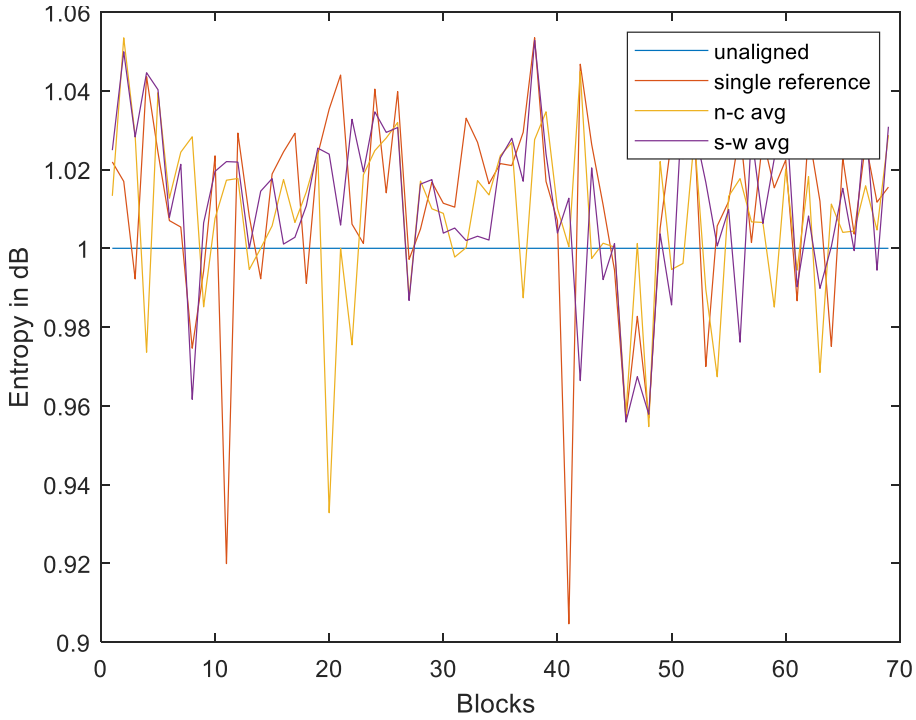

Figure 5.4 Plot of the block number vs normalised entropy (dB)

6. Conclusion

The main objectives of this project were to analyse the current implementation of range alignment algorithms, specifically their performance across different datasets. These objectives were met, to the extent described below, in the following way.

6.1 Review of Range alignment techniques

Chapter 2 provided the theory relating to radar as well as radar signal processing. Furthermore, it looked at range alignment algorithms, relating to ISAR, that have been previously researched. Moreover, quality measures of these techniques were recognised. Lastly, a critical review of the previous literature on range alignment algorithms was presented.

6.2 Implementation and assessment of Range alignment techniques

In chapter 4, the algorithms explaining how these techniques were implemented, were explored. In particular, 8 algorithms were explored, all related to envelope correlation. This was further split into integer shift techniques and sub-integer shift techniques. A discussion of the strengths and weaknesses of these algorithms was conferred. The quality of these techniques was assessed by qualitative measures as well as quantitative measures such as contrast and entropy. As expected, the different techniques had different performances.

6.3 Performance of the different algorithms on different datasets

Moreover, Chapter 4 further looked at the comparison of the performance of the algorithms across two different datasets, namely the Spanish dataset and the CSIR dataset. This performance was once more measured by qualitative means as well the quantitative measures such as contrast and entropy. For the most part, the performance of the algorithms was consistent apart from a few minor differences. The single reference profile sub-integer shift algorithm produced the best results for the data blocks analysed, across the two datasets.

6.4 Intra-dataset performance

In chapter 5, the performance of the techniques within different blocks of the dataset was tested. With the Spanish dataset having little data to work with, the results were inconclusive. However, the CSIR dataset contained more information and the variation in performance could be accurately concluded. The single reference profile algorithm integer shift was the best among the integer shift algorithms. With the sub-integer shift algorithms, no algorithm was consistently better than the others.

6.5 Future work

A large room for improvement exists as there are many topics left out of this project. Furthermore, these improvements are worth pursuing as enhancements in the topic of ISAR imaging could be very beneficial.

6.5.1 Exploring more techniques

Many range alignment techniques discussed in the literature were not implemented. Using these techniques in future iterations of the project can lead to more findings and better results.

6.5.2 Exploring more quantitative measures

As with exploring more range alignment techniques, other measures apart from the contrast and entropy can be used to quantify the performance of algorithms, leading to more justifiable results.

6.5.3 Using more datasets

Better conclusions could be made and justified with the use of more datasets. Furthermore, higher quality and larger datasets could be used to provide more justifiable results.

6.5.4 Phase correction and autofocus

Lastly, phase correction techniques were left out of the scope of this project. Inclusion of this, and ISAR images could display the performance of range alignments and their propagating effects more visually.

List of References

[1] M. Martorella, J. Palmer, J. Homer, B. Littleton, and D. Longstaff, "On_Bistatic_Inverse_Synthetic_Aperture_Radar," 2007, doi: 10.1109/TAES.2007.4383602.

[2] R. Vehmas and N. Neuberger, "Inverse Synthetic Aperture Radar Imaging: A Historical Perspective and State-of-the-Art Survey," *IEEE Access*, vol. 9. Institute of Electrical and Electronics Engineers Inc., pp. 113917–113943, 2021. doi: 10.1109/ACCESS.2021.3104799.

[3] M. Martorella *et al.*, "Inverse Synthetic Aperture Radar," 2006. doi: 10.1155/ASP/2006/63465.

[4] V. Janse Van Rensburg, A. Mishra, and W. Nel, "High Range Resolution Profile Alignment," 2012.

[5] A. Zyweck, "Preprocessing Issues in High Resolution Radar Target Classification," 1995.

[6] L. I. Xi, "Autofocusing of ISAR images based on entropy minimization," *IEEE Transactions on Aerospace and Electronic Systems*, vol. 35, no. 4, pp. 1240–1252, 1999, doi: 10.1109/7.805442.

[7] M. Martorella and F. Berizzi, "Time Windowing for Highly Focused ISAR Image Reconstruction," 2005. doi: 10.1109/TAES.2005.1541444.

[8] M. Y. Abdul Gaffar, W. A. J. Nel, and M. R. Inggs, "Selecting suitable coherent processing time window lengths for ground-based ISAR imaging of cooperative sea vessels," *IEEE Transactions on Geoscience and Remote Sensing*, vol. 47, no. 9, pp. 3231–3240, Sep. 2009, doi: 10.1109/TGRS.2009.2019729.

[9] J. M. Muñoz-Ferreras and F. Pérez-Martínez, "Subinteger range-bin alignment method for ISAR imaging of noncooperative targets," *Eurasip Journal on Advances in Signal Processing*, vol. 2010, 2010, doi: 10.1155/2010/438615.

[10] W. Nel, E. Giusti, M. Martorella, and M. Y. Abdul Gaffar, "A time domain phase-gradient based ISAR autofocus algorithm," in *Proceedings of 2011 IEEE CIE International Conference on Radar, RADAR 2011*, 2011, vol. 1, pp. 541–544. doi: 10.1109/CIE-Radar.2011.6159598.

[11] X. Mao, D. Zhu, and Z. Zhu, "Polar format algorithm wavefront curvature compensation under arbitrary radar flight path," in *Proceedings of 2011 IEEE CIE International Conference on Radar, RADAR 2011*, 2011, vol. 2, pp. 1382–1385. doi: 10.1109/CIE-Radar.2011.6159816.

[12] R. M. O'donnell, "Introduction to Radar Systems," 2002.

[13] M. A. (Mark A.) Richards, J. Scheer, and W. A. Holm, *Principles of modern radar. Volume I, Basic principles*. SciTech Pub, 2010.

[14] O'donnell R, "The Radar Equation MIT Lincoln Laboratory Disclaimer of Endorsement and Liability," 2002.

[15] O'donnell R, "Detection of targets in noise and pulse compression techniques," 2002.

[16] A. K. J. W. H. J. and E. P. D. Ausherman, *Developments in radar imaging, Aerospace and Electronic Systems*, vol. 4. Aerospace and Electronic Systems, IEEE Transactions on, 1984. doi: 10.1109/TGRS.2011.2151865.

[17] Junfeng Wang and D. Kasilingam, "Global range alignment for ISAR," *IEEE Transactions on Aerospace and Electronic Systems*, vol. 39, no. 1, pp. 351–357, Jan. 2003, doi: 10.1109/TAES.2003.1188917.

[18] L. Zhang, Z. J. Qiao, M. Xing, Y. Li, and Z. Bao, "High-resolution ISAR imaging with sparse stepped-frequency waveforms," *IEEE Transactions on Geoscience and Remote Sensing*, vol. 49, no. 11 PART 2, pp. 4630–4651, Nov. 2011, doi: 10.1109/TGRS.2011.2151865.

[19] C. Ozdemir, *Inverse Synthetic Aperture Radar Imaging with MATLAB Algorithms*, vol. 210. Wiley-Interscience, 2012.

[20] B. Haywood and R. Evans, *Motion compensation for ISAR imaging*, vol. 89. Proceedings of ASSPA, 1989.

[21] C. Chen and M. Martorella, *Inverse Synthetic Aperture Radar Imaging*. SciTech publishing, 2014.

[22] C. C. Chen and H. C. Andrews, "Target-motion-induced radar imaging," *IEEE Transactions on Aerospace and Electronic Systems*, vol. AES-16, no. 1, pp. 2–14, 1980, doi: 10.1109/TAES.1980.308873.

[23] J. Son, G. Thomas, and B. Flores, *Range-Doppler radar imaging and motion compensation*, vol. 1. Artech House Publishers, 2000.

[24] Li Xi, Liu Guosui, and Jinlin Ni, "Autofocusing of ISAR images based on entropy minimization," *IEEE Transactions on Aerospace and Electronic Systems*, vol. 35, no. 4, pp. 1240–1252, 1999, doi: 10.1109/7.805442.

[25] B. Haywood and R. J. Evans, "Motion compensation for ISAR imaging," in *Proceedings of Australian Symposium on Signal Processing and Applications*, 1989, pp. 113–117.

[26] Daiyin Zhu, Ling Wang, Yusheng Yu, Qingnian Tao, and Zhaoda Zhu, "Robust ISAR Range Alignment via Minimizing the Entropy of the Average Range Profile," *IEEE Geoscience and Remote Sensing Letters*, vol. 6, no. 2, pp. 204–208, Apr. 2009, doi: 10.1109/LGRS.2008.2010562.

[27] R. Bocker and S. Jones, "ISAR motion compensation using the burst derivative measure as a focal quality indicato," *International Journal of Imaging Systems and Technology*, vol. 4, pp. 285–297, 1992.

[28] J. M. Munoz-Ferreras and F. Perez-Martinez, "Extended envelope correlation for range bin alignment in ISAR," in *IET International Conference on Radar Systems 2007*, 2007, pp. 39–39. doi: 10.1049/cp:20070515.

[29] M. Y. A. Gaffar, W. A. J. Nel, K. Naicker, J. Steyn, T. Alanazi, and A. Alzamil, "Synthetic range profiling, ISAR imaging of sea vessels and feature extraction, using a multimode radar to classify targets: Initial results from field trials," in *2011 Saudi International Electronics, Communications and Photonics Conference (SIECPC)*, Apr. 2011, pp. 1–6. doi: 10.1109/SIECPC.2011.5876925.

Appendices

Appendix A: Sub-Integer algorithm steps and derivation

Sub-integer algorithm steps

The sub-integer algorithm consists of the following seven steps [4], [9]:

1. First profile. $\overline{P_0} = P_0$
2. Calculate, R_m, the reference profile.
3. Calculate, x_m, the envelope correlation, for each integer shift value of τ_m.
4. Determine, $\tau_{m,0}$, which is the τ_m value which caused the maximum cross-correlation.
5. With $\tau_{m,0}$, as the initial guess to the Nelder-Mead algorithm, get the optimal shift which is $\widehat{\tau_m}$.
6. Obtain the aligned profile, $\hat{P}_m$.
7. If $m < M - 1$, where M is the number of profiles, go to step 2. $(m = m + 1)$

Haywood's algorithm

Haywood's algorithm consists of 3 stages as follows [4]:

1. Radial motion compensation
2. Adaptive beamforming
3. Doppler processing

The first is explored. Assume *N* complex HRR profiles, each with *n* range bins as $r_1 \ldots . r_n$. This gives an HRR profile matrix of $N \times n$ given by Equation A.1. [4]

$$\begin{bmatrix} r_1 \\ \vdots \\ r_N \end{bmatrix} = \begin{bmatrix} A_{11}e^{j\emptyset_{11}} & \cdots & A_{1n}e^{j\emptyset_{1n}} \\ \vdots & A_{lm}e^{j\emptyset_{lm}} & \vdots \\ A_{N1}e^{j\emptyset_{N1}} & \cdots & A_{Nn}e^{j\emptyset_{Nn}} \end{bmatrix} \tag{A.1}$$

Where $\emptyset_{lm}$ is a real number between $[0,2\pi)$, A_{lm} is a real number, $l=1 \ldots N$ is an HRR profile index and m is the range bin index.

A reference profile given by Equation A.2 is cross-correlated with each HRR profile (magnitude), to achieve radial compensation. This calculation, c_l, is shown in Equation A.3.[4]

$$r_p = [A_{p1}e^{j\emptyset_{p1}} \ldots A_{pn}e^{j\emptyset_{pn}}] \tag{A.2}$$

In Equation A.3 DFT and IDFT are the Discrete Fourier Transform operation. The location of the peak of c_l, indicates the required range shift for alignment, d_l, as seen in Equation A.4.[4]

$$c_l = \left|IDFT\left(DFT\left(|r_p|\right)DFT(|r_l|)^*\right)\right| \qquad \forall\, l = 1 \ldots N \tag{A.3}$$

$$d_l = location[\max(c_l)] \qquad \forall\, l = 1 \ldots N \tag{A.4}$$

The sequence of shifts, $d_1 \dots d_n$, are smoothed by fitting a low-order polynomial to them. The smoothed sub-integer shifts, s_l, are applied to the HRR profiles by multiplying them in the frequency domain with a phase shift vector, $\mathbf{\Phi}$. The calculation is shown in Equation A.5 with $\mathbf{\Phi}$ shown in Equation A.6. [4]

$$r'_l = IDFT(\mathbf{\Phi} DFT\left(\left[A_{l1}e^{j\emptyset_{l1}} \dots A_{lm}e^{j\emptyset_{lm}} \dots A_{ln}e^{j\emptyset_{ln}}\right]\right)) \qquad \forall\, l = 1 \dots N \tag{A.5}$$

$$\mathbf{\Phi} = e^{j\frac{2\pi}{\beta}} \times [e^{-js_l(f_s+\Delta f)} \dots e^{-js_l(f_s+m\Delta f)} \dots e^{-js_l(f_s+n\Delta f)}] \qquad \forall\, l = 1 \dots N \tag{A.6}$$

Where $\beta = N\Delta f$ is the bandwidth, Δf is the frequency increment and f_s is the start frequency.
After range alignment, the HRR profiles can be represented by Equation A.7.

$$\begin{bmatrix} r'_1 \\ \vdots \\ r'_N \end{bmatrix} = \begin{bmatrix} A'_{11}e^{j\emptyset'_{11}} & \cdots & A'_{1n}e^{j\emptyset'_{1n}} \\ \vdots & A'_{lm}e^{j\emptyset'_{lm}} & \vdots \\ A'_{N1}e^{j\emptyset'_{N1}} & \cdots & A'_{Nn}e^{j\emptyset'_{Nn}} \end{bmatrix} \tag{A.7}$$

Where A'_{lm} is real, $\emptyset'_{lm}$ is a real number between $[0,2\pi)$, $l=1 \dots N$ is an HRR profile index and m is the range bin index.

Appendix B: Global Method flow diagram

The shift value, τ_m, applied to profile *m*, is calculated using Equation B.1 [4], [17]:

$$\tau_m = \sum_{i=1}^{\infty} \beta(i)\left(\frac{2m}{M} - 1\right)^i \tag{B.1}$$

The value *β(i)*, is calculated by the algorithm presented in Fig B.1 [4].

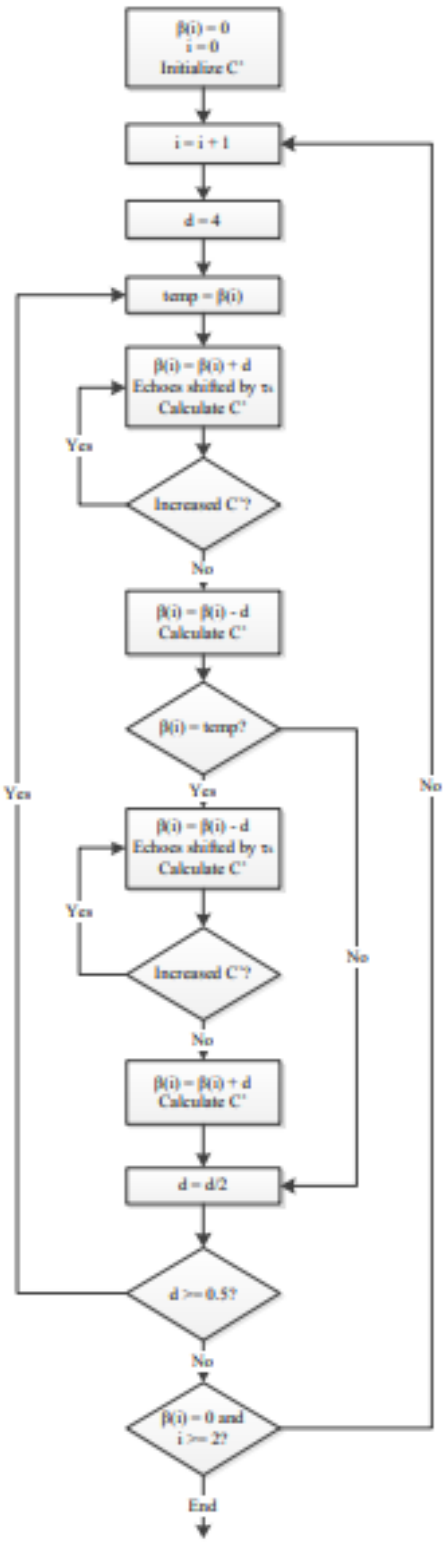

Fig B.1: Algorithm to calculate β(i), for optimal contrast [4]

Appendix C: Sum Envelope Entropy derivation

The sum envelope entropy which was presented in [26], makes use of the definition of the sum envelope defined in Equation C.1. [4]

$$H = -\sum_{n=0}^{N-1} \frac{a(n)}{A} \ln \frac{a(n)}{A} \tag{C.1}$$

Where n, N and A remain as previously stated.

Envelopes of different profiles found in a data set have similar shapes but have varying time delays. Thus, when the alignment of the profiles takes place, *a(n)* is the sharpest and subsequently the entropy, *H*, would be a minimum. Equation C.1 is rewritten as Equation C.2. [4]

$$H = ln\, A - \frac{1}{A}\sum_{n=0}^{N-1} a(n) \ln a(n) \tag{C.2}$$

A stays constant in alignment, so *H* is redefined by Equation C.3, which is calculated more efficiently than Equation C.1. [4]

$$H' = -\sum_{n=0}^{N-1} a(n) \ln a(n) \tag{C.3}$$

Appendix D: Code to obtain the results

This section provides the GitHub link required to access the code used to obtain the results in this report. The following link can be used to access the code in the GitHub repository:

https://github.com/azharebrahim1/EBRAZH001_Matlab_Scripts_22.git

EBE Faculty: Assessment of Ethics in Research Projects

Application for Approval of Ethics in Research (EiR) Projects
Faculty of Engineering and the Built Environment, University of Cape Town

ETHICS APPLICATION FORM

Please Note:
Any person planning to undertake research in the Faculty of Engineering and the Built Environment (EBE) at the University of Cape Town is required to complete this form **before** collecting or analysing data. The objective of submitting this application *prior* to embarking on research is to ensure that the highest ethical standards in research, conducted under the auspices of the EBE Faculty, are met. Please ensure that you have read, and understood the **EBE Ethics in Research Handbook** (available from the UCT EBE, Research Ethics website) prior to completing this application form: http://www.ebe.uct.ac.za/ebe/research/ethics1

APPLICANT'S DETAILS		
Name of principal researcher, student or external applicant		Azhar Ebrahim
Department		Electrical Engineering
Preferred email address of applicant:		EBRAZH001@myuct.ac.za
If Student	Your Degree: e.g., MSc, PhD, etc.	BSc in Eng in Mechatronics
	Credit Value of Research: e.g., 60/120/180/360 etc.	40
	Name of Supervisor (if supervised):	DR. Yunus Abdul Gaffar
If this is a researchcontract, indicate the source of funding/sponsorship		n/a
Project Title		Range Alignment for ISAR imaging of sea vessels

I hereby undertake to carry out my research in such a way that:

- there is no apparent legal objection to the nature or the method of research; and
- the research will not compromise staff or students or the other responsibilities of the University;
- the stated objective will be achieved, and the findings will have a high degree of validity;
- limitations and alternative interpretations will be considered;
- the findings could be subject to peer review and publicly available; and
- I will comply with the conventions of copyright and avoid any practice that would constitute plagiarism.

APPLICATION BY	Full name	Signature	Date
Principal Researcher/ Student/External applicant	Azhar Ebrahim		3/27/2022
SUPPORTED BY	Full name	Signature	Date
Supervisor (where applicable)	Dr Abdul Gaffar		31/03/2022

APPROVED BY	Full name	Signature	Date
HOD (or delegated nominee) Final authority for all applicants who have answered NO to all questions in Section 1; and for all Undergraduate research (Including Honours).			
Chair: Faculty EIR Committee For applicants other than undergraduate students who have answered YES to any of the questions in Section 1.			